Role of Ca Doping and Process Variables in the Dielectric Properties of Barium Titanate Ceramics

by

Abu Mohammed Rashed Chowdhury

MASTER OF SCIENCE IN ENGINEERING

Department of Materials and Metallurgical Engineering

BANGLADESH UNIVERSITY OF ENGINEERING AND TECHNOLOGY

2005

The thesis titled "Role of Ca Doping and Process Variables in the Dielectric Properties of Barium Titanate Ceramics", submitted by Abu Mohammed Rashed Chowdhury, Roll no 9611006P Session 95-96-97 has been accepted as satisfactory in partial fulfillment of the requirement for the degree of Master of Science in Engineering (Materials and Metallurgy) on the 27th August 2005

Board of Examiners

1. Dr. Md Fakhrul Islam
Professor
Department of Materials and Metallurgical Engineering
BUET, Dhaka — Chairman (Supervisor)

2. Dr Mominul Huq
Professor and Head
Department of Physics
BUET, Dhaka — Member (Co- Supervisor)

3. Dr. Md. Nasrul Haque
Professor and Head
Department of Materials and Metallurgical Engineering
BUET, Dhaka — Member (Ex-Officio)

4. Dr. Md. Mohar Ali
Professor
Department of Materials and Metallurgical Engineering
BUET, Dhaka — Member

5. Dr. A.K. M. Bazlur Rashid
Professor
Department of Materials and Metallurgical Engineering
BUET, Dhaka — Member

6. Dr. Md. Tafazzal Hussain
Professor
Department of Physics
University of Dhaka, Dhaka — Member (External)

CANDIDATE'S DECLARATION

It is hereby declared that this thesis or any part of it has not been submitted elsewhere for the award of any degree or diploma.

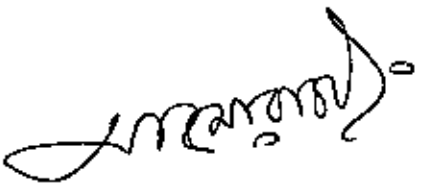

(Abu Mohammed Rashed Chowdhury)

Dedicated

To

Moulana Abdus Samad Chowdhury

and

my Grand Parents

Contents

List of Figures

List of Tables

Acknowledgements

Firstly, I would like to express sincere gratitude to my supervisor Prof. Dr. Md. Fakhrul Islam for his guidance, valuable comments, encouragement, enthusiasms and all round support. This thesis would not have realized without his extra ordinary support, I am indeed indebt to him. He was there, where I needed, when I needed regardless the place or time. I do also admire his patience, profoundly. He organized for me to carry out some experiments at MTEC at Bangkok which helped greatly in the research of this thesis.

Prof. Dr. Mominul Huq, Professor and Head of Physics Department, BUET was kind enough to be my co-supervisor. He guided me with valuable comments, suggestions and facilitated with equipments of his department. My sincere gratitude to him. In this connection I would like to thank Prof. Dr. Abu Hashan Bhuiyan for the help with the instruments also.

Bulk of the experimental works was carried out at MTEC, Bangkok, Thailand under the supervision of Dr. Apinya Panupat My gratitude to her for all the suggestions. help and time she has given in this project And also for all the trouble she has taken from the day I was in Bangkok to the day I left Dr. Arech Thanaboonsombut, despite her busy schedule spared time for advice and assistance whenever needed, my gratitude to her also. I also like to thank Ms. Naruporn, Mr. Bandit and all other technicians and colleague for their time provided during my stay at MTEC My gratitude to the Royal Thai Government for the financial support

I would like to express my thanks to Prof. Dr. Md. Nasrul Haque providing laboratory facilities and suggestions in completing this thesis He has been very kind to me and took the trouble of teaching X ray diffraction that really helped me a lot. I am grateful to all other teachers of MME Department for their continuous inspiration, help, particularly to Prof. Dr. Haseeb for valuable comments. All the technicians and staffs did extend their help whenever I needed. I like to thank them all.

Dr Md. Abdul Hakim and Dr. Dilip Kumar Saha of Magnetic Material Division of Atomic Energy Commission (AEC) helped me with the experimental and XRD. I gratefully acknowledge their cooperation and extend my gratitude. Special thanks to my co-worker Mr. Tareque Chowdhury of AEC for the help with the experiments and support.

My acknowledgement and gratitude to my parents, my family, wife and specially my daughter *Ibtisama* for their sacrifice and whole hearted support. My wife, Fatema, was behind the scene from the start, inspiring me continuously to complete this thesis.

A. M. Rashed Chowdhury

Dhaka

June 2005

Abstract

Effects of Ca doping, calcination and sintering temperature on the dielectric properties of $BaTiO_3$ based ceramic were studied in this thesis. Conventional mixed oxide method was used to prepare disc shape sample. The three doping levels were 0.05, 0.08 and 0.12 mole fraction of Ca substituting Ba. Regardless the stoichiometry or sintering parameters, the first set of samples exhibited the Curie temperature (T_c) at 55°C, much lower than 120°C - the usual transition temperature of $BaTiO_3$. Instead of sharp peak, they exhibited bell shaped hump at 55°C. These anomalies were due to iron pickup during milling with steel balls in water media. For verification, another two batches of samples were prepared following identical powder processing technique. One batch was prepared using BUET precursor powder and another from MTEC source. The later one was normal $BaTiO_3$ but the other one did not even sinter to 75% of theoretical density. TiO_2 and $BaCO_3$ used at BUET seem to contain impurities and detrimental phases.

In general the dielectric constant (k') was better for denser samples and so was tangent loss. Density seems to be a conjugate result of calcination and sintering. Incomplete calcination, or incomplete reaction, leads to the formation of gas or blowhole during sintering and most importantly desired properties not realized owing to non-formation (or partial formation) of required phase(s). Due to sluggish nature of solid-state reaction, calcination at 1100°C for 7 hours seems to be satisfactory.

Sintering temperature and timing should be tuned to achieve about 95% of theoretical density. Properly calcined un-doped $BaTiO_3$ can be sintered at 1325°C for 4 hours to achieve that goal. It was observed that Ca did act as a sintering aid for doping level of 0.08 mole fraction and above. Densities of doped sample did follow a non-linear relationship with doping concentration and the change over was observed at 0.07 mole fraction. This effect was observed irrespective of sintering thermal profile.

Iron inclusion in samples turned the expected normal ferroelectric ceramic into relaxor type, with peak k' nearly 4000. In conjunction with Ca doping the Tc was shifted to 55°C which; with the increase of Ca doping level above 0.08 mole fraction shifted the Tc to 90°C. The k' also changed non-linearly with the Ca concentration level. From the XRD examination, it was seen that the extent of tetragonal distortion was the governing factor fixing the T_c. Also observed a preferred orientation of {002} plane at the surface of during sintering, contributing to increase k' near Tc and beyond.

1 Introduction

1.1 Barium Titanate – the pioneer electronic ceramic

Barium Titanate is a ferroelectric material belonging to the sub-class of piezoelectric material. Ferroelectricity is a phenomenon discovered in 1921. The name refers to certain magnetic analogies, though it is somewhat misleading, as it has no connection with iron (ferrum) at all. Ferroelectric materials exhibit spontaneous polarization (*cf* ferromegnetic material - spin orientation) on cooling below the Curie point (T_c), ferroelectric domains and a ferroelectric hysteresis loop. Prior to 1940, naturally found crystals were the only source of ferroelectric material that were available. Work by Thurnauer and Deaderick [1] brought the extraordinary electrical properties of barium titanate to lay the foundation of electronic ceramic. In fact, $BaTiO_3$ was the first ferroelectric ceramic – electronic ceramic in that matter - synthesized and still used widely. These ceramics are referred as electronic because of their extra ordinary electrical properties leading to significant use in electrical applications.

Dielectric constant of $BaTiO_3$ was order of magnitude higher than the best material (Rutile, for instance) available at that time. A huge leap in the research on ferroelectric materials followed immediately in the 1950's, leading to the widespread use of barium titanate ($BaTiO_3$) based ceramics in capacitor applications and piezoelectric transducer devices. Since then, many other ferroelectric ceramics including lead titanate ($PbTiO_3$), lead zirconate titanate (*PZT*), lead lanthanum zirconate titanate (PLZT), and relaxor ferroelectrics like lead magnesium niobate (PMN) have been developed and utilized for a variety of applications. The largest use of ferroelectric ceramics have been in the areas such as dielectric ceramics for capacitor applications, ferroelectric thin films for non volatile memories, piezoelectric materials for medical ultrasound imaging and actuators, and electro-optic materials for data storage and displays.

Among the electronic ceramic used world wide, undoubtedly $BaTiO_3$ in polycrystalline form is ranked highest in volume and variety of application wise. To get a high volumetric efficiency (capacitance per unit volume) the dielectric material between the electrodes should have a large dielectric constant, a large area and a small thickness. $BaTiO_3$ based ceramics having a perovskite type structure show dielectric

constant values as high as 15,000 as compared to 5 or 10 for common ceramic and polymer materials. The high dielectric constant $BaTiO_3$ based ceramic disk capacitors are simple to make. The volumetric efficiency can be further enhanced by using multi layer ceramic (MLC) capacitors. MLC have captured more than 80% of the capacitor market in the year 2002 as shown in Figure 1-1 valued more than US $6.7 billion in Bangladesh Taka that would be 40,200 crore![2]

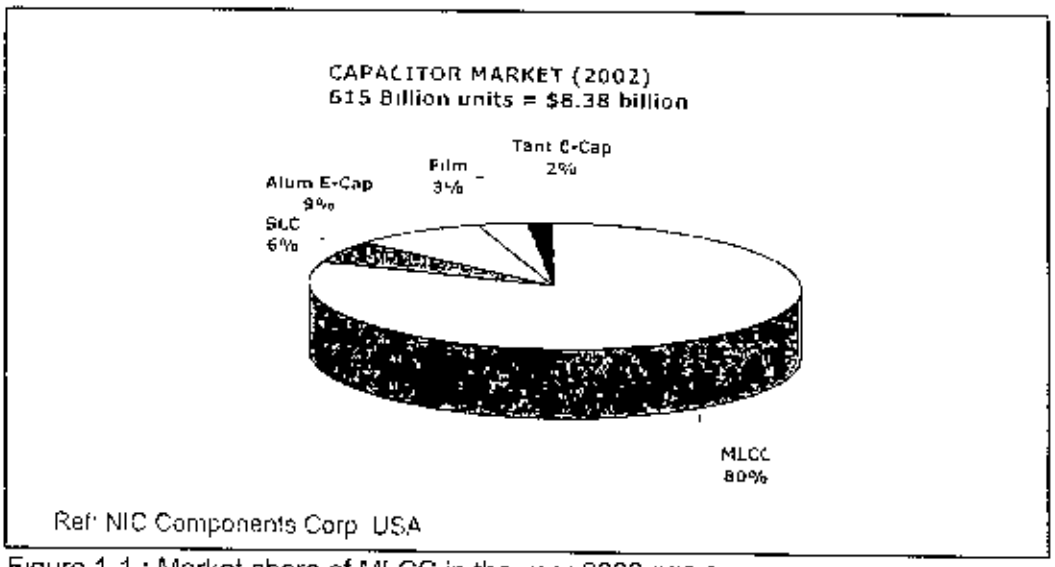

Figure 1-1 : Market share of MLCC in the year 2002 (NIC Components Corp USA)

1.2 Demerits and short falls of $BaTiO_3$

Dielectric constant of $BaTiO_3$ sharply peaks at T_c and loss characteristics follow the same pattern. These anomalies of electrical properties result in extreme change of electrical characteristics of components. For instance, the capacitance of a capacitor would increase by order of magnitude at around T_c than what was at the room temperature. Overall, electrical performance of the circuit would change to extremity, if temperature rises to around T_c. This is not desirable at all, as component in electrical circuit seldom heat up to close proximity of T_c.

In the past few decades, many books and reviews have been written explaining the concepts of electronic ceramic materials [3,4,5,6,7]. An excellent review on piezoelectric ceramic with emphasis on $BaTiO_3$ is compiled by Jaffe [8]. However, it is recognized that the true values of properties of a polycrystalline ceramic are difficult to quote. Almost all chemical and physical deviation from purity has substantial effect on the properties. For instance, universally accepted Curie point (T_c) of $BaTiO_3$ is 120°C but ultra pure $BaTiO_3$ crystal grown using Remeika's process exhibit Curie point at 130°C [9]. Curie point of ceramics also depends on particle or grain size.

Hennings, *et al* [10] has described solid state preparation using ultra fine raw material yielding better results. Grain size is a major factor affecting the dielectric properties of $BaTiO_3$ ceramics [11]. On the other hand, Ba/Ti ratio plays a role determining the grain size and density besides sintering parameters [12]. Seldom do these events occur at the same time during ceramic processing and hence it is difficult to isolate the effect of a single factor at a time. Some time a combination of factors yield different properties than a single factor would. Research followed on for increased performance, higher dielectric constant (k'), smooth dielectric change near T_c, ease of manufacture in bulk and so forth. Doping was one popular and easy option. Other than Ca, many dopants were used stretching from rear earth metal to common ones in search of better $BaTiO_3$ for various applications.

1.3 Scope of this study

Process variables such as sintering temperature, holding time and milling procedures were varied to observe their effect on dielectric properties along side variation of Ca doping level. Un-doped $BaTiO_3$ were also prepared to compare the properties for each combination of variations. In the literature review chapter, the basic principles governing ferroelectricity and means to improve the properties, covering the various materials exhibit these properties were discussed. Particular emphasis was given on $BaTiO_3$ and its dielectric properties. The general processing of ferroelectric ceramics with a few examples were described, since processing is a major factor affecting the final properties of a ceramic. Finally, a few important applications of ferroelectric materials are briefly discussed. Manufacturer's chemical analyses of powers used for sample preparation were included in Appendix 7.1 through 7.3.

Sintering temperature was varied form 1200°C to 1350°C and hold time form 2 hours to 4 hours. Calcium doping level was 5, 8 and 12 % mole fraction of Ba. Their effect on sintered body density, dielectric constant and dielectric loss were measured. Extent of processing was also assessed. For instance, particle size was analyzed for ball milling effect, pre and post calcination XRD were carried out to examine the extent of reaction. Results were explained in the light of finding of crystal structure through XRD investigation, microstructural study by SEM and optical microscopy.

2 Literature Review

2.1 Electronic Ceramics - Classification

Properties of material have its origin in the crystal structure. Having identical chemical composition may yield entirely different properties owing to the difference in crystal structure and vice versa. A property of ceramics is dictated by its crystal structure and so its classification is based on symmetry element of crystal. The seven crystal system can be classified into 32 point group according to symmetry (Appendix 7.5). The thirty-two point groups can be further classified into (a) crystals having a center of symmetry and (b) crystals that do not possess a center of symmetry. Crystals with a center of symmetry include the 11 point groups labeled as centrosymmetric. These point groups do not show polarity. The remaining 21 point groups do not have a center of symmetry (i.e. non-centrosymmetric) possesses one or more crystallographically unique directional axes. All non-centrosymmetric point groups, show piezoelectric effect along unique directional axes. The following classification, based on the symmetry of crystals, is useful in considering electronic ceramics.

2.1.1 Piezoelectric Ceramic

Crystals that lack center of symmetry of ion distribution are electrically polarized (i.e. they develop surface charges) when they are mechanically stressed. This is the definition of piezoelectricity. The most important piezoelectric ceramics are those that are also ferroelectric. This means that the ferroelectric (and therefore also piezoelectric) domains within a polycrystalline sample of material can be reoriented ("poled") under the influence of an external electric field, and the reorientation is permanent. Thus, polycrystalline piezoelectric transducers can be produced. One very important applications of piezoelectric ceramics transducers for the conversion of electrical energy into mechanical vibration, as in ultrasonic cleaners, ultrasound generators (imaging devices, detection devices) and for the conversion of mechanical vibration into electrical signals, as in ultrasonic sensors.

2.1.2 Pyroelectric Ceramic

Some of crystals that lack center of symmetry of ion distribution, (i.e. piezoelectric) can also spontaneously develop electric dipoles (polarize), with the degree of polarization dependent on temperature. This is called the pyroelectric effect, which was first discovered in tourmaline by Teophrast in 314 B.C. and so named by

Brewster in 1824 [8] The spontaneous polarization is given by the value of the dipole moment per unit volume or by the value of the charge per unit area on the surface perpendicular to the axis of spontaneous polarization. The axis of spontaneous polarization is usually along a given crystal axis. Although a crystal with polar axes (20 non-centrosymmetric point groups) shows the piezoelectric effect, it is not necessary for it to have a spontaneous polarization vector. It could be due to the canceling of the electric moments along the different polar axes to give a zero net polarization. Only crystals with a unique polar axis (10 out of 21 non-centrosymmetric point groups) show a spontaneous polarization P_s vector along this axis and its value depends on the temperature The pyroelectric effect can be described in terms of the pyroelectric coefficient π A small change in the temperature ΔT, in a crystal, in a gradual manner, leads to a change in the spontaneous polarization vector ΔP_s given by,

$$\Delta P_s = \pi \Delta T \qquad \text{---} \qquad (1)$$

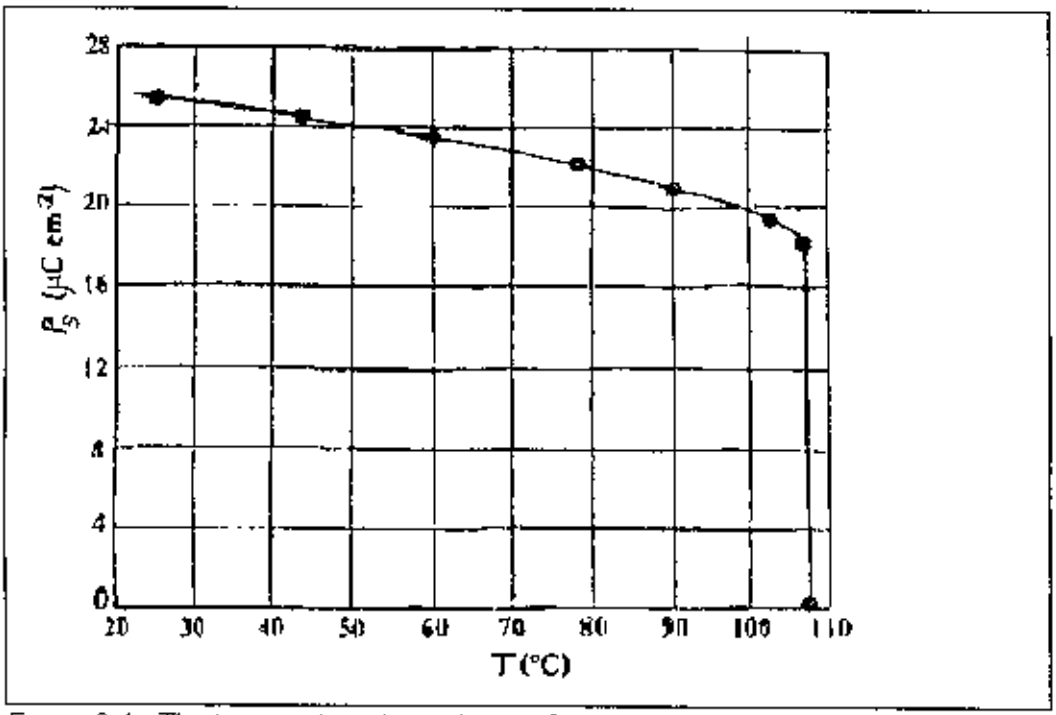

Figure 2-1 : The temperature dependence of spontaneous polarization Ps for $BaTiO_3$ ferroelectric crystal [13]

Figure 2-1 shows the variation of the P_s with temperature for a $BaTiO_3$ ferroelectric crystal. An increase in the temperature leads to a decrease in the spontaneous polarization $BaTiO_3$ has a negative pyroelectric coefficient.

The polarization suddenly falls to zero on heating the crystal above T_c [13]

2.1.3 Ferroelectric ceramics

A subgroup of pyroelectrics has an unusual property of spontaneous alignment of the electric dipoles within domains (~1μm) and the polarization direction can change under the influence of an electric field. This is the definition of ferroelectricity. The spontaneous alignment of electric dipoles (in a pyroelectric material) by their mutual interaction results in the high dielectric constant and P-E_e hysteresis loop. All ferroelectrics are pyroelectrics and piezoelectric, but not vice versa. For example, tourmaline shows pyroelectricity but is not ferroelectric. The alignment of electric dipoles is opposed by thermal vibrations and at the Curie temperature T_c the alignment disappears. For $T > T_c$, Curie-Weiss law holds:

$$\chi = \frac{P}{(\varepsilon.E)} = \frac{\varepsilon}{\varepsilon_o} - 1 = \kappa' - 1 = \frac{3T_c}{(T - T_c)} \qquad \text{---} \qquad (2)$$

χ represent the electrical susceptibility, P represents polarization, E electric field, ϵ and ϵ_0 permittivity of material and vacuum respectively and k' represents dielectric constant.

The classic example of a ferroelectric ceramic is $BaTiO_3$. A relatively small Ti^{4+} ion is located in a large octahedral site, with some room for free movement. The rattling Ti hypothesis suggests that there are minimum energy positions for Ti off center, by less than 0.01 nm, giving an electric dipole in each unit cell.

Because of spontaneous alignment of the dipoles, the dielectric constant ($k' = \varepsilon/\varepsilon_0$) for barium titanate exceeds 2000 at room temperature. The largest dielectric constant is achieved when critical temperature is approached, at $T = T_c = 125°C$, $k' = 12{,}000$. However, structural modifications of the classic $BaTiO_3$ are required if variations in dielectric constant vs temperature and polarization voltage are of concern.

2.1.3.1 Ferroelectric Domains

Ferroelectric crystals possess regions with uniform polarization called ferroelectric domains. Within a domain, all the electric dipoles or the polar axis transformation occur and spontaneous polarization takes place. The electrical stray field energy caused by the non-compensated polarization charges is reduced by the formation of ferroelectric domains as shown in Figure 2-2. The configuration of the

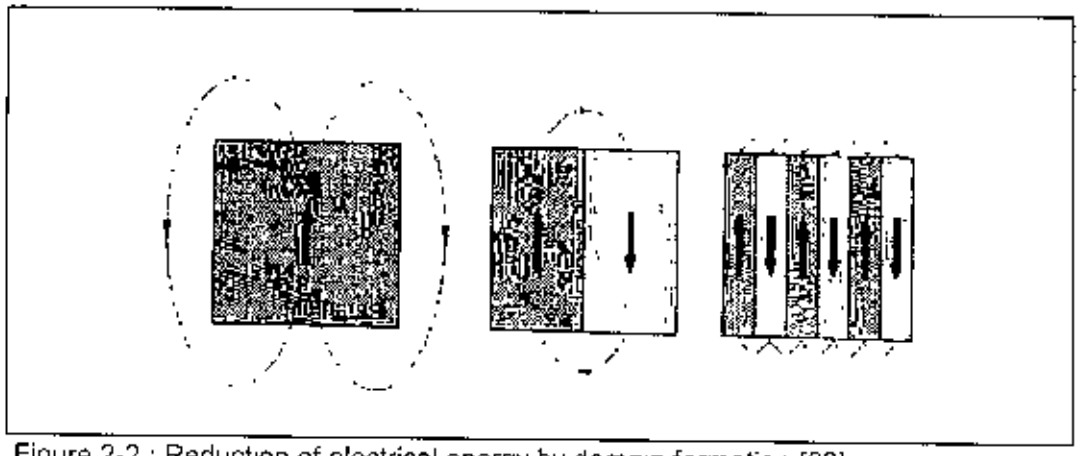

Figure 2-2 : Reduction of electrical energy by domain formation [03]

domains follows a head-to-tail condition in order to avoid discontinuities in the polarization at the domain boundary

In cubic crystals the polarization may be orientated in any of the six pseudo cubic <001> directions. Therefore, the polar axis may be aligned orthogonally (90° domains) and anti-parallel (180° domains) with respect to each other (Figure 2-3)

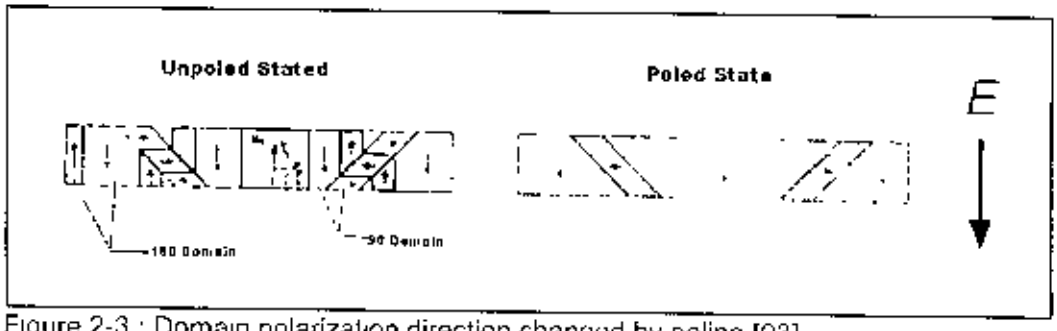

Figure 2-3 : Domain polarization direction changed by poling [03]

A single domain can be obtained by domain wall motion made possible by the process called poling. An appropriate electric field is applied to the sample at a temperature slightly below the Tc. Overall performance of the ferroelectric material greatly influenced by the nature of domain and its movement. Many research are on going to characterize the domain and its activities. The 180° domains are easily removed by polling as illustrated in Figure 2-3. The 90° domains are difficult to remove because the surface strain generated during cooling and the crystal fabrication restrict the motion of the domain. Mechanical force is used by many [14] to pole 90° domain and recently Chen [15] described a new technique. There may be many domains in a crystal separated by interfaces called domain walls. These walls have a thickness of only 100nm or less [16]. Muller [17] described a new laser technology that provides information about domain structure, their nucleation, and their dynamics

Atomic force microscopy [18] and TEM [19] was used to characterize domain. A very strong field could lead to the reversal of the polarization in the domain, known as domain switching [20]. Domains can be observed under the optical microscope and in SFM after the polished sample being etched with concentrated HCl [22] The relationships between etch pattern and the domain orientation in $BaTiO_3$ crystal in tetragonal state had been described by Hooton [21]. During etching processing the positive ends of the electric dipoles etch rapidly, forming a rough surface, the negative ends etch slowly, forming smooth surface and the sides (dipoles parallel to the surface) etch at an intermediate rate, forming a semi smooth surface.

The built-up of domain wall, elastic stress fields as well as free charge carriers counteracts the process of domain formation. In addition, an influence of vacancies, dislocations and dopants exits [23].

2.1.3.2 Ferroelectric Hysteresis Loop

The main difference between pyroelectric and ferroelectric materials is that

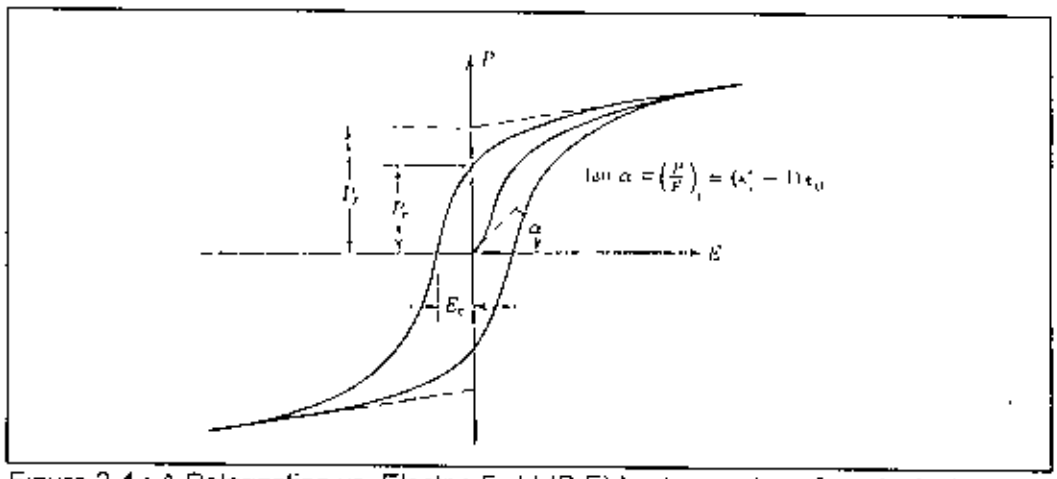

Figure 2-4 : A Polarization vs Electric Field (P-E) hysteresis loop for a typical ferroelectric crystal [9]

the direction of the spontaneous polarization in ferroelectrics can be switched by an applied electric field. The polarization reversal can be observed by measuring the ferroelectric hysteresis (analogous to ferromagnetic behavior) as shown in Fig. 2-4. As the electric field strength is increased, the domains start to align in the positive direction giving rise to a rapid increase in the polarization. At very high field levels, the polarization reaches a saturation value (P_{sat}). The polarization does not fall to zero when the external field is removed. At zero external field, some of the domains remain aligned in the positive direction, hence the crystal will show a remnant polarization P_r.

The crystal cannot be completely depolarized until a field of magnitude is applied in the negative direction. The external field needed to reduce the polarization to zero is called the coercive field strength E_c. If the field is increased to a more negative value, the direction of polarization flips and hence a hysteresis loop is obtained. The value of the spontaneous polarization Ps is obtained by extrapolating the curve onto the polarization axes.

The ferroelectric hysteresis originates from the existence of irreversible polarization processes by polarization reversals of a single ferroelectric lattice cell. However, the exact interplay between this fundamental process, domain walls, defects and the overall appearance of the ferroelectric hysteresis is still not precisely known The separation of the total polarization into reversible and irreversible contributions might facilitate the understanding of ferroelectric polarization mechanisms. Especially, the irreversible processes would be important for ferroelectric memory devices, since the reversible processes cannot be used to store information. For ferroelectrics, mainly two possible mechanisms for irreversible processes exist. First, lattice defects which interact with a domain wall and hinder it from returning into its initial position after removing the electric field that initiated the domain wall motion ("pinning"). Second, the nucleation and growth of new domains that do not disappear after the field is removed. In ferroelectric materials, the matter is further complicated by defect dipoles and free charges that contribute to the measured polarization and can also interact with domain walls [17].

Reversible ferroelectrics are the basic requisite of dielectric materials for application such as capacitors. Reversible contributions in ferroelectrics are due to ionic and electronic displacements and to domain wall motions with a small amplitude. These mechanisms are very fast The reorientation of dipoles and/or defect or free charges also contributes to the total polarization These mechanisms are usually much slower, but they also might be reversible (relaxation)

Remanent polarization and coercive voltage are of critical importance to the design of external circuits of FeRAMs or DRAMs

2.1.3.3 Curie Point and Phase Transitions

All ferroelectric materials have a transition temperature called the Curie point (Tc) At a temperature T > Tc the crystal does not exhibit ferroelectricity, below Tc it

is ferroelectric. On decreasing the temperature through the Curie point, a ferroelectric crystal undergoes a phase transition from a non-ferroelectric phase to a ferroelectric phase. If there are more than one ferroelectric phases, the temperature at which the

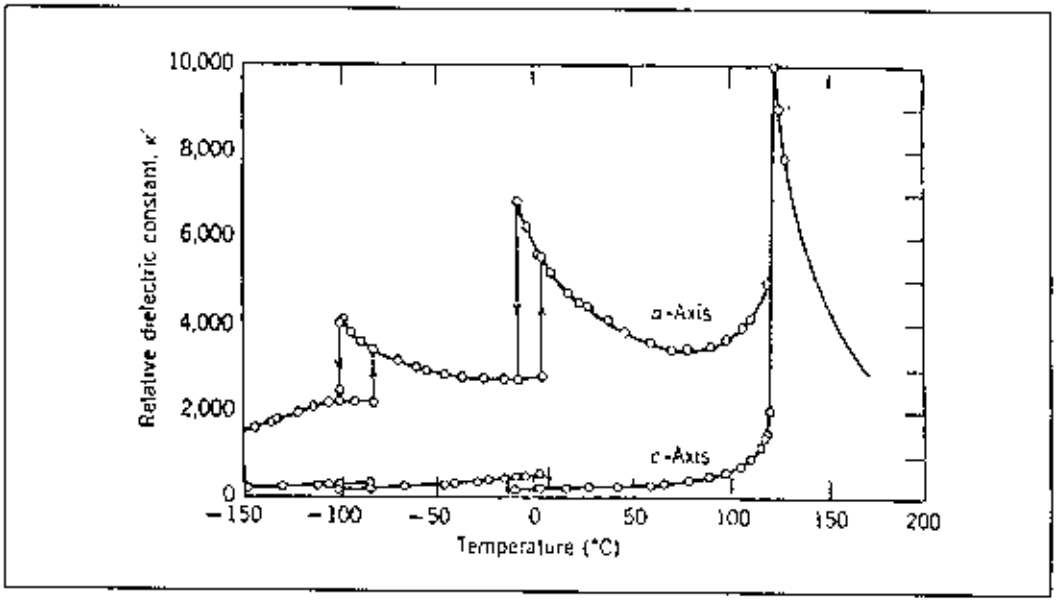

Figure 2-5 : Variation of dielectric constants (a and c axis) with temperature for $BaTiO_3$. [12]

crystal transforms from one ferroelectric phase to another is called the transition temperature.

The phase transition in $BaTiO_3$ is of first order, and as a result, there is a discontinuity in the polarization, lattice constant, and many other properties, as becomes clear in Figure 2-6. It is also clear in the figure that there are three phase transitions in barium titanate having the following sequence upon heating: rhombohedral, orthorhombic, tetragonal and cubic. There is a small thermal hysteresis of the transition temperature, which depends on many parameters such as the rate of temperature change, mechanical stresses or crystal imperfections.

From a crystal chemical view, the Ba-O framework evokes an interstitial for the central Ti^{4+} ion which is larger than the actual size of the Ti^{4+} ion. As a result, the series of phase transformations takes place to reduce the Ti cavity size. Certainly, the radii of the ions involved impact the propensity for forming ferroelectric phases; thus both $PbTiO_3$ and $BaTiO_3$ have ferroelectric phases, while $CaTiO_3$ and $SrTiO_3$ do not [24]. Early research works on ferroelectric transitions have been summarized by Nettleton [25, 26]. Figure 2.6 shows the variation of the relative permittivity ϵ_r with temperature as a $BaTiO_3$ crystal is cooled from its paraelectric cubic phase to the

ferroelectric tetragonal, orthorhombic, and rhombohedral phases. Near the Curie point or transition temperatures, thermodynamic properties including dielectric, elastic,

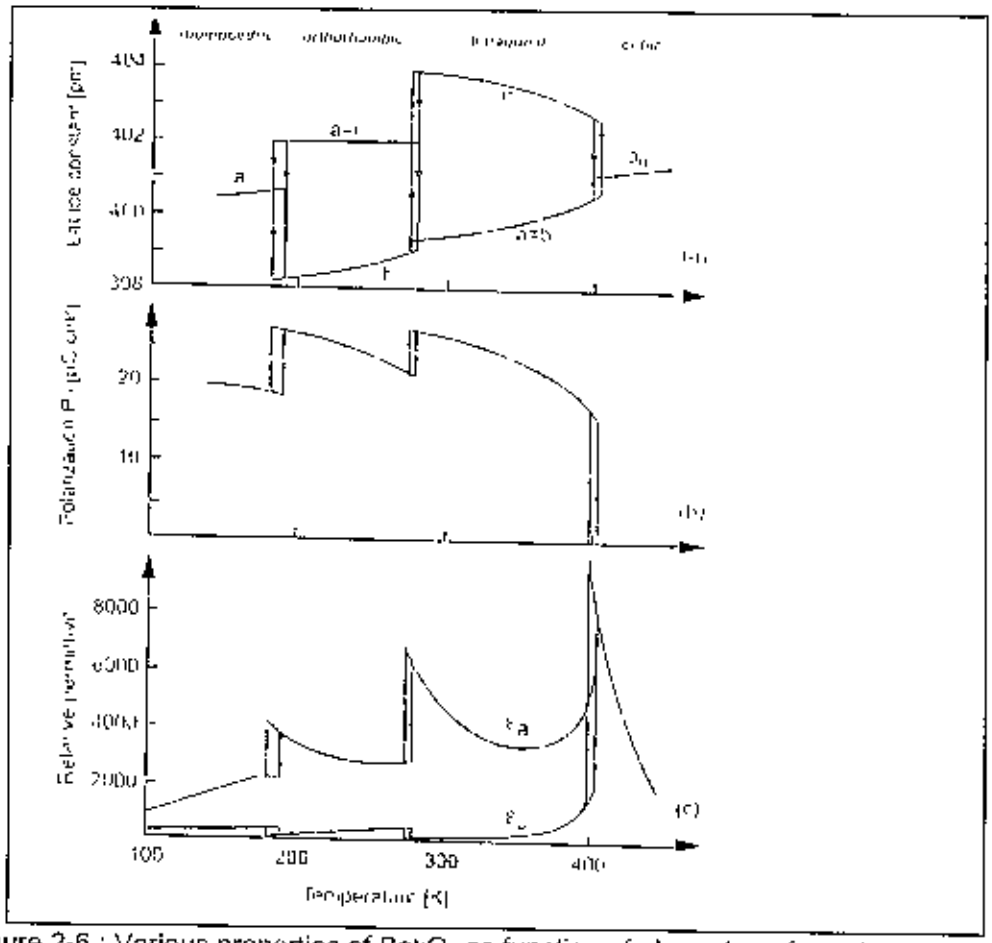

Figure 2-6 : Various properties of $BaTiO_3$ as function of phase transformation

optical, and thermal constants show an anomalous behavior. This is due to a distortion in the crystal as the phase structure changes. The temperature dependence of the dielectric constant above the Curie point ($T > T_c$) in ferroelectric crystals is governed by the Curie-Weiss law mentioned in section 2.1.3

2.1.3.4 Type of Ferroelectric materials

Ferroelectric materials can be grouped according to their structure, into four main types. These are the corner sharing oxygen octahedra, compounds containing hydrogen bonded radicals, organic polymers and ceramic polymer composites. Corner sharing octahedra can be classified into Perovskites (ABO_3), tungsten bronze type compounds (K_xWO_3, x<1, such as $PbNb_2O_6$), Bismuth oxide layer structured (such as $Bi_4Ti_3O_{12}$) and Lithium Niobate & Tantalate. Hydrogen bonded ferroelectric usually water soluble made in single crystal. Rochelle salt ($NaKC_4H_4O_6$, $4H_2O$) is one

example of this type and this was the first ferroelectric material discovered. These are now gradually replaced by ceramic ferroelectrics. Interesting type of ferroelectric material are organic polymers for medical applications. These piezo-polymers have some properties, which make them better suited for use in medical imaging applications. The density of these polymers is very close to that of water and the human body tissues, hence there is no acoustic impedance mismatch with the body. Polyvinylidene fluoride (PVDF, $(CH_2\text{-}CF_2)_n$) and copolymers of PVDF with trifluoroethylene {P(VDF-TrFE)} have found applications as piezoelectric and pyroelectric materials. The drive for piezoelectric composites stems from the fact that desirable properties could not be obtained from single phase materials such as piezoceramics or piezopolymers. Piezoelectric composites are made up of an active ceramic phase embedded in a passive polymer. The properties of the composite depend on the connectivity of the phases, volume percent of ceramic, and the spatial distribution of the active phase in the composite. The concept of connectivity developed by Newnham et al. [27] describes the arrangement of the component phases within a composite.

2.1.3.5 Corner Sharing Octahedra and Perovskite

A large class of ferroelectric crystals are made up of mixed oxides containing corner sharing octahedra of O^{2-} ions schematically shown in Figure 2-7. Inside each octahedron is a cation B^{b+} where 'b' varies from 3 to 6. The spaces between the octahedra are occupied by A^{a+} ions where 'a' varies from 1 to 3. In prototype forms, the geometric centers of the A^{a+}, B^{b+} and O^{2-} ions coincide, giving rise to a non-polar lattice. When polarized, the A and B ions are displaced from their geometric centers with respect to the O^{2-} ions, to give a net polarity to the lattice. These displacements occur due to the changes in the lattice structure when phase transitions take place as the temperature is changed. The formation of dipoles by the displacement of ions will not lead to spontaneous polarization if a compensation pattern of dipoles are formed which give zero net dipole moment.

Perovskite is a family name of a group of materials and the mineral name of calcium titanate ($CaTiO_3$) having a structure of the type ABO_3. A wide variety of cations can be incorporated into perovskite structure as long as they obey the relationship: $t = (R_A + R_B)/\sqrt{2}(R_B + R_O)$

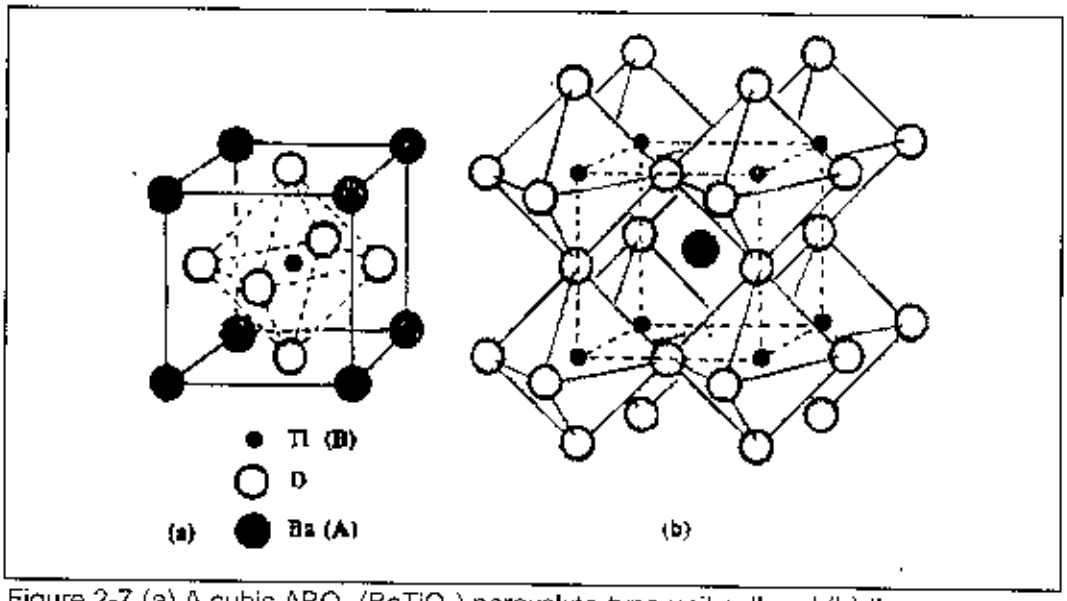

Figure 2-7 (a) A cubic ABO_3 ($BaTiO_3$) perovskite-type unit cell and (b) three dimensional network of corner sharing octahedra of O_2- ions [12].

For an ideal perovskite structure t = 1, and R_A, R_B and R_O the ionic radius of large cation, small cation and oxygen [28] The structure takes cubic from with the t value between 0.95 to 1.0; lower thus slightly distorted cubic but not ferroelectric but slightly above 1.0 tends to be ferroelectric [29].

Many piezoelectric (including ferroelectric) ceramics such as Barium Titanate ($BaTiO_3$), Lead Titanate ($PbTiO_3$), Lead Zirconate Titanate (PZT), Lead Lanthanum Zirconate Titanate (PLZT), Lead Magnesium Niobate (PMN), Potassium Niobate ($KNbO_3$), Potassium Sodium Niobate ($K_xNa_{1-x}NbO_3$), and Potassium Tantalate Niobate ($K(Ta_xNb_{1-x})O_3$) have a perovskite type structure.

2.2 Electrical Properties

Ceramics are mostly covalently bonded material hence electrically non-conductive or insulator. Importance of particular property depends on the application demand. For instance, dielectric strength is an important parameter for application of ceramic as insulators used in power transmission line, load bearing general insulators, in house hold appliances, etc. In this kind of applications where frequency do not exceed 1kHz, the breakdown strength, measured in kV/cm, and mechanical strength are prime important factors. The dielectric constant (k') or loss factor (k") does not matter much. On the other hand, for capacitor and electronics applications just the opposite required. The values of k' and k" are of prime importance, not only their room temperature values but also as function of temperature and frequency. These are

intrinsic properties of material, can be modified by doping, micro structural variation, etc. $BaTiO_3$ is used extensively as a principal ingredient for multi layer ceramic capacitor (MLCC) manufactured commercially in billions. In the following sections basic concept and factors governing dielectric constant, dielectric losses are discussed. Materials are treated as polycrystalline and linear dielectric.

2.2.1 Dielectric constant

The overall Dielectric constant (k') of an insulator material is given by the relation:

$$D = \varepsilon E = \varepsilon_o \kappa' E \qquad \text{--- ---} \qquad \{2\}$$

D represents the electric displacement, E the electric field in the dielectric, k' the dielectric constant and ε_o permittivity of vacuum. The electric displacement describes the extent to which the electric field has been altered by the presence of the dielectric material. The dielectric constant k' is an intrinsic property of a material and a measure of the ability of the material to store electric charge relative to vacuum. It is measured indirectly from the capacitance of a capacitor in which the material is used as electrode separator or dielectric. From eq {2} and the capacitive cell illustrated in Figure 2-8 the dielectric constant k', total charge Q (coulombs) and capacitance C (farads) can be developed as follows:

$$\kappa' = \frac{D}{\varepsilon_o E} = \frac{Q/A}{\varepsilon_o V/d} \qquad \text{--- ---} \qquad \{3\}$$

Therefore, $$Q = \varepsilon_o \kappa' \frac{A}{d} V = CV \qquad \text{--- ---} \qquad \{4\}$$

Where, $$C = \varepsilon_o \kappa' \frac{A}{d} \qquad \text{--- ---} \qquad \{5\}$$

$$C_o = \varepsilon_o \frac{A}{d} \qquad \text{--- ---} \qquad \{6\}$$

and $$\kappa' = \frac{C}{C_o} = \frac{\varepsilon}{\varepsilon_o} \qquad \text{--- ---} \qquad \{7\}$$

Here, A represents the area of the capacitive cell, d its thickness (or gap

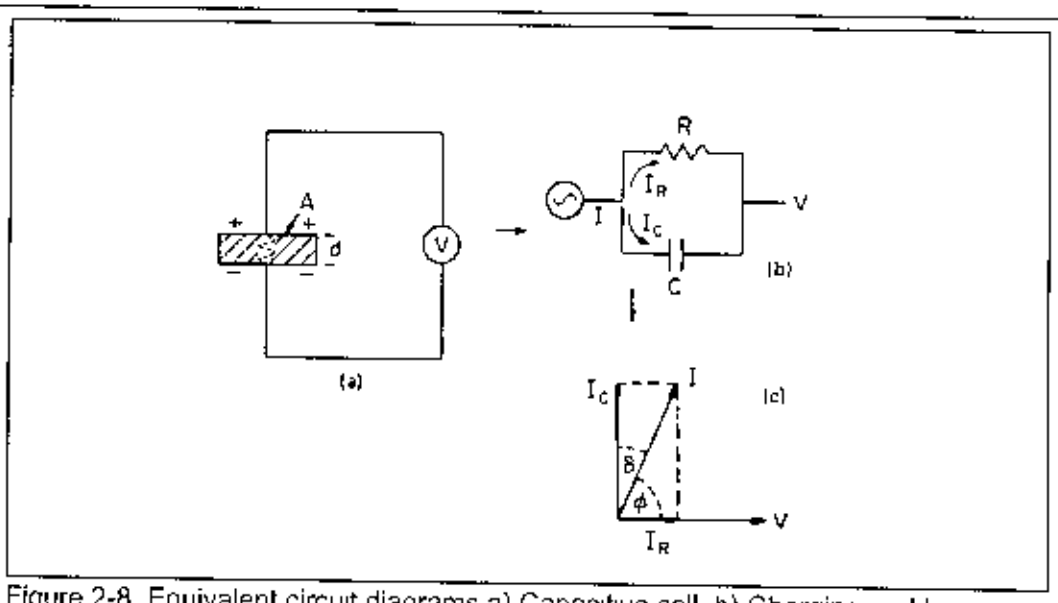

Figure 2-8 Equivalent circuit diagrams a) Capacitive cell, b) Charging and loss current c) loss tangent

between the electrodes), Co and C the respective capacitance of the capacitor with air and material, V the voltage across the cell and ϵ the material permittivity (F/m). Thus k' represents the ratio of the permittivity or charge storage capacity relative to air or vacuum as dielectric. It is clear from eq. {5} that for a given size capacitor and applied voltage the higher the k' the higher the capacitance of the capacitor. This is the only variable left with the material scientist to increase the capacitance per unit volume value of capacitor for modern electronics applications.

2.2.2 Dielectric Loss

An ideal dielectric would allow no flow of electronic charge, only a displacement of charge via polarization. If a plate of such ideal material were placed between the capacitive cell shown in Figure 2-9 (a) and a dc voltage was applied, the current through the circuit would decay exponentially to zero with time. But this would not be case if an alternating (sine wave) electric field was applied. In this case the eq. {4} may be written as

$$Q = CV_o e^{i\omega t} \qquad \text{--- ---} \qquad \{8\}$$

Therefore,

$$I = \frac{dQ}{dt} = i\omega CV = i\omega C_o \varepsilon_o \kappa' V \qquad \text{---} \qquad \{9\}$$

here, I represents the current flow on discharge of the capacitor in time t. For real dielectric material, the current I has two vector components, real I_R and imaginary I_C. The condition of a lossy (not so good) dielectric illustrated in Figure 2-9 (c) as an

equivalent circuit analogous of a resistance in parallel with the capacitor. The current I_C represents a (watt less) capacitive current proportional to the charge stored in the capacitor. It is frequency dependent and leads the voltage by 90°. On the other hand the current I_R is an ac conduction current in phase with the voltage V, which represents the energy loss or power dissipated in the dielectric. The resultant angle between the current and the voltage is ϕ somewhat less than 90°. Ideal dielectric under this circumstance would not absorb any power and the capacitor would have zero loss. The current would lead the voltage exactly 90°. The current in real capacitor lags slightly behind what it would be in an ideal capacitor. The angle of lag is defined as δ and the amount of lag becomes tan δ or loss tangent

Eq. {9} can be written for real and imaginary part,

$$I = I_C + I_R \qquad \text{--- ---} \qquad \{10\}$$

$$= i\omega C_o \varepsilon_o \kappa' V + \omega C_o \varepsilon_o \kappa'' V \qquad \text{---} \qquad \{11\}$$

By definition, $$\tan\delta = \left|\frac{I_R}{I_C}\right| = \frac{\kappa''}{\kappa'} \qquad \text{--- ---} \qquad \{12\}$$

Dielectric loss often attributed to ion migration, ion vibration & deformation and electronic polarization. Ion migration is particularly important and strongly affected by temperature and frequency. The losses due to ion migration increase at low frequency and the temperature increases.

2.2.3 Material Aspect

Intrinsic properties such as k' and k" can be explained in terms of chemical composition and structure. Material behavior in a dielectric field is a direct result of three vector quantities a) dielectric displacement D, b) electric field E, and c) polarization P.

$$D = \varepsilon_o \kappa' E = \varepsilon_o E + P \qquad \text{--- ---} \qquad \{13\}$$

Affect of dielectric in capacitor illustrated in Figure 2-9. The contribution of vacuum is the term $\varepsilon_o E$ and is the electrical polarization contribution of the dielectric.

Therefore, $$P = \varepsilon_o(\kappa'-1)E = \varepsilon_o \chi E \qquad \text{--- ---} \qquad \{14\}$$

It is clear from eq. {1} and {14} polarization is the key factor attributing to the dielectric property of material. For ceramic material, polarization can be further

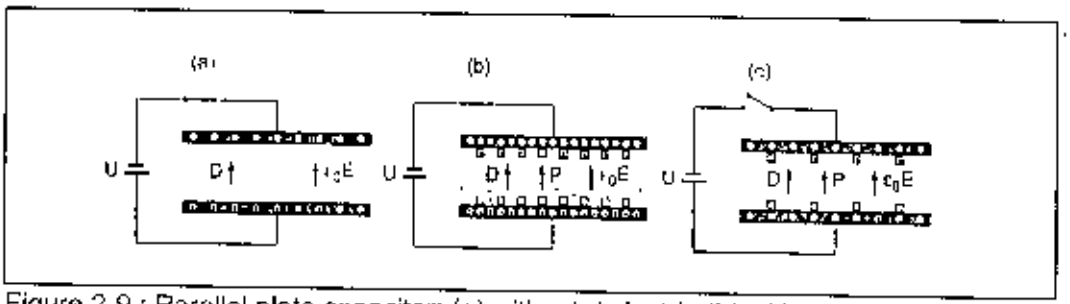

Figure 2-9 : Parallel plate capacitor: (a) without dielectric (b) with dielectric E constant (c) with dielectric with D constant

described in terms of a volume charge density related to the concentration of dipole per unit volume N and the local field E' in the dielectric:

$$P = \alpha N E' \qquad \text{--- ---} \qquad \{15\}$$

and

$$E' = \frac{\varepsilon_r + 2}{3} E \qquad \text{--- ---} \qquad \{16\}$$

where, α represents the polarizability, arising from different polarization mechanism of the material.

$$\alpha = \alpha_e + \alpha_i + \alpha_a + \alpha_s \qquad \text{--- ---} \qquad \{17\}$$

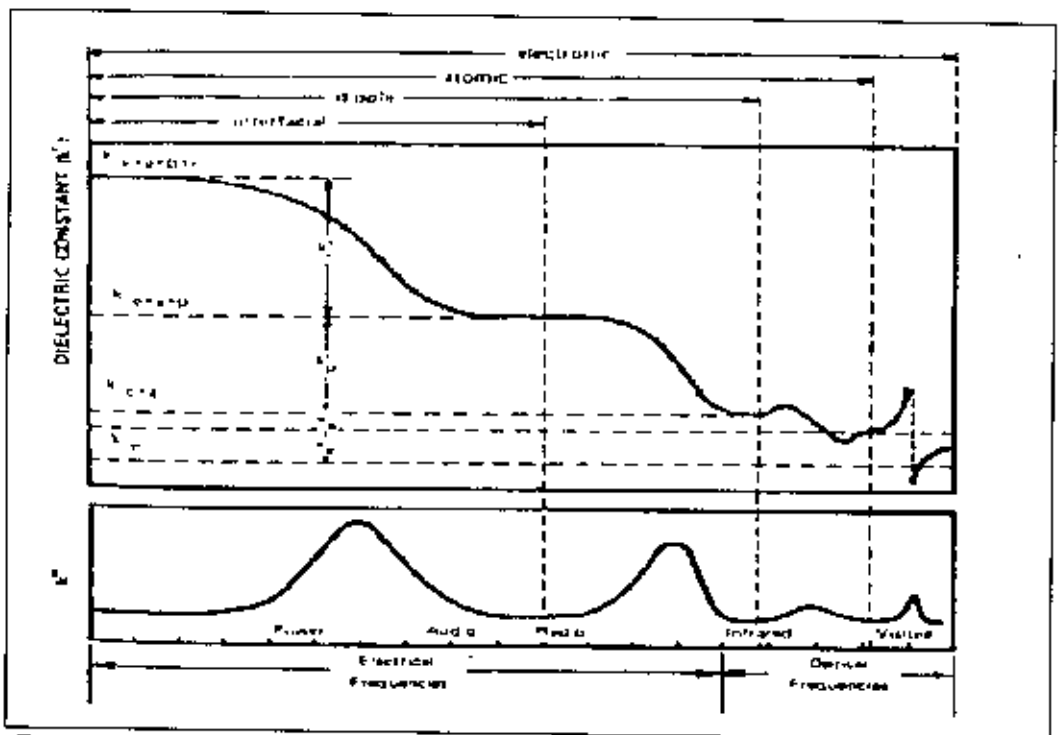

Figure 2-10 : Frequency dispersion behavior of dielectric material as function of frequency

representing the susceptibility associated with electronic, ionic, orientational and space charge polarization, respectively. Mechanism of polarization described in the following section

For cubic structures and for induced dipoles (ionic and electronic polarization), the calculation reveals a relation between the atomic polarizability α and the macroscopic permittivity $\epsilon = \epsilon_0 \epsilon_r$ which is referred to the Clausius-Mossotti equation [30].

$$\varepsilon = \frac{\varepsilon_o + 2N\alpha}{\varepsilon_o - N\alpha} \qquad \text{--- ---} \qquad \{18\}$$

In Figure 2-10, the frequency dependence of k' and associated polarization mechanism are illustrated. Affect of different polarization mechanism to the overall dielectric constant is related to the composition, frequency and temperature of the dielectric material. In general, α_e increases with ion concentration, ion size and ion polarizability, hence ions like Ba^{2+}, Pb^{2+}, La^{3+} are used in order to achieve a higher dielectric constant and refractive index. In ionic solids (such as MgO, Al_2O_3) α_i is the predominant polarization mechanism, where ion size and separation have the significant effect. For ceramic materials with mobile ion, the orientational polarization can be a factor. This can be attributed to ion jump polarization α_j, where

$$\alpha_e = \frac{p^2}{3kT} \qquad \text{and} \qquad \alpha_j = \frac{(eZd)^2}{3kT} \qquad \text{---} \qquad \{19\}$$

$p = eZd$, represents the dipole moment associated with the jump of an ion of charge eZ through a distance d. The relaxation time τ and the number of successful ion jumps per second are given in Arhenius form

$$\tau = \tau_0 e^{\mu/kT} \qquad \text{and} \qquad n = n_0 e^{-\mu/kT} \qquad \text{--- ---} \qquad \{20\}$$

here, μ is the activation energy, k Boltzman constant and T absolute temperature. In other word, for ceramic τ decreases with temperature, the relaxation move to higher temperature with increasing frequency and n increases with the temperature. Hence it is normally observed that at a given frequency k' increases with the temperature and at a given temperature k' decreases as frequency increased.

2.2.4 Mechanism of Polarization

In general, there are five different mechanisms of polarization which can contribute to the dielectric response [31].

• Electronic polarization exists in all dielectrics. It is based on the displacement of the negatively charged electron shell against the positively charged core. The electronic polarizability α_e is approximately proportional to the volume of the electron shell. Thus, in general α_e is temperature-independent, and large atoms have a large electronic polarizability.

• Ionic polarization is observed in ionic crystals and describes the displacement of the positive and negative sublattices under an applied electric field.

• Orientation polarization describes the alignment of permanent dipoles. At ambient temperatures, usually all dipole moments have statistical distribution of their directions. An electric field generates a preferred direction for the dipoles, while the thermal movement of the atoms perturbs the alignment. The average degree of orientation is given by the Langevin function $\langle \alpha_o \rangle = p^2/(3k\,T)$ where k denotes the Boltzmann constant and T the absolute temperature.

• Space charge polarization could exist in dielectric materials which show spatial inhomogeneities of charge carrier densities. Space charge polarization effects are not only of importance in semiconductor field-effect devices, they also occur in ceramics with electrically conducting grains and insulating grain boundaries (so-called Maxwell-Wagner polarization).

• Domain wall polarization plays a decisive role in ferroelectric materials and contributes to the overall dielectric response. The motion of a domain wall that separates regions of different oriented polarization takes place by the fact that favored oriented domains with respect to the applied field tends to grow

2.3 Processing of Barium Titanate ceramic

Property of the final product depends on the processing from raw material to the final sintering. Every step in the process chain has its own influence on the

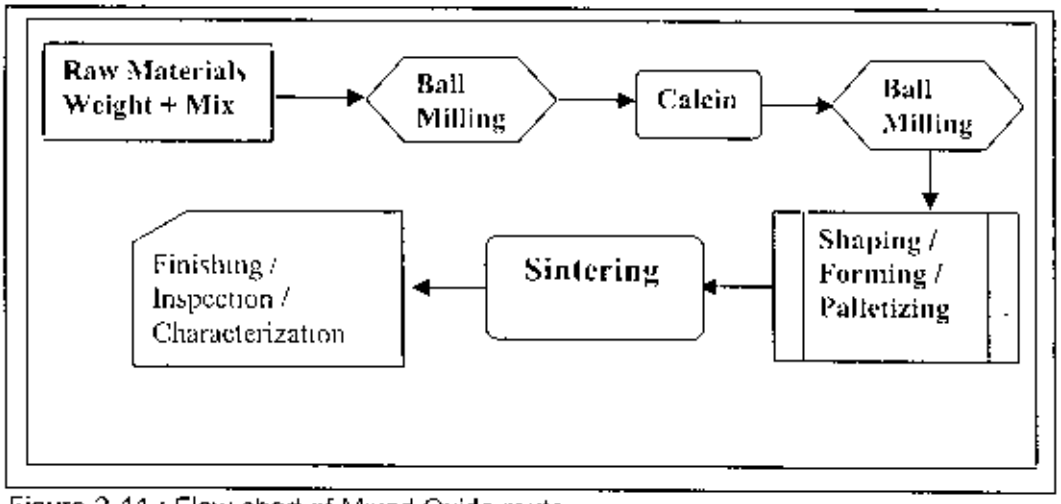

Figure 2-11 : Flow chart of Mixed Oxide route

successive step and the final product. Many methods are used to syntheses $BaTiO_3$, a) conventional mixed oxide, b) sol-gel, c) chemical precipitation, d) hydrothermal and e) combustion reaction. Choice of route depends on the application. Nanopowders are prepared using the electrophoretic (EPD) method for making films. Even thin film was prepared from bulk single crystal using ion slicing method [31]. Ultra fine $BaTiO_3$ powder obtained by combustion reaction are used to make bulk material was described as relatively efficient method [32]. By far the first method is widely in the industrial application as well as at laboratories. However, powder obtained in other routes is superior in terms of homogeneity and fineness. This method also known as solid-state method, was used to prepare sample in this study.

Processing route of this method illustrated in Figure 2-11. In the following sections important steps are discussed briefly with their influence on dielectric property of $BaTiO_3$ ceramics. The raw materials $BaCO_3$ and TiO_2 (rutile or anatase) are first weighed according to the stoichiometric formula. The raw materials should be of high purity.

2.3.1 Ball Milling

The weighted powders are mixed mechanically by either ball milling or attrition milling. Milling is carried out to reduce the particle size of the powders to the micron range for the ease of solid phase reactions to occur by atomic diffusion.

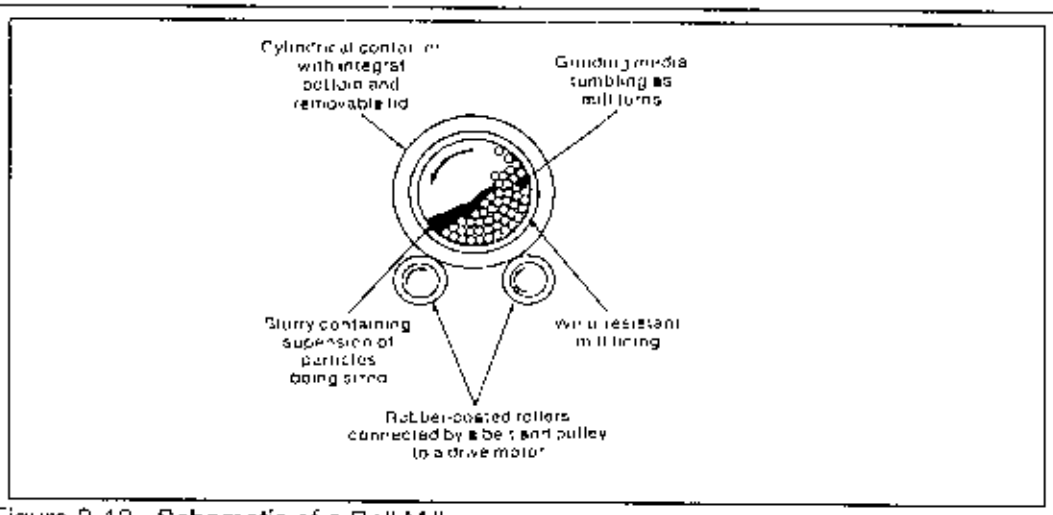

Figure 2-12 . Schematic of a Ball Mill

The schematic of a ball mill is illustrated in Figure 2-12. Size and distribution of the ball is an import factor determining the product quality. Particle size is reduced by the action of impact and friction of balls with the powder. Thumb rule is, smaller the size of balls finer the particle but it take longer time to break down big particles, hence use mix of different size balls Motion of ball is controlled by the rotation speed of the mill At higher speed balls cling at the inner side of the mill due to centrifugal force. too low speed would set the balls almost stationary at the bottom. In both case insufficient friction between balls and particle would not break down the particle. Optimum speed is achieved when balls are in circular motion and roll back to bottom from about three quarter way to the top as shown in Figure 2-12.

Media is another important consideration for two reasons. It must not react with the ball, the container, or the powder. Secondly, must avoid decrease of colloidal stability For instance, milling of $BaTiO_3$ in water media set of tribochemical reaction The reaction forms strongly alkaline $Ba(OH)_2$ which upset the pH balance, decreasing the colloidal stability of the suspension [33]. Either non-polar liquid such as acetone, alcohol, is used or polyelectrolyte stabilizers are used with water Usually the same set up is used for milling the calcined powder. Finer particle can lower the sintering temperature and firing time significantly. Extent of ball milling is usually assessed by particle size analysis.

2.3.2 Calcination

Chemically as well as ceramic point of view, this is an important step. Desired compound are formed and necessary reactions are accomplished During the

calcination step the mixed powder is exposed to high temperature at a specified atmosphere and time. The purposes of calcinations are:

a) To remove residual media form milling process

b) To remove water of hydration, carbon dioxide forming oxide, and any volatile impurities

c) To effect solid phase reaction between the constituents giving the desired phase or solid solution

d) The reaction would reduce the volume shrinkage in the final sintering.

The calcination of $BaTiO_3$, starting raw materials $BaCO_3$ and TiO_2 are mixed

$$BaCO_3 \rightarrow BaO + CO_2 \uparrow$$

$$BaO + TiO_2 = BaTiO_3$$

in the molar ratio of 1:1, ball milled, then calcined in ambient air at 1000°C to obtain the perovskite phase through the diffusion controlled reaction [34]. Degree of calcinations can be assessed by weight loss of CO_2 as a function of time and temperature using TGA. Under isothermal condition, the reaction obeys a parabolic time law. Newnham [24] has detailed the model of kinetic of solid state reaction between spherical particles. According to him, the reaction rate is inversely proportional to the square of the particle radius. Importance of milling before calcinations is realized and so is the fineness of the powder.

2.3.2.1 Formation of phases and Phase Diagram

$BaTiO_3$ formed during reaction above through formation number of intermediate phases. Templeton [35] detected the intermediate second phases Ba_2TiO_4, $BaTi_4O_9$ and $BaTi_3O_7$. The final conversion to monophase $BaTiO_3$ determined by decomposition of the intermediate phases, ie, the diffusion exchange between Ba and Ti rich region in the powder. The calcinations temperature and the amount of intermediate phases critically depends on the morphology and degree of mixing of the raw material. During ball milling this is an important point aimed to accomplish. According to Bauger [34], during this solid-solid reaction BaO act as the mobile agent. At the contact interface BaO is formed which diffuses into the TiO_2 forming as intermediate layer of Ba_2TiO_4, which slowly reacts with the residual TiO_2 to form

$BaTiO_3$. Hence, particle size is an important factor especially the size of TiO_2 as it determines the particle size of $BaTiO_3$.

The phase diagram of BaO-TiO_2 is shown in Figure 2-13. As per phase diagram stoichometric $BaTiO_3$ can accommodate little more TiO_2 with the compound. Formation of Ba_2TiO_4 is inhibited below 1100°C by the presence of a CO_2 atmosphere. This phase is particularly harmful, since it is hygroscopic and decomposed with swelling in slightly moist air. Incomplete mixing and reaction will yield small amounts of Ba_2TiO_4 and $BaTi_3O_7$ and other intermediate phases. The same kind of harmful phases may also occur when alkaline earth oxides, such as Ca, Sr used in substituted $BaTiO_3$ [36]. Effect of calcination temperature was studied by Maison *et al* [37] suggest at 700°C tetragonal $BaTiO_3$ do not form whereas at 1100°C it does at the expenses of particle agglomeration.

Dopent and other additives are added at this stage of processing. A great advantage of this method is that dopes and additives can be homogeneously incorporated into the perovskite lattice during calcinations [3]

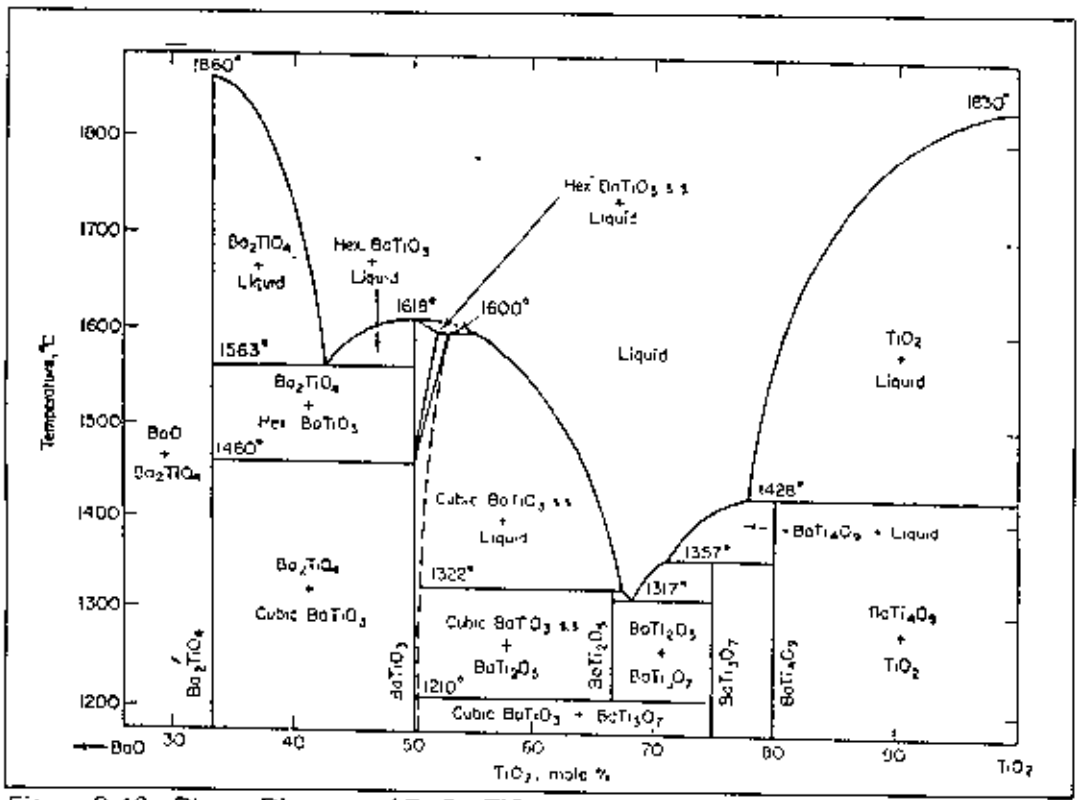

Figure 2-13 : Phase Diagram of BaO - TiO_2 system

The calcining temperature is important as it influences the density and hence the electromechanical properties of the final product. The higher the calcination temperature, the higher the homogeneity and density of the final ceramic product. Many calcination temperature and time scheme has been suggested. Higher temperature and longer time usually yield completely reacted powder but coarser particle size posing difficulties during subsequent milling. So, proper calcination at the right temperature is necessary to obtain the best electrical, mechanical properties and minimizing the presence of harmful phases.

2.3.2.2 Effect of particle size

Reaction kinetics greatly influenced by the fineness of the particle size. Henning *et al* [3] studies the effect of grain size of particle on the reaction during sintering and the final product using TGA. They concluded that the decomposition temperature of $BaCO_3$ in mixtures with TiO_2 is largely independent of the particle size of $BaCO_3$. However, the particle size of TiO_2 widely determines the grain size of $BaTiO_3$. This is in good agreement with diffusional solid state reaction suggested where BaO act as a mobile agent. Sub micron sized $BaCO_3$ however, strongly inhibits the formation of harmful phase Ba_2TiO_4. The Ba/Ti atomic ratio has a strong influence on the calcination temperature. Higher temperature required for Ba rich composition.

2.3.3 Shaping and drying

After calcining, the lumps are ground by milling as described previously. The milled powder ready for further processing is commonly referred at 'green' body. The green bodies should have a certain minimum density before they can be sintered. Common practice is to achieve 60% of the theoretical density during shaping and pre-sintered state. The desired shape and a minimum green density can be provided by various techniques including powder compaction, slip-casting, extrusion, doctor blading, dipping, etc. Hot pressing (both axial and isotactic), although expensive method, is becoming popular for better quality ceramic material used in high end application. The choice of the method depends on the type of powder used, particle size distribution, state of agglomeration, desired shape, and thickness of the part. Hydraulic or mechanical presses are used to press powder in to desired shape at the pressure of ~100 to 300MPa. Owing to the nature of this process, only simple and symmetric shape can be prepared. No sintering aid or liquid is added to the powder for

solid phase sintering route. Hence, strength of the green powder compact is achieved through addition of a suitable binder such as PVA, glycol phthalate, etc.

After shaping, the green bodies are heated very slowly to between 400-600°C in order to remove any binder present. Initial heating rate to burnout the binder is about ~1-2°C/min in order to allow the gases to come out slowly without forming cracks and blisters in the ceramic part. After the binder burnout is over, the samples are taken to a higher temperature for sintering to take place.

2.3.4 Sintering

In this step, powder so prepared finally transforms to usable ceramic body. In ceramic industries, this step is also known as firing. $BaTiO_3$ matures in the 1350°C to 1450°C range [11]. This is the most important processing step in making of ceramic material. All properties of ceramic depends on the sintered body which is the direct result of the sintering parameter such sintering temperature, hold time, atmosphere, thermal profile, etc. There are many sintering methods used but this discussion would be limited to solid phase method.

Heat causes the powder particles to develop inter granular bonds by surface diffusion and other physical driving force. Mechanism of sintering and allied topics detailed elsewhere [7]. The typical green density of ceramic body at the start is about 60% of TD. Strength starts to develop gradually as more and more particles bond. At about ~80% to 90% density the pores are still open and the ceramic has a typical "chalky" appearance. The dielectric constant is usually low and the T_c is not pronounced strongly. The pores of a ceramic are generally closed at ~95% of TD. Additional heat work causes grater densification as trapped gasses diffuse out along grain boundaries. At densities below 95% of TD the presence of open pores would cause the dielectric loss and undoubtedly inferior dielectric properties

Setting of sintering temperature is not that straight forward. Low temperature sintering results in ceramic of poor density and formation of Ba_2TiO_4. On the other hand, too high temperature and long hold time may cause open structure with low density [11]. Also, at high temperature grain growth is accelerated resulting in low dielectric properties. Another harmful hexagonal phase of $BaTiO_3$ may form at the temperature higher than 1460°C (Figure 2-10). The sintering temperature and time should be optimum for proper densification to occur without abnormal grain growth.

This is best done by trail and error for particular material, volume and other process parameters.

In MLC manufacturing industries, sintering high temperature such as 1300°C is not practicable, due to use of low melting point electrode material. Commercial formulation is aimed to lower temperature (~1100°C) sintering with the addition of many sintering and dopants, for instance X7R, Z5U, etc.

2.4 Dielectric Properties of $BaTiO_3$

Ferroelectric ceramics and dielectric behaviors were discussed in length in the previous sections. Ferroelectric nature of $BaTiO_3$, the mechanism of superior dielectric properties, factors affecting properties discussed in the following sections. Effect of doping specially doping effect of Ca, process variables such as ball milling practice, calcination thermal profiles, sintering temperature and hold time on the dielectric properties discussed.

2.4.1 Crystal Structure and Phase Transformation

Different phase transformations and cell dimensions of $BaTiO_3$ are illustrated in figure 2-14. $BaTiO_3$ has a paraelectric cubic phase above its Curie point of about 130°C. In the temperature range of 130°C to 0°C the ferroelectric tetragonal phase with a c/a ratio of ~1.01 is stable. The spontaneous polarization is along one of the [001]

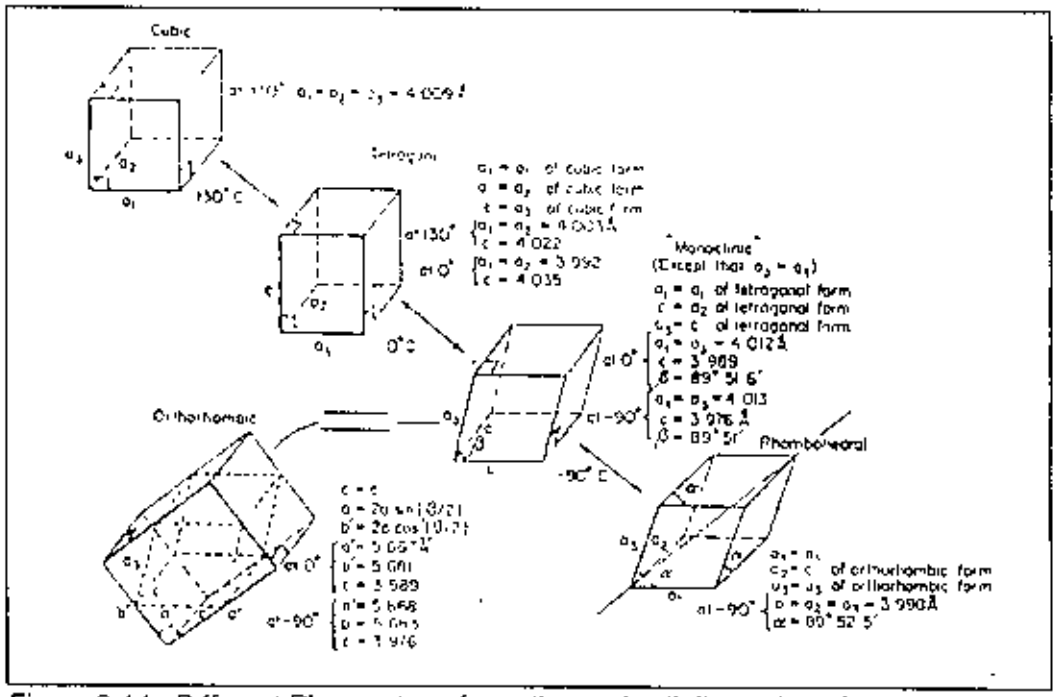

Figure 2-14 . Different Phases, transformation and cell dimension of $BaTiO_3$

directions in the original cubic structure. Between 0°C and -90°C, the ferroelectric orthorhombic phase is stable with the polarization along one of the [110] directions in the original cubic structure. On decreasing the temperature below -90°C the phase transition from the orthorhombic to ferroelectric rhombohedral phase leads to polarization along one of the [111] cubic directions

On cooling from high temperatures, the permittivity increases up to values well above 10,000 at the phase transition temperature T_c. The inverse susceptibility as well as the dielectric permittivity follows a Curie-Weiss law. The appearance of the spontaneous polarization is accompanied with a spontaneous (tetragonal) lattice distortion. The phase transition in barium titanate is of first order, and as a result, there is a discontinuity in the polarization, lattice constant, and many other properties, as becomes clear in Figure 2-6.

2.4.1.1 Significance of tetragonal phase

The phase of ferroelectric interest is the tetragonal existing between 130°C (T_c) to 0°C. The extent of tetragonality i.e c/a ratio can be calculated from XRD pattern. Separation of (002) and (200) peak is a good indication of formation of tetragonal $BaTiO_3$ as indicated in Figure 2-15 for sample calcined at 700°C, 900 °C and 1100 °C

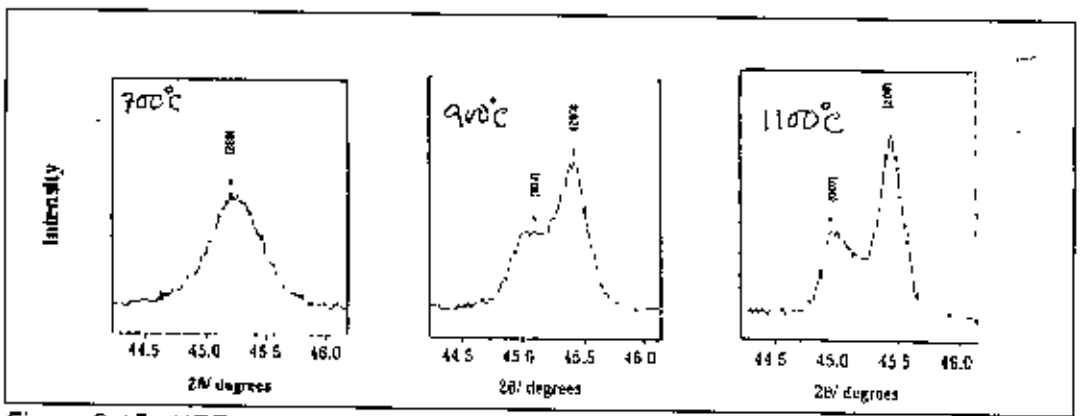

Figure 2-15 : XRD pattern showing separation of (002) and (200) peaks

[37]. The JCPDS file for tetragonal and cubic phase are 5-626 and 31-174 respectively. The lattice parameters are given as a_o=3.994Å and c_o=4.038Å for tetragonal phase and a_o=4.031Å for cubic phase. The c/a ratio was also increased from 1.0065 to 1.010 for calcination at 900 °C and 1100 °C respectively. Extreme anomalies of properties at T_c are associated with the extent of tetragonality of $BaTiO_3$ ceramic.

On the other hand, ferroelectric properties will diminish with the absence of tetragonal phase.

2.4.1.2 Factors influencing tetragonal phase

Apart from the calcination temperature of $BaTiO_3$ formation the other major factor is the Ba/Ti molar ratio. Lee [12] reported the extent of dielectric peak at Tc lowed as Ba/Ti ratio increased. Impurities such as Fe, Cr, Mn present also suppress tetragonal phase Curie point also suppressed in ultra fine-grained ceramic. Arlt el al [11] shown the dependence of lattice constants (c/a - 1)% of tetragonal $BaTiO_3$ ceramic on average grain size as illustrated in Figure 2-16. With the change of grain size different ferroelectric phases coexist at room temperature.

At gain size above 1μm normal tetragonal XRD reflection occur for (004) and (400) planes. As the grain size is reduced to 0.84μm these peaks shift closer and a third pseudo cubic reflection of (040) appear within. This pseudo cubic phase most probably ascribed to the orthorhombic phase, that exits below 10°C

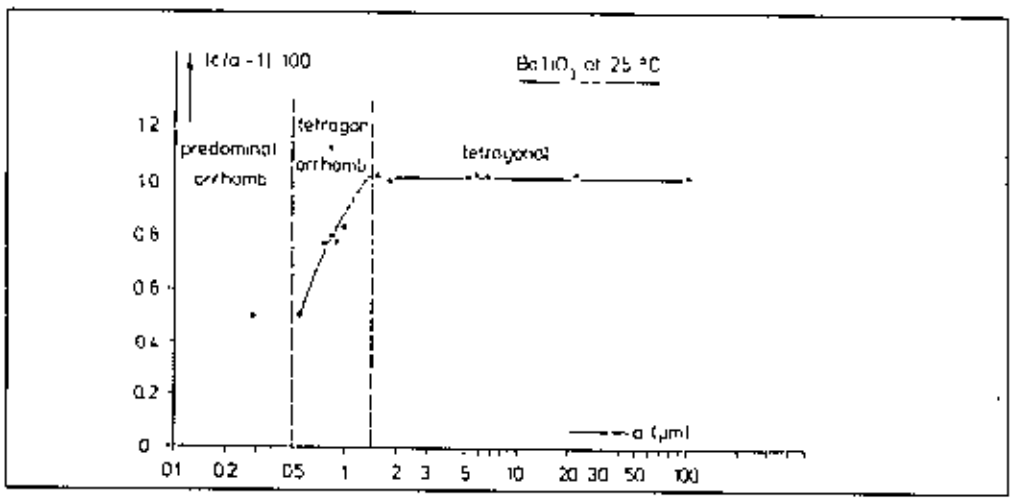

Figure 2-16 : Ratio of the lattice constants as a function of grain size

At grain size of 0.28μm only two reflections are observed which cannot be ascribed to any know ferroelectric phases of $BaTiO_3$ [4].

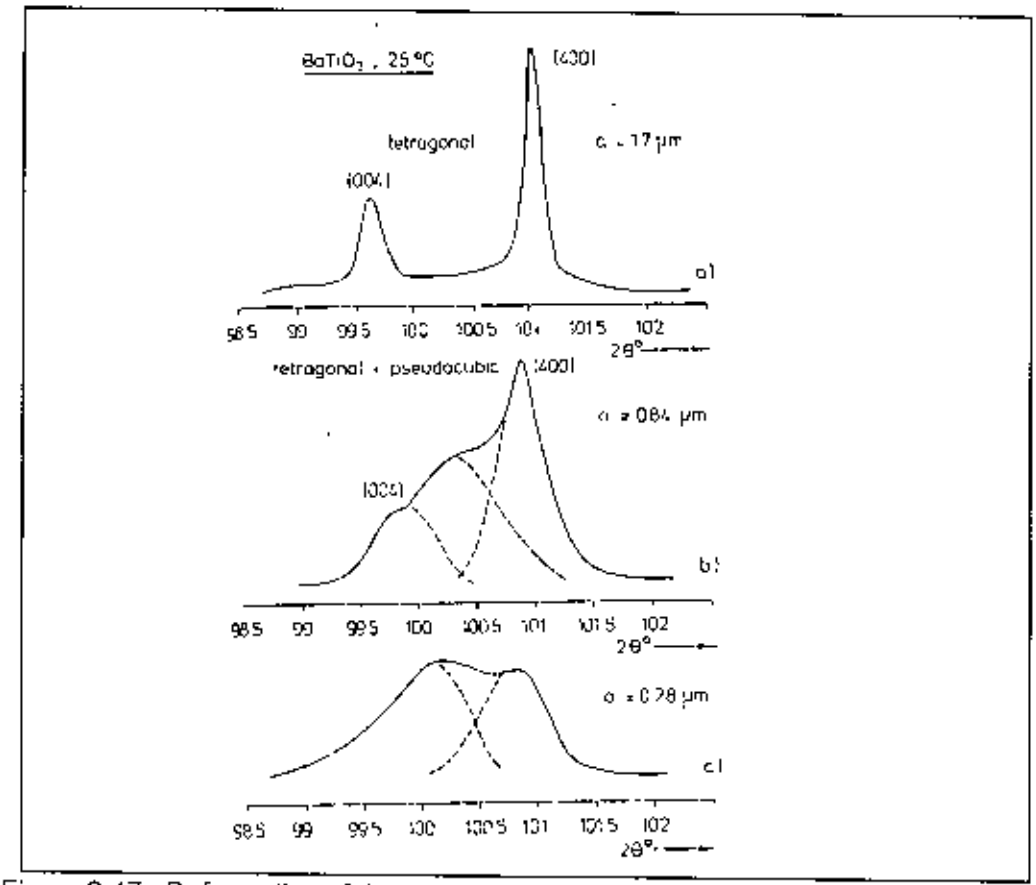

Figure 2-17 : Deformation of the tetragonal (400)/(004) x ray diffraction peaks due to grain size [4]

2.4.1.3 Displacement of ion

Off center dimension of atoms with in the unit cell of $BaTiO_3$ is given in figure

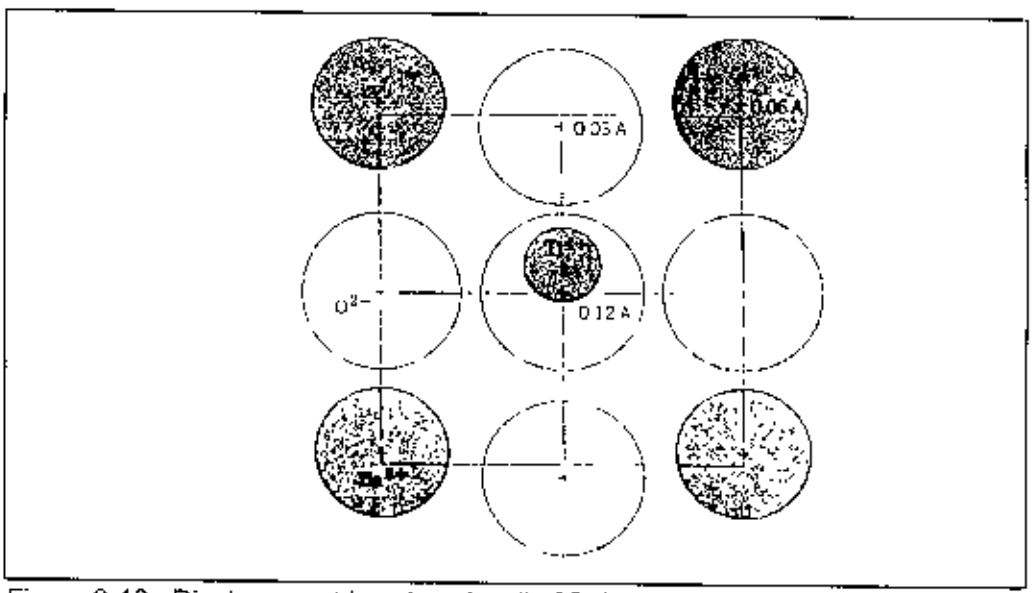

Figure 2-18 : Displacement ions in unit cell of $BaTiO_3$

2-18. Titanium ion is displaced by 0.12Å towards oxygen ion in [001] direction and that oxygen ion also displaced by 0.03Å towards [001] titanium atom. Barium ion also displaced by 0.06Å towards [001] direction. Under the influence of electric field of opposite direction the displacement will be towards opposite direction. On cooling below the Curie point T_c, the tetragonal structure so develops where the center of Ba^{2+} and Ti^{4+} ions are displaced relative to the O^{2-} ions, leading to the formation of electric dipoles. Spontaneous polarization developed is the net dipole moment produced per unit volume for the dipoles pointing in a given direction [22].

Large octagonal space compared to Ti atom size is responsible for this displacement. This is the basis of spontaneous polarization of $BaTiO_3$ or ferroelectric ceramic. This large octagonal hole is also the reason of $BaTiO_3$ undergoing many phase transformation at different temperatures. The relative displacement of ions in a unit cell illustrated in Figure 2-18.

2.4.2 Domain Structure effect

In polycrystalline bulk ceramics the pattern of domains is quite different because the domain structure of each grain is formed under elastic clamped conditions by its surrounding neighbors, whereas a single crystal is free [4]. It should be noted that only non-180 domains, i.e. 90 domains (for tetragonal structures) or 71 and 109 domains (for rhombohedral structures), have the potential to reduce elastic energy.

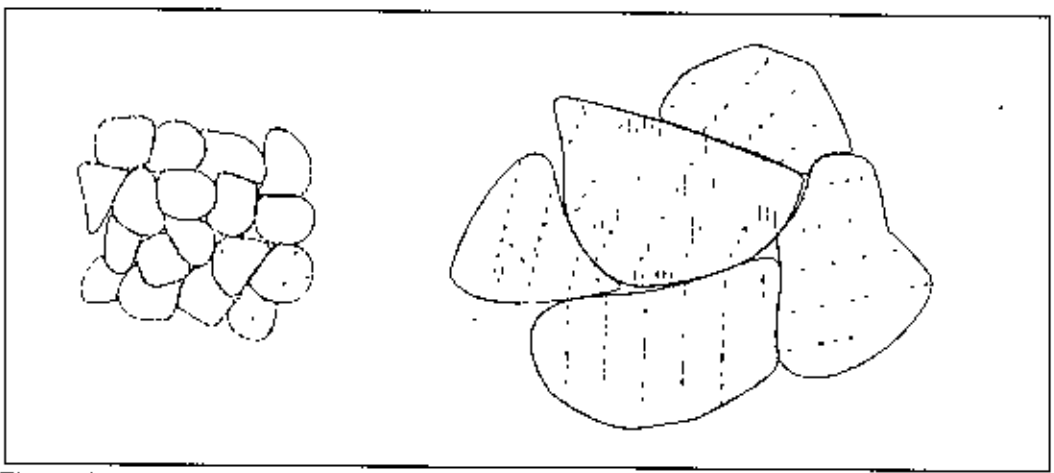

Figure 2-19 : Domain pattern of fine grained (left) and coarse grained (right) $BaTiO_3$ ceramic

There exist two types of domain in coarse grained $BaTiO_3$, called herring bone and square net pattern. The first one is by far the most common in unpoled ceramics.

As shown in Figure 1-19, by decreasing the grain size the domain pattern changes from a banded to a laminar structure [13]

2.4.3 Grain Size Effect

In bulk $BaTiO_3$ ceramics the grain size has a strong effect on the low frequency permittivity for grain sizes below approx. 10 µm as shown in Figure 2-17 (a). The permittivity is rising at decreasing grain sizes up to a maximum at grain size

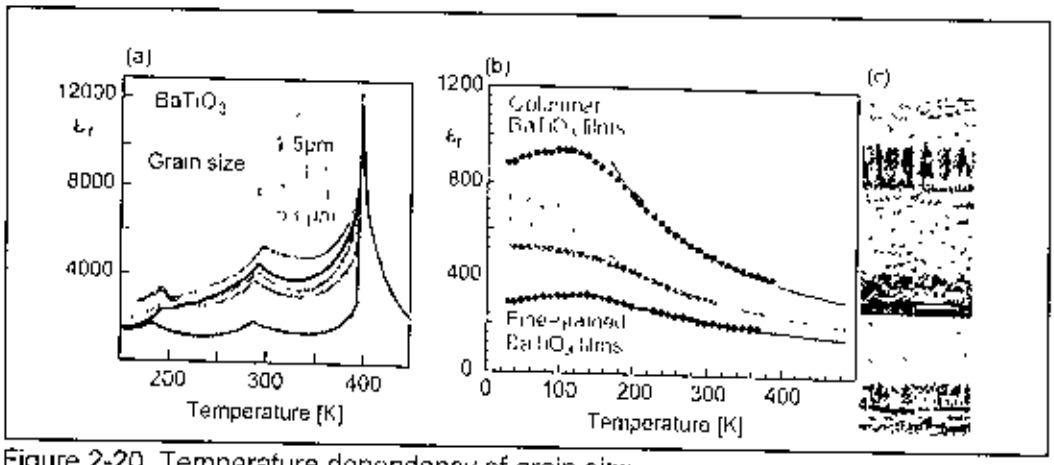

Figure 2-20 Temperature dependency of grain size

~ 0.7µm [4] The increase of k' could have caused by internal stresses because each grain is clamped by its surrounding neighbors or by the increase of the number of domain walls contributing to the dielectric constant. Below this grain size the permittivity sharply decreases again in conjunction with a reduction of the tetragonality and of the remanent polarization.

The drop in permittivity may be interpreted by the effect of a low permittivity interfacial layer of 0.5 to 2 nm thickness at the grain boundaries. This layer shows no difference of the composition and crystal structure in comparison to the bulk and is believed to be of photonic nature. In Figure 2-20 the temperature dependence of the permittivity for (a) bulk ceramics with different grain sizes and (b) thin films with different grain sizes and (c) microstructure of thin films are illustrated. For $BaTiO_3$ thin films a significant increase in the room temperature permittivity from 500 to 900 is observed which was induced by the change in the morphology from a granular to a columnar microstructure (Figure 2-20 (b) and (c)).

In contrast to $BaTiO_3$ bulk ceramics, which exhibit a paraelectric to ferroelectric phase transition with decreasing temperature accompanied by a sharp

peak of the permittivity at around 123°C, only a broad maximum in the permittivity vs. temperature curve is observed for polycrystalline thin films. Additionally, the $BaTiO_3$ thin films do not show a ferroelectric hysteresis at room temperature. While the absence of a remanent polarization is typical for paraelectric material, the grain size dependence indicates a super-paraelectric behavior of $BaTiO_3$ thin films. Compared to bulk ceramics, thin $BaTiO_3$ films of the same average grain size show a significantly lower permittivity, although the grain size dependence is still observed. The difference in the absolute permittivity values may be explained by a combination of thin film effects, which result in a further decrease of the permittivity, as for example film-electrode interfaces and stress effects.

Figure 2-21 shows the variation of dielectric constant with temperature for $BaTiO_3$ ceramics with a fine (<1μm) and coarse (>50μm) grain size. Large grained $BaTiO_3$ (>1μm) shows an extremely high dielectric constant at the Curie point. This is because of the formation of multiple domains in a single grain, the motion of whose walls increases the dielectric constant at the Curie point. For a $BaTiO_3$ ceramic with fine grains (<1μm), a single domain forms inside each grain. The movement of domain walls are restricted by the grain boundaries, thus leading to a low dielectric constant at the Curie point as compared to coarse grained $BaTiO_3$ [38].

The room temperature dielectric constant, k' of coarse grained (>50μm) $BaTiO_3$ ceramics was found to be in the range of 1500-2000. On the other hand, fine grained (~1μm) $BaTiO_3$ ceramics exhibit a room temperature dielectric constant between 3500-6000. The grain size effect on the dielectric constant at room temperature has been explained by the work of Arlt et. al [4] and Buessem et. al [39] coworkers proposed that the internal stresses in fine grained $BaTiO_3$ must be much greater than

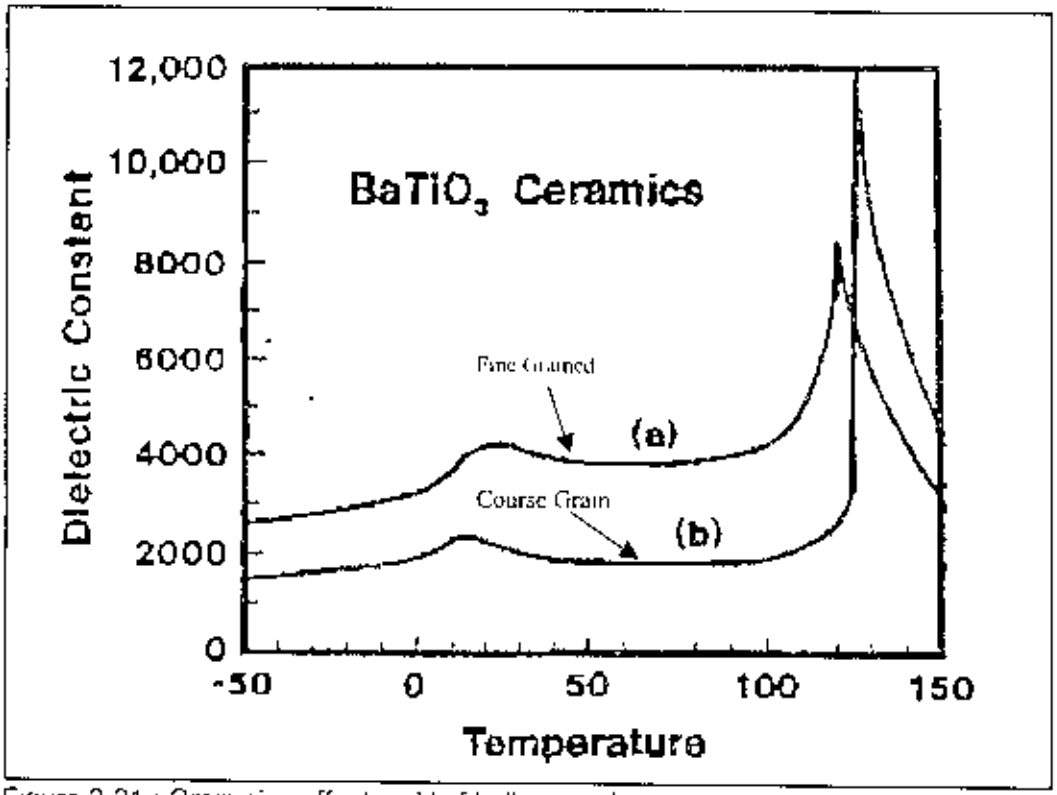

Figure 2-21 : Grain size effect on k' of bulk ceramic

the coarse grained ceramic, thus leading to a higher permittivity at room temperature. Arlt studied the domain structures in $BaTiO_3$ ceramics and showed that the room temperature k' reached a peak value at a critical grain size of ~0.7μm. He concluded that the enhanced dielectric constant was due to the increased 90° domain wall density. The mobility of the 90° domain walls in very fine grained $BaTiO_3$ is hindered and only less than 25 % of the k' was achieved.

As the $BaTiO_3$ ceramics have a very large room temperature dielectric constant, they are mainly used multilayer capacitor applications. The grain size control is very important for these applications

2.4.4 Morphology

Dielectric constant strongly depends on the microstructure specially porosity and other phase present. The effect of grain size discussed earlier. Ideally sintering should provide a ceramic body close to its theoretical density, around 95% or more Gerson et al [40] expressed the relation between porosity and κ' as

$$Log_{10}(k') = \sum_n V_n \log_{10}(k'_n) \qquad \text{---} \qquad \text{---} \qquad \{21\}$$

where, V_1, V_2, ... are volume fraction with κ' of κ_1', κ_2', ... Relationship with the experimental data shown in Figure 4-22

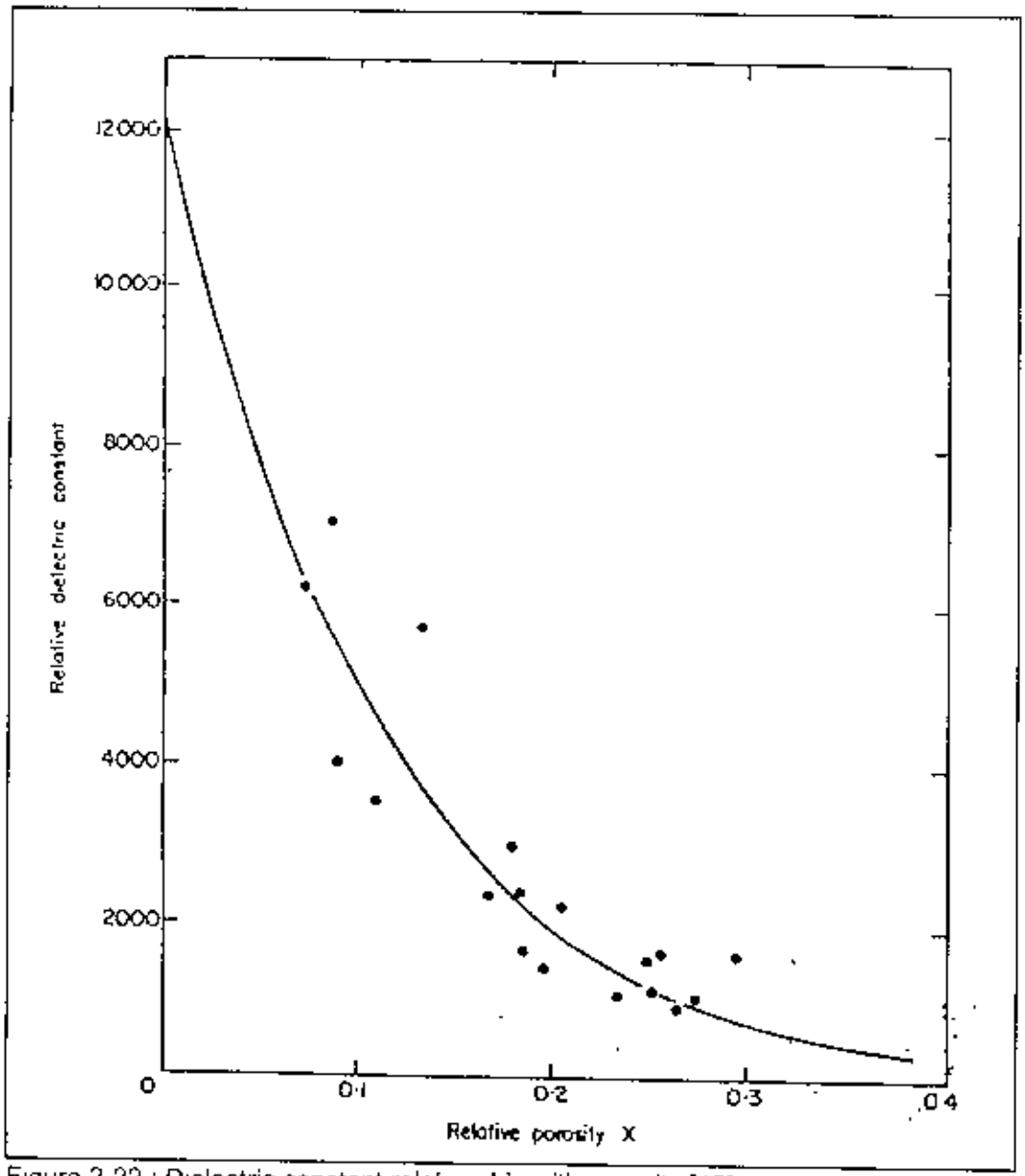

Figure 2-22 : Dielectric constant relationship with porosity [40]

Another feature of is the core shell structure develops owing to doping and other factors are discussed in section 2.7 7 2

2.4.5 Doping effect

Various A and B site substitutions in different concentrations have been tried to see their effect on the dielectric and ferroelectric properties of $BaTiO_3$. Sr^{2+} and substitutions to the A site have been found to reduce the Curie point linearly towards room temperature. The substitution of Pb^{2+} for Ba^{2+} raises the Curie point. The substitution of Zr^{4+} tend to decrease T_c but increases other transition temperatures. These effect shown in Figure 2.23 with effect on dielectric property. The simultaneous substitution into both A and B sites with different ions can be used to tailor the

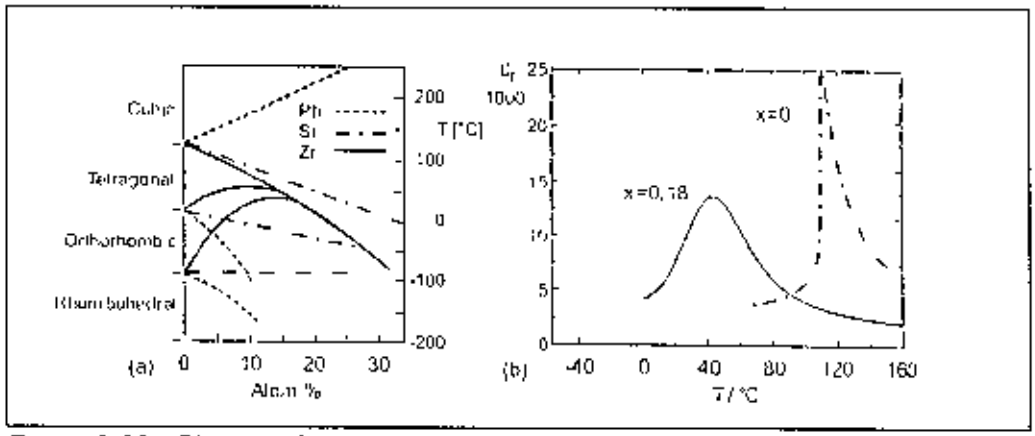

Figure 2-23 : Change of transition temperature with dopents and effect on dielectric constant

properties of $BaTiO_3$. The effects of various isovalent substitutions on the transition temperatures of $BaTiO_3$ ceramic are shown in Figure 2-24

Doping is necessary to.

-avoid time variations of $\kappa = \varepsilon/\varepsilon_0$

-broaden the κ' - T dependence

-decrease T_c to close to room temperature, if maximum κ' is required

If an ion of the perovskite structure $BaTiO_3$ is replaced by a different ion of the same valence, isovalent doping is present. e.g. Ca^{2+} on the Ba^{2+}-site $Ba_{1-x}Ca_xTiO_3$. Aliovalent doping exists when donors like La^{3+} on Ba-site or Nb^{5+} on Ti-site as well as acceptors like Ni^{2+} or Mn^{3+} on Ti-site are incorporated in the crystal. At least the site occupancy is determined by the size and the valence of the dopant, e.g. Ca^{2+} may be isovalent A-site or aceptor-type on B-site.

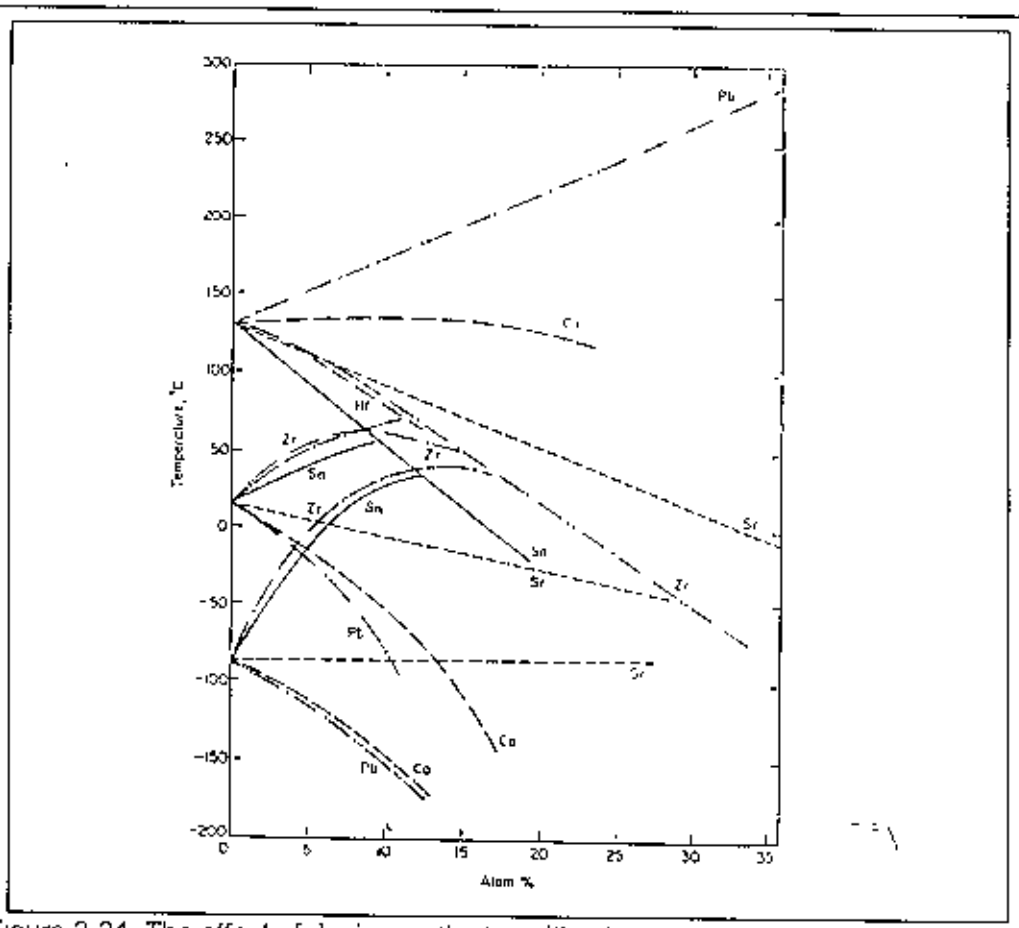

Figure 2-24 The effect of doping on the transition temperatures of $BaTiO_3$ ceramic

Besides Sr, Pb and Zr. Ba can be replaced by Pb, Sr, Ca, or Cd, and Ti can be replaced by Sn, Hf, Zr, Ce, or Th.

2.4.6 Ca doping effect and mechanism

Several reporters have found that Ca addition to $BaTiO_3$ causes negligible change [41] or only a slight decrease of the T_c [42,,43]. Increasing Sr doping level in $BaTiO_3$ ceramic decreases the Tc systematically to 90°K as observed my many researchers. This is normally attributed to the smaller ion size of Sr^{2+} compared to Ba^{2+} which caused reduction of unit cell volume with the increase of concentration of Sr. It was suggested that Tc was lower by the action of hydrostatic pressure [44]. Doping of Pb cause just the opposite although. Pb^{2+} ion is smaller than Ba^{2+}. It was explained in terms of larger electronic polarizability of Pb^{2+} than Ba^{2+} or Sr^{2+}, this polarizability intensifies the interactions between the Ti ions and thus raises the T_c [45].

Ca on the other hand has smaller ionic radius and a smaller electronic polarizability than either Ba^{2+} or Sr^{2+} Whereas Ca doping up to 25 mole % has almost

the same T_c as pure $BaTiO_3$. It was speculated that, Ca ions are not uniformly

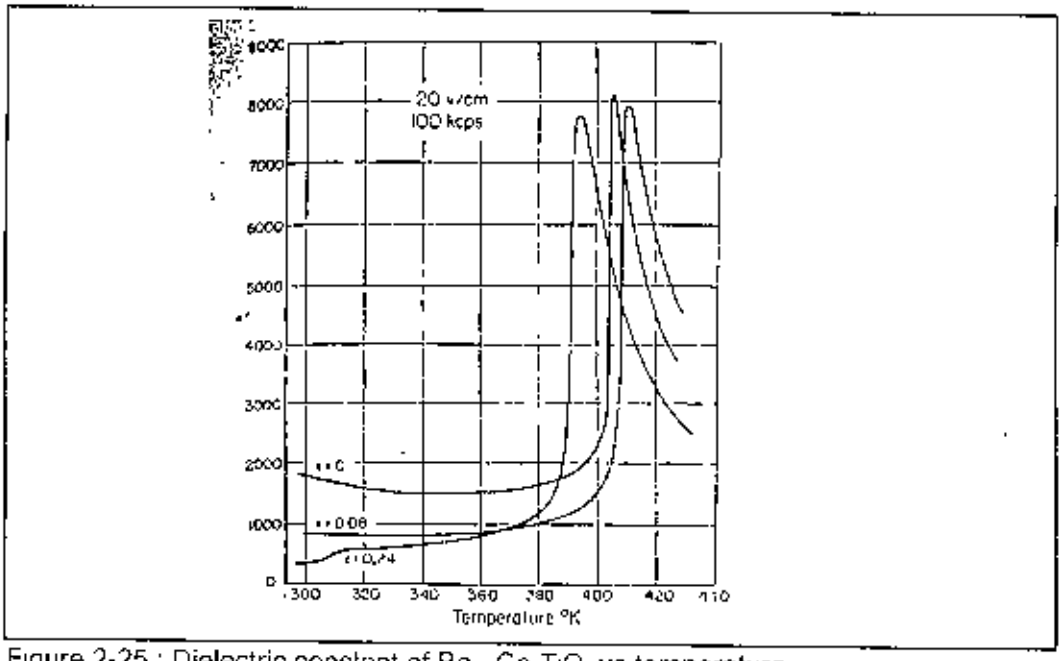

Figure 2-25 : Dielectric constant of $Ba_{1-x}Ca_xTiO_3$ vs temperature

distributed in the (Ba, Ca)TiO_3 solid solutions. In that case (Ba, Ca)TiO_3 might behave to some extent like a simple mixture of $CaTiO_3$ and $BaTiO_3$, resulting in a lowering of the dielectric peak at the Tc and in a broadening of the x-ray back reflection

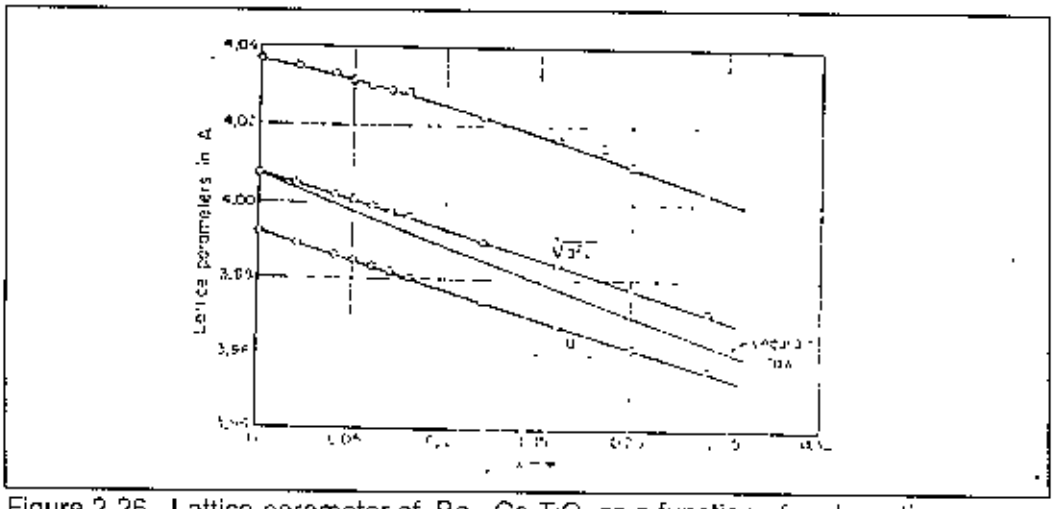

Figure 2-26 . Lattice parameter of $Ba_{1-x}Ca_xTiO_3$ as a function of molar ratio

lines with increasing Ca concentration. Mitsui et al [38] examined doping effect of Ca with concentration of x=0.08 and 0.24. They reported the calcination longer calcination time is required as Ca concentration increased. The temperature dependence of dielectric constant as shown in Figure 2-25 where T_c shifted to maximum of 136 1°C for Ca x= 0.08 then started to decrease as Ca concentration increased. Electron Paramagnetic Resonance (EPR) study by Babu *et al* [46] reported

a clear evidence for existence of dynamic fluctuation between cubic and tetragonal phases at the proximity of the phase transition temperature of $Ba_{1-x}Ca_xTiO_3$ (x=0 & 0.05). This might be one of the reason of T_c fluctuation with the Ca concentration. In the lattice of the perovskite type, each Ba or Ca is coordinated to twelve oxygen. Since Ca^{2+} has smaller ionic radius than Ba^{2+}, the space available to Ca^{2+} in $Ba_{1-x}Ca_xTiO_3$ solid solution must be larger than in $CaTiO_3$ and that for Ba^{2+} smaller than in $BaTiO_3$. The observed deviation from Vegard's law as shown in Figure 2-25 proves that a compromise is made in favour of the $BaTiO_3$ lattice, i.e., the space for Ca^{2+} is increased beyond that of an ideal solid solution. In $Ba_{1-x}Ca_xTiO_3$ the Ca ion therefore seems to have greater atomic polarizability.

Electronic structure of $Ba_{1-x}Ca_xTiO_3$ studied by X-ray absorption spectroscopy and theoretical calculation reported by Askan et al [47] reported that CaO and/or BaO, with TiO_2 enhance the effective charge of the O ions. Thus, a large dipole moment may result from the displacement of the Ti ion from the centre of the Ti-O octahedron leading to collective displacement of Ti ions through attractive dipole-dipole coupling and may give rise to ferroelectricity. This increased atomic polarizability might have increased the T_c as it does in case Pb doping to a certain point. But, the marked shrinkage of the unit cell volume of $Ba_{1-x}Ca_xTiO_3$ due to further Ca addition lowers the T_c as hydrostatic pressure would.

2.4.7 Commercial formulations

As discussed in detail so far, the permittivity of ferroelectric perovskites shows marked changes with temperature, particularly close to the phase transition. From the device point of view a high dielectric permittivity with stable properties over a wide

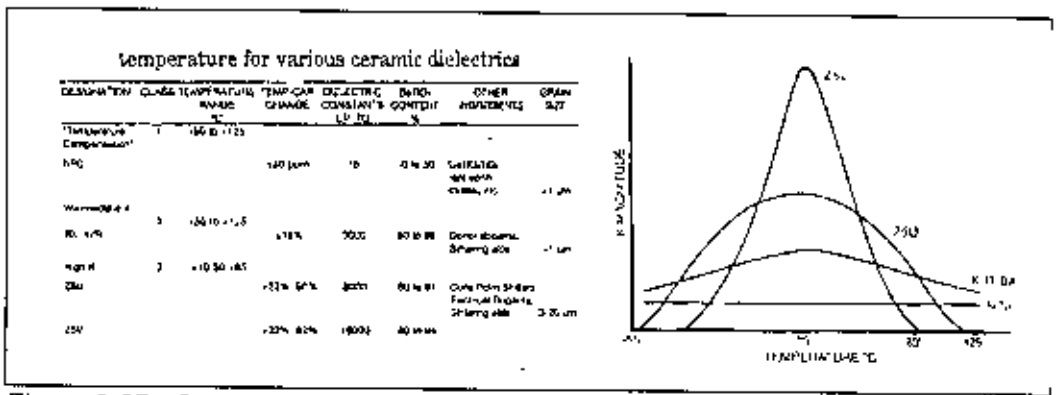

Figure 2-27 : Commercial formulations and their k' vs T characteristics [48]

temperature range is required. There are various commercial specifications which have to be fulfilled (e.g. X7R: $C/C_{T=25°C} < \pm 0.15$ in a range between -55°C and 125°C).

By substitution or doping it becomes possible to tailor the ferroelectric materials to different properties. In Figure 2-27 dielectric constant vs temperature behavior of commercial formulation as illustrated.

2.4.7.1 T_c Suppression

Doping generally leads to a shift of the phase transition temperature. In Figure 2-23 and 2-24, the change of the transition temperatures is plotted as function of dopant concentration for different dopants in $BaTiO_3$. It is found that Pb-doping stabilizes the tetragonal phase in the sense of their existence over a wide temperature range whereas Sr-doping destabilized the tetragonal phase. This behavior could be understood by the fact that the larger Pb-ions on the A-site form a larger cavity giving the central ion more space for off-center positions than the Sr-ions. In case of high dopant concentrations sequence of the phase transitions in $BaTiO_3$ tends to be suppressed. For $Ba(Zr_xTi_{1-x})O_3$ all phase boundaries meet at a Zr content $x = \sim 0.18$ (Figure 2-23). Because of the superposition of the particular phase transitions the resulting transition becomes diffuse with a broad maximum of the dielectric permittivity as shown in Figure 2-23. Therefore, this composition has the potential as suitable temperature-stable dielectric for ceramic capacitors.

2.4.7.2 Core Shell Structure

A different approach to over come the temperature instabilities of the dielectric coefficient is the addition of more complex compositions (than doping with atoms) as $CdBi_2Nb_2O_9$ [49]. By controlling the reaction kinetic of the sintering process the microstructure exhibits a grain core-grain shell structure. The core consists of $BaTiO_3$, and the perovskite material in the shell shows a mixture of $BaTiO_3$ with the complex perovskites $Ba(Bi_{0.5}Nb_{0.5})O_3$ and $Ba(Cd_{2/3}Nb_{2/3})O_3$ having an approximate Curie point at T_c 80°C. Figure 2-28 displays schematically the ferroelectric core and the paraelectric shell. The material fulfills the X7R specification for its dielectric behavior. The chemical inhomogeneity emerges during a process of reactive liquid-phase sintering. Application of too high sintering temperatures leads to uniform distributions of the additives via solid-stated diffusion and to the loss of the X7R characteristic.

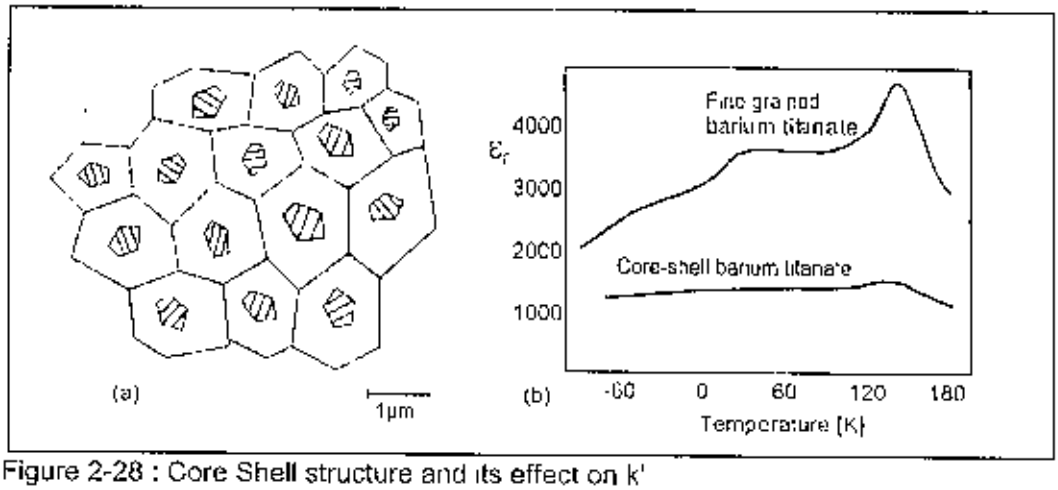

Figure 2-28 : Core Shell structure and its effect on k'

2.4.8 Relaxor Ferroelectric

These are special type of ferroelectric ceramic in their own right. Strictly, they are neither a derivative of $BaTiO_3$ nor a result of doping effect. The reason of their relevance in this study was to high light few aspects, which was observed in the $BaTiO_3$ samples of this study. Relaxor ferroelectrics are a class of lead based perovskite type compounds with the general formula $Pb(B_1,B_2)O_3$ where B_1 is a lower valency cation (like Mg^{2+}, Zn^{2+}, Ni^{2+}, Fe^{3+}) and B_2 is a higher valency cation (like Nb^{5+}, Ta^{5+}, W^{5+}). Pure lead magnesium niobate (PMN or $Pb(Mg_{1/3}Nb_{2/3})O_3$) is a representative of this class of materials with a Curie point at $-10^{\circ}C$. The main differences between relaxor and normal ferroelectrics are shown in Appendix 7.6.

Relaxor ferroelectrics like PMN can be distinguished from normal ferroelectrics such as $BaTiO_3$ and PZT, by the presence of a broad diffused and dispersive phase transition on cooling below the Curie point. Figure 2-29 shows the variation in the dielectric properties with temperature for PMN ceramic. It shows a very high room temperature dielectric constant and a low temperature dependence of dielectric constant. The diffused phase transitions in relaxor ferroelectrics are due to the compositional heterogeneity seen on a microscopic scale.

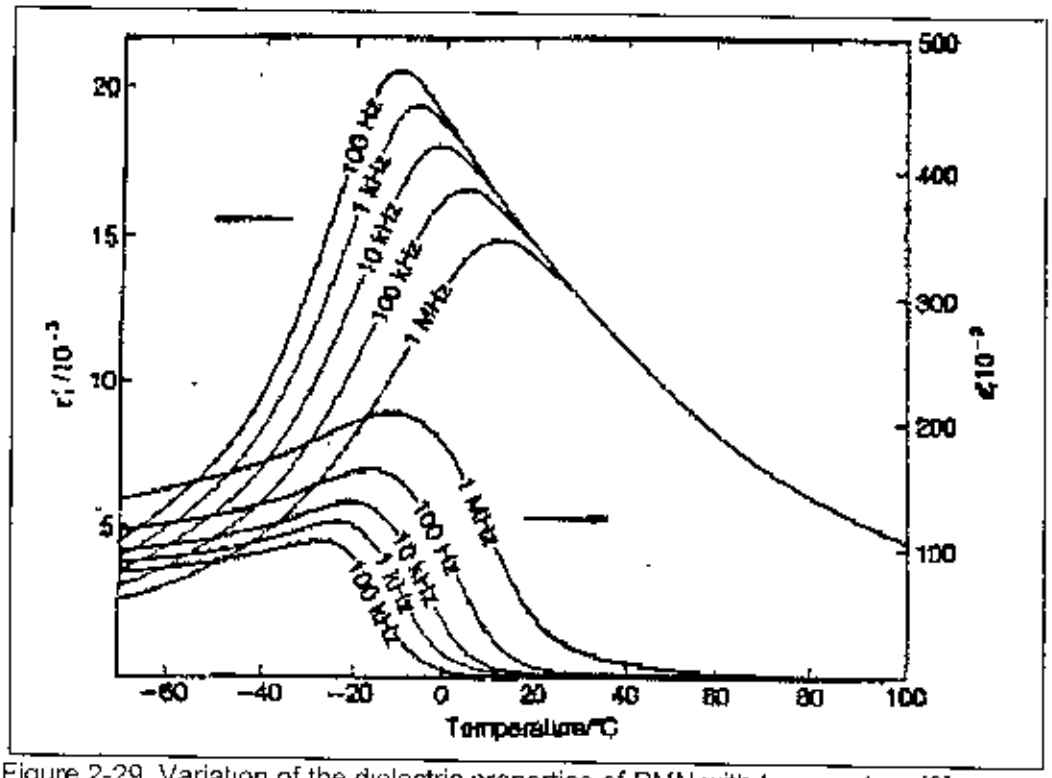

Figure 2-29 Variation of the dielectric properties of PMN with temperature [9]

The relaxors also show a very strong frequency dependence of the dielectric constant. The Curie point shifts to higher temperatures with increasing frequency. The dielectric losses are highest just below the Curie point, T_t. Relaxors which have a second order phase transition, the remnant polarization, P_r, is not lost at the Curie point but gradually decreases to zero on increasing the temperature beyond T_c [50].

2.5 Applications

Barium titanate can be regarded as 'role model' of electronic ceramic from application point of view. Its piezoelectric, pyroelectric and ferroelectric properties were successfully applied in many commercial applications. Vast majority of commercially important application are in polycrystalline bulk or film form. In the following sections, property wise applications are briefly discussed. Since dielectric properties of $BaTiO_3$ were studied in this thesis, capacitor application especially MLCC emphasized. Cut-away schematic of MLCC is shown in Figure 2-30 and a actual MLCC shown in Figure 2-31

2.5.1 Ferroelectric applications as bulk

Notable application of ferroelectric $BaTiO_3$ is in the manufacture of capacitor for electrical appliances. Basics of capacitor have been discussed in the section 2.2

with example of simple ceramic capacitor. From application point of view MLCC capacitors are most important and technologically challenging. The volumetric

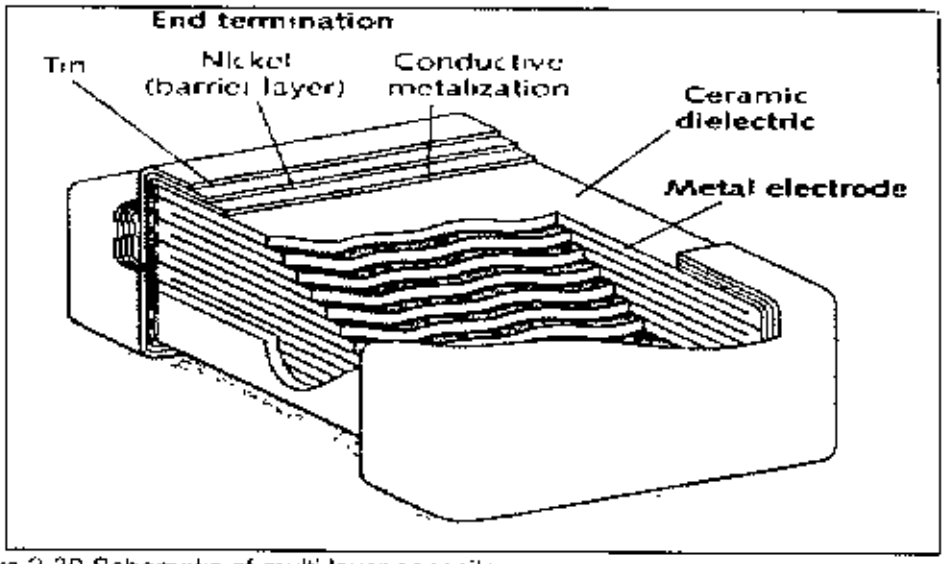

Figure 2-30 Schematic of multi layer capacitor

efficiency (more capacitance from given capacitor size) further enhanced by using multilayer ceramic (MLC) capacitors. As shown in Figure 2-30, the MLC capacitor structure consists of alternate layers of dielectric and electrode material. Each individual dielectric layer contributes capacitance to the MLC capacitor as the electrodes terminate in a parallel configuration.

Hence, the effective equation (cf. equation 5) for capacitance becomes,

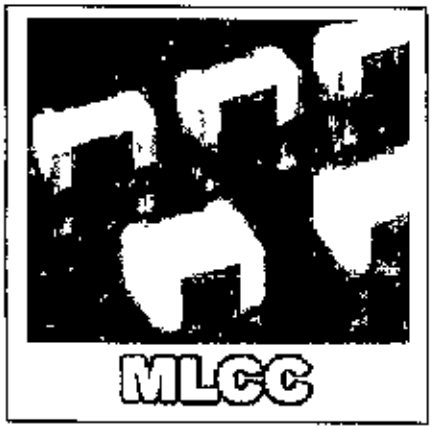

$$C = \frac{n\varepsilon_o \kappa' A}{d}$$

Here, n is the number of dielectric layer. The advances in tape casting technology have made it possible to make dielectric layers < 20 μ m thick. This, combined with the use of a high dielectric constant ceramic like $BaTiO_3$,

Figure 2-31 MLCC capacitor

allows large capacitance values to be achieved in relatively small volume capacitor devices [9]. MLC capacitors are made by the tape casting process.

2.5.1.1 MLCC processing

Slurry with a suitable binder/solvent system is first made from the dielectric ceramic powder. Thin green sheets of the ceramic are then made by the tape casting process. Ink consisting of an electrode (Pd, Ag-Pd, etc.) and organics is screen printed on the dielectric sheets and then hundreds of sheets are stacked one on top of the other. A low pressure at a temperature between 50°C and 70°C is applied to laminate the sheets. These laminates are then diced to form a monolithic green MLC capacitor. The binder removal is accomplished by heating the green body very slowly to a temperature of ~ 300-400°C. The MLC capacitor is then sintered at a high temperature depending on the type of ceramic. After applying the terminations for the internal electrodes of the MLC capacitors, the capacitor is mounted on the electronic substrate by soldering.

The critical steps in the fabrication of the MLC capacitors include the formation of thin uniform green sheets from the ceramic slurry. Any non-uniformity in the thickness could lead to dielectric breakdown during operation of the device. The co-firing of the ceramic tapes and metal electrodes should be compatible and should not lead to any reactions between the two.

2.5.2 Ferroelectric Thin Films

Ferroelectric thin films have attracted attention for applications in many electronic and electro-optic devices. Beside $BaTiO_3$ other important ferroelectric materials being used for making thin films include the perovskite type materials such as, $Pb(Zr_xTi_{1-x})O_3$ and $Pb(Mg_{1/3}Nb_{2/3})O_3$. Applications of ferroelectric thin films utilize the unique dielectric, piezoelectric, pyroelectric, and electro-optic properties of ferroelectric materials. Some of the most important electronic applications of ferroelectric thin films include nonvolatile memories, thin films capacitors, pyroelectric sensors, and surface acoustic wave (SAW) substrates. The electro-optic devices being studied include optical wave guides and optical memories and displays.

2.5.3 Piezoelectric Applications

In the early days, piezoelectric property of $BaTiO_3$ was used in phonographic pick-ups. Piezoelectric ceramics can be used for both active and passive transducer applications in ultra sound application. In the passive mode the transducer acts as a sound receiver i.e. there is conversion of sound energy into an electrical signal. The

converse piezoelectric effect permits a transducer to act as an active sound transmitter. In the pulse echo mode, the transducer is used to perform both the active and passive functions at the same time. A sound wave is propagated into the medium and a faint echo is received back after a small time gap due to the acoustic impedance mismatch between the interface materials. This principle is used in transducers for ultrasonic medical imaging applications. Other applications are gas igniter, displacement transducer, accelerometers, piezoelectric transformers, impact printer head for dot matrix, etc.

2.5.4 Other applications

Recently $BaTiO_3$ has been used as in-built thermal switches on motors. When the temperature rises above a set point, the resistance through the switch increases, shutting off the motor. Also for constant temperature heating devices as the device becomes self-regulating at the set temperature by the increase of resistance. However, in spite of all of this interest, an accurate model of the cause of the PTCR (positive temperature coefficient of resistivity) effect remains a contentious issue. At a particular temperature, which can be tuned by the choice of dopants and the doping level, a rather sharp increase in resistivity covering several orders of magnitude is observed. The resistance drops normally on either side of this sharp transition. The nature of this PTCR effect occurs in the same temperature range where the sample undergoes a structural phase transition from a tetrahedral to a cubic unit cell. However, the phase transition also occurs in the single crystal sample where no PTCR effect is observed. Apparently, the grain boundary region must be in control of this phenomenon. In 1992, worldwide production of $BaTiO_3$ thermistors exceeded a half billion units.

3 Experimental

3.1 Introduction and sample identification

Disc shape samples were prepared in this experiment. Four sets of samples were prepared with different materials and process variables. Pre sinter powder processing of one set samples was carried out at MME Dept, BUET. Pallets so made were then sintered and properties measured at MTEC Lab (NSTDA, Bangkok, Thailand). This set of sample referred as set '**A**'. Next set of sample, labeled as set '**B**' was prepared entirely at MTEC Lab using powder of MME and MTEC Lab. Third set of sample, labeled as set '**C**', was prepared entirely at MME using processing technique of MTEC and powder different from the ones used in Set A. Last set of sample, labeled as '**D**' was prepared using high purity TiO_2 powder form Atomic Energy Commission (AEC) and Ca doped as $CaTiO_3$. Alongside doped samples, un-doped sample was also prepared for comparison. The raw powder sources were different for these sets and processing parameters of each batch or trial as shown in Table 3-1. Specifications of raw powders used are given in Appendix-I.

Table 3-1 Process variables in sample preparation

Set	Raw Powder source	Trial / Batch	Calcination	Sinter	Remarks
A	MME (Ca doping and pure $BaTiO_3$)	B – I	900°C for 3hrs	1225°C for 3hrs	calcination three times
		B – II	900°C for 3hrs	1200°C for 3hrs	
		B – III	900°C for 3hrs	1300°C for 1hr	
B	MME and MTEC (only $BaTiO_3$)	E – M	900°C for 3hrs	1300°C for 3hrs	MTEC powder
		E – B	900°C for 3hrs	1300°C for 3hrs	MME powder
		EI – M	900°C for 3hrs	1250°C for 1hr	MTEC powder
		EII - M	1000°C for 2hrs	1350°C for 0.5hr	
C	MME (2) (Ca doping and $BaTiO_3$)	B – IV	1000°C for 7hrs	1325°C for 2.5hr	MME new powder
D	MME (2) and AEC ($CaTiO_3$ doping and $BaTiO_3$)	B – V	1200°C for 10hrs	1350°C for 4hr	MME new and AEC powder

The test results of set A and B for each batch were compiled from the average of at least five samples. Three doping levels were used in this experiment. Samples were designated as per following Table 3-2 for samples of every set.

Table 3-2 Sample identity accroding to doping level

$BaTiO_3$	$Ba_{0.95}Ca_{0.05}TiO_3$	$Ba_{0.92}Ca_{0.08}TiO_3$	$Ba_{0.88}Ca_{0.12}TiO_3$
P	**Q**	**R**	**S**

Therefore, regardless the set or batch P would be refered to undoped $BaTiO_3$ sample. Q for Ca doing of 5mole percent, R for 8 mole percent and S for 12 mole percent. At MTEC lab only un doped $BaTiO_3$ samples were prepared. This sample identification convention would be referred through out the later sections of this study.

3.2 Sample Preparation

Conventional mixed oxide method was used throughout. Appropriate weight of Barium Carbonate ($BaCO_3$), Titanium Oxide (TiO_2) and calcium doping source were mixed and milled in a ball mill under the condition given in Table 3-3. The doping sources were Calcium Oxide (CaO). Calcium Carbonate ($CaCO_3$) and $CaTiO_3$ for set A, C and D respectively. $CaTiO_3$ was prepared for use as dopant instead of CaO or $CaCO_3$ for set D. Shape of the sample shown in Figure 3-1.

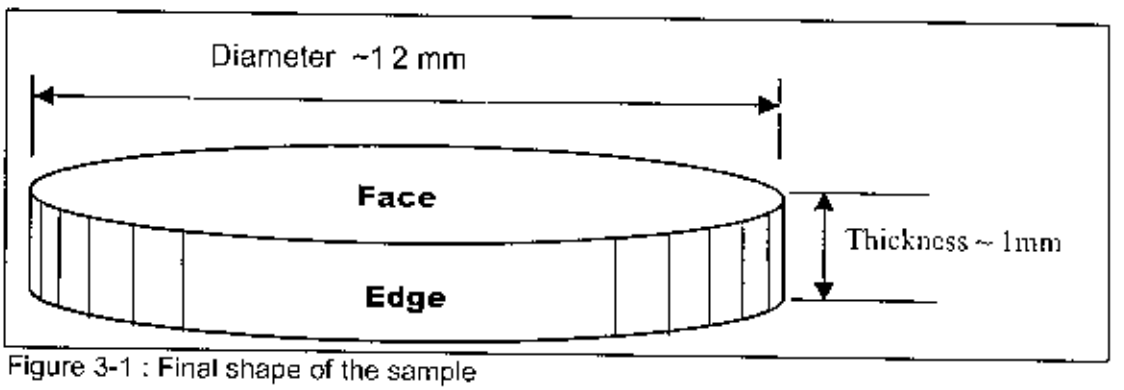

Figure 3-1 : Final shape of the sample

3.2.1 Ball Milling

At MME, milling was carried out in porcelain pot with steel balls and distilled water was used as media for set A. At MTEC, plastic bottle (HDPE - capacity 150cc), zirconia ball (dia. 7mm) and acetone were used instead. This milling procedure was followed for set C and D at MME. Typical milling time was 24 hours; except for set A. Samples of set A were calcined three consecutive times followed by milling every time. Identical procedure was followed for pre and post calcination milling.

Some samples of set B were analyzed to assess the extent of milling using Malvern Laser particle size analyzer, *Mastersizer-S*.

Table 3-3 Milling and doping parameters

Set	Milling Media	Time	Dopant source	Remarks
A	Steel Balls / distilled water	3 h to 10 h	CaO	3 times consecutive calcination and milling
B	Zirconia balls / acetone	24 h	no doping	
C	- do -	24 h	$CaCO_3$	
D	- do -	24 h	$CaTiO_3$	

3.2.2 Calcination

Temperature profile of calcinations is given in Table 3-1 for each set of samples. Calcination was carried out at air in muffle furnace equipped with micro-controller based temperature controller. Alumina crucible was used through out. Extent of calcinations, i.e. formation of $BaTiO_3$, was examined by pre and posts calcined powder samples of set B using XRD

3.2.3 Compaction

Milled calcined powder was mixed with 2% Poly Vinyl Alcohol (PVA) and then dried in oven at 100°C before pressed into pallets. Samples were pressed into pallets using pressure of ~100MPa for set A and ~150MPa for set B, C and D, using hydraulic press. The Green pallets were dried in oven, then lightly ground with grit #600 and #800 SiC paper to a flat and smooth surface, removing surface irregularities. Green densities of the pallets were measured before sintering for set A.

3.2.4 Sintering

Muffle furnace was used to sinter the pallets in air atmosphere. General thermal profile of sintering is given in Figure 3-2. Pallets were placed in the furnace on alumina plate. Binder burnout temperature was 450°C, while the hold time was 2 hours. A Thermo Gravimetric Analysis (TGA) test was carried out to confirm the weight loss characteristics of green pallet of set B. Sintering temperature and hold time was varied to observe their effect on the density and dielectric properties.

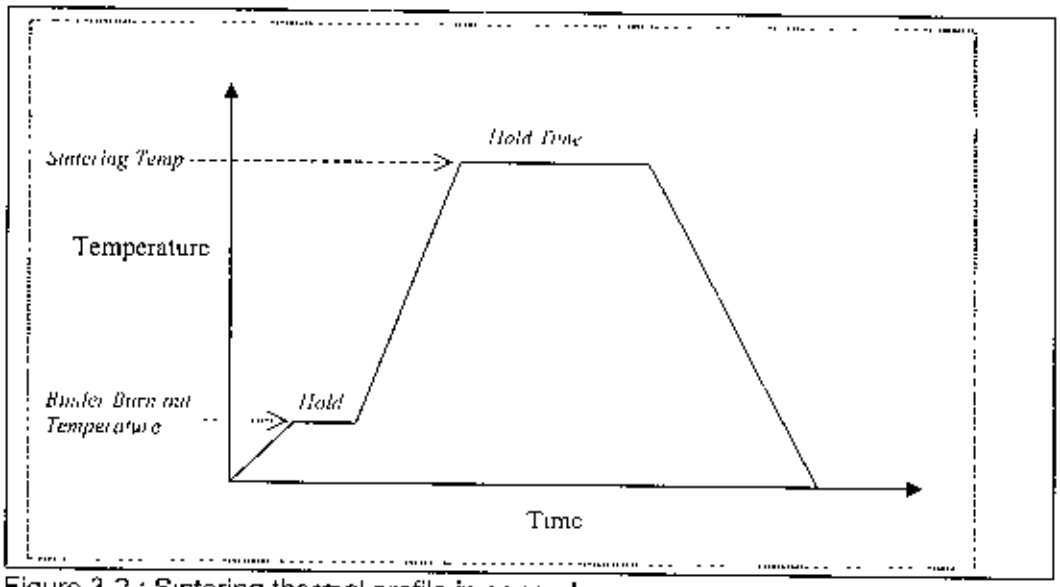

Figure 3-2 : Sintering thermal profile in general

3.2.5 Post Sinter

After sintering, the samples were ground successively with SiC paper of grit #600, #800 and #1200 to obtain a flat and polished surface. Dimension of the pallets were taken for dielectric constant and density calculation Prior to electrical measurements samples were cleaned and dried then, painted with high purity conductive Silver paint on the both faces of the sample. Gold sputtered electrode was applied for samples of set C. Edges were ground and cleaned with acetone

3.3 Property Measurement

3.3.1 Density

Dimension of the sample were taken using micrometer with digital read'out and weighed using analytical weighing scale. Density of the sample was calculated from these data Density results were presented as percentage of theoretical density (TD) TD of doped samples was calculated based on volume fraction of respective phase as shown in Table 3-4

Table 3-4 Theoretical Density of BaTiO3 and doped sample in g/cm³ [8, 51]

$BaTiO_3$	$Ba_{0.95}Ca_{0.05}TiO_3$	$Ba_{0.92}Ca_{0.08}TiO_3$	$Ba_{0.88}Ca_{0.12}TiO_3$	$CaTiO_3$
6.017	5.921	5.864	5 787	4.10

To compare the accuracy of density calculated from the dimensions and weight of pallets, the Archimedean method was also used for some sample of Set B This was done following ASTM standard C 373-88.

3.3.2 Dielectric constant and loss

Electrical properties of the sample were measured using a Hewlett-Packard 4194A impedance and phase gain analyzer at MTEC. Applied voltage was $40V_{pp}$ of sine wave shape. Dielectric constant k' was calculated from the capacitance value obtained from the analyzer according to equation 5 as below

$$\kappa' = \frac{C_p d}{\varepsilon_0 A} \qquad \text{--- ---} \qquad \{20\}$$

At MTEC, thermal chamber made by Delta Design, model Delta 9029 was used to heat the samples. It has the facility of maximum eight samples to be tested simultaneously in the chamber and an electronic switching device was used to select the particular sample.

A tube-furnace type oven and custom sample holder was designed by the author and built at MME. These set-up was used to heat the sample of set 'B' and 'C' during electrical property measurement at Physics Department of BUET. An *Agilent* model 4129A impedance analyzer was used. Five samples could be tested simultaneously in this arrangement.

3.3.3 Thermo Gravimetric Analysis (TGA)

TGA test was carried out at MTEC to observe weight loss and binder burn out characteristics of the sample added with 2% PVA. Sample was tested to 850°C in air and heating rate was 20°C/min.

3.3.4 Particle size analysis

Ball mill slurry of $BaTiO_3$ powder was tested for particle size and their distribution using Malvern Instrument's *Mastersizer-s* at MTEC. Powder suspension was prepared in de-ionized water and '*Nonidet 40*' was used as dispersant agent. The suspension was treated in ultrasonic bath for 10 minutes. The refractive index of $BaTiO_3$ and dispersant were 2.40 and 1.33 respectively.

3.4 Microstructure

Sintered samples (disc shaped) were polished using conventional ceramographic technique. Concentrated HCl was used as etching agent. The microstructure of samples was examined using Scanning Electron Microscope (SEM)

and conventional optical microscope Samples were gold sputtered (few nanometer thick) prior to SEM examination. At MTEC Jeol JSM-6301F SEM was used with acceleration voltage up to 20kV and at MME, Phillips XF 30 was used with acceleration voltage of 10kV.

3.4.1 X ray Diffraction (XRD)

Extent of reaction or $BaTiO_3$ formation was examined by XRD in powder form Sintered samples were examined in solid form. At MTEC a *Jeol model XD320* and at Magnetic Material Division (MMD) of AECD *Phillips X'Pert Pro* were used following identical scanning parameter given in Table 3-5 in all XRD experiment:

Table 3-5 XRD operational conditions

X Ray Source:	**Cu Kα**	for calculation Cu $K\alpha_1$ λ = **1.54056 Å** Used
Tube Voltage: Current:	**40 kV** **20 mA**	
Degree range:	**20 ° to 60 °**	Speed: **0.02° per sec**

4 Results and Discussions

Dielectric property results quoted are the average of at least four samples of a batch. Especially for set A and B standard deviation was less than 1%. Abnormal results were double-checked and some of them were excluded. The abnormally low Tc of set A samples were rechecked for temperature correction and several tests were carried out to confirm the calibration of the instrument. Frequency dependence of electrical properties are presented for the temperature of 60°C.

4.1 Particle size of milling product

Un-doped $BaTiO_3$ samples of set B were tested for particle size analysis distribution and results are given in Table 4-1. The volumetric particle size distribution-curve shown in the Figure 4-1. Samples tested were processed under identical milling procedure. The volumetric distribution of particle size of post calcined powders are relatively finer than their pre calcined counterpart.

Table 4-1 Particle size distribution data of set B [1]

	Calcination	Volumetric particle size distribution in μm				S. Surface Area	
Set	Condition	D [4, 3]	D (v, 0.1)	D (v, 0.5)	D (v, 0.9)	m^2/g	Uniformity
E – M	Pre	3.30	0.84	3.11	5.94	3.9709	0.4997
E – B	Pre	2.53	1.07	2.39	4.19	3.4504	0.4105
E – M	Post	2.51	0.31	2.23	4.94	7.2561	0.6278
E – B	Post	1.62	0.52	1.36	3.13	6.5925	0.5917
EII – M	Post	1.61	0.60	1.36	2.97	5.9541	0.5395

The same pattern observed for specific surface area and uniformity. These were quite expected; pre calcined powders are mixture of component materials (in powder form), whereas post calcined powders are supposed to be single phase compound. Furthermore, pre calcined powders are as produced by manufactures, going thorough complete reaction and refinement. Hence, raw powder particles' surfaces were much smoother and round. On the other hand, post calcined powder particles are product of calcination reaction, hence rough surface. Difference of particle size and distribution was observed between MME and MTEC powders.

[1] D(v, 0.1), D(v, 0.5) and D(v, 0.9) are the particle under-size below 10%, 50% and 90% of the volume respectively, v stands for volume, D[4, 3] is the mean diameter value by volume.

Both pre and post calcination powder particle size of MME powder are finer than MTEC powder and the specific surface area is the lower. Calcination temperature for batch E and EI were 900°C for 3 hours and for EII was 1000°C for 2 hours. Relatively powder size distribution is finer and uniform for E-II batch. The D (v,0.9) is 2.97μm of EII series whereas other post calcination sizes of the same distribution is much higher. This might have been due to single-phase composition of the powder as the calcination had completed forming $BaTiO_3$ confirmed by XRD pattern

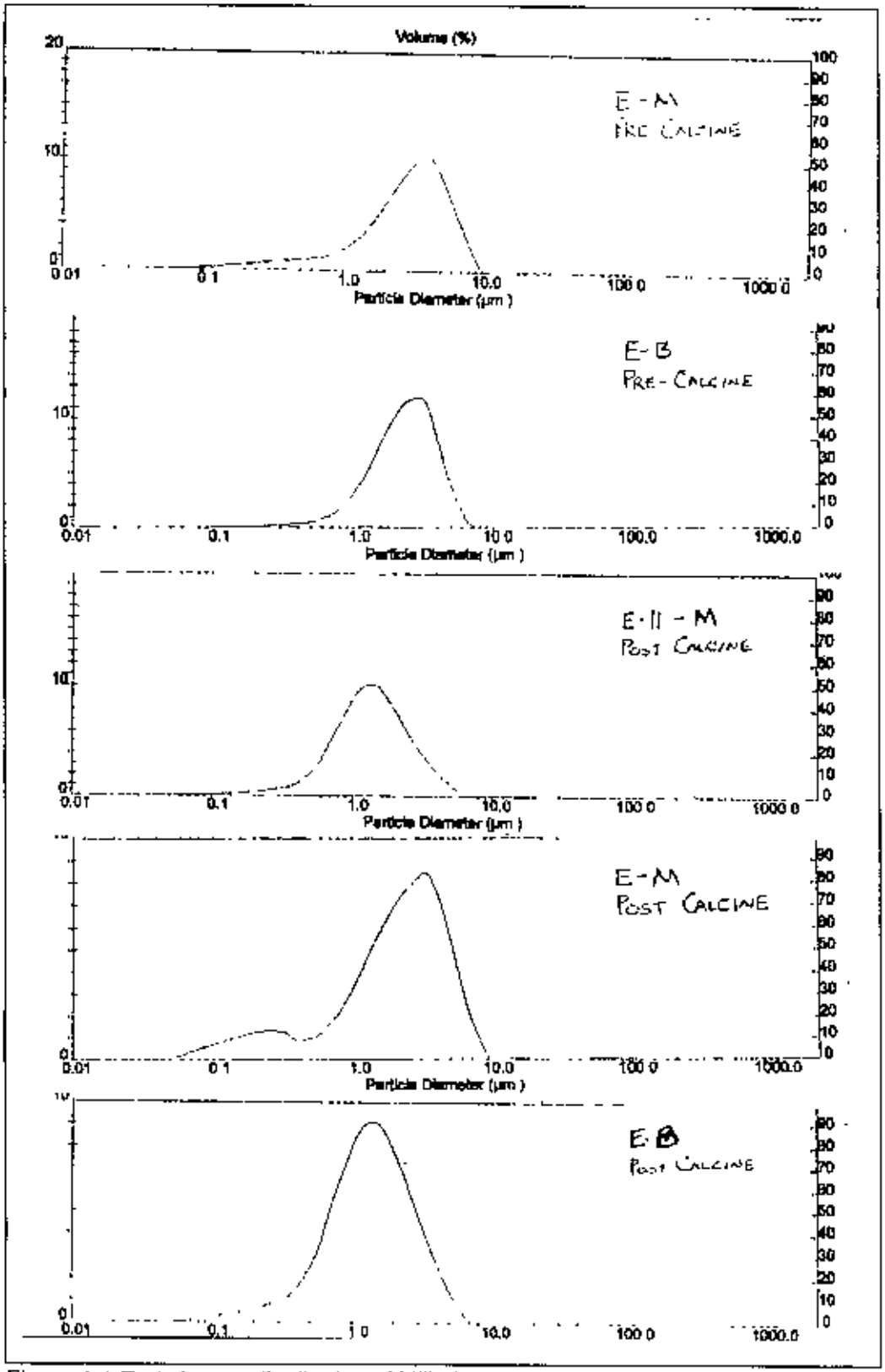

Figure 4-1 Particle size distribution of Milled powder

4.2 Density of sintered body

Densities of the samples were represented as percentages of theoretical density (TD) calculated based on the data given in Table 3-4. The average green densities of compacted pallets are given in Table 4-2. Suggested green density should be around 60% of TD. None of the pallets of series P attained that except for a trial pressure at 220MPa for batch EII-M. However, this increased green density did not translate into

Table 4-2 Average green density of pallets

	Pressure	Average Green Density % of TD			
Batch	MPa	P	Q	R	S
B - I	150	53.42	50.02	50.42	50.10
B - II	150	53 64	49 37	49.99	49.91
E – M	150	53.34	Ca doped sample not prepared for Set B		
E – B	150	53.41			
EI – M	150	54.25			
EI – B	150	54.51			
EII – M	220	58.72			
EII – M	150	54.25			

increased sintered density. The green densities of series P are better than doped ones by approx. 4% under identical pressing conditions. This is due to mixture of two different phases. The sintered body densities calculated from volume and weight are given in the Table 4-3.

Table 4-3 Calculated density of sintered samples

		Calcination		Sintering		Average density % of TD			
Set	Batch	°C	Hour	°C	Hour	P	Q	R	S
A	B – I	900	3	1225	3	90.32	89 08	89.73	92.15
	B – II	900	3	1200	3	88.58	82.72	89.99	89.85
	B – III	900	3	1300	1	90.31	89.78	89 16	94.16
B	E – M	900	3	1300	3	85.00	Ca Doped sample not prepared		
	E – B	900	3	1300	3	73 22			
	EI – M	900	3	1250	1	84.77			
	EI – B	900	3	1250	1	67 07			
	EII – M	1000	7	1350	0.5	91 89			
C	B – IV	1000	2	1325	2.5	90.87	87.89	85.36	94 64
D	B – V	1200	10 [2]	1350	4	samples fused and cracked			

[2] Calcined two time, first 4hours followed by another calcination for 6hours

During sintering many samples of set A, specially the doped ones were cracked, stuck with the alumina substrate and others left brownish stain on the substrate. Exception was series P. Staining and these sintering anomalies do suggest inclusion of elements other than Ca in the samples. This aspect of inclusion discussed in later sections.

4.2.1 Calcination

From Table 4-3, it is apparent that the deciding factor on densification is not straightforward. Analysis of data and microstructural study do suggest three major factors; calcination thermal profile, particle size of milling product and sintering thermal profile. The principal aim of calcination is to form the desired phase through solid-state reaction. This kind of reaction is very sluggish and time consuming. SEM micrograph of a sample (B-1 of set A) sintered at 1225°C shown in Figure 4-2. Un etched sample seem to contain acceptable level of porosity. The average bulk density of this sample was 89% of TD. Close examination of the pore suggests that these pore were result of gas escape and un-reacted powder that did not coagulate.

These gas escape holes might have formed due to CO_2 formation from the reaction of un-reacted particles that did not from $BaTiO_3$ during calcination. Close up of such pore shown in Figure 4-3. The same sample was etched with concentrated HCl

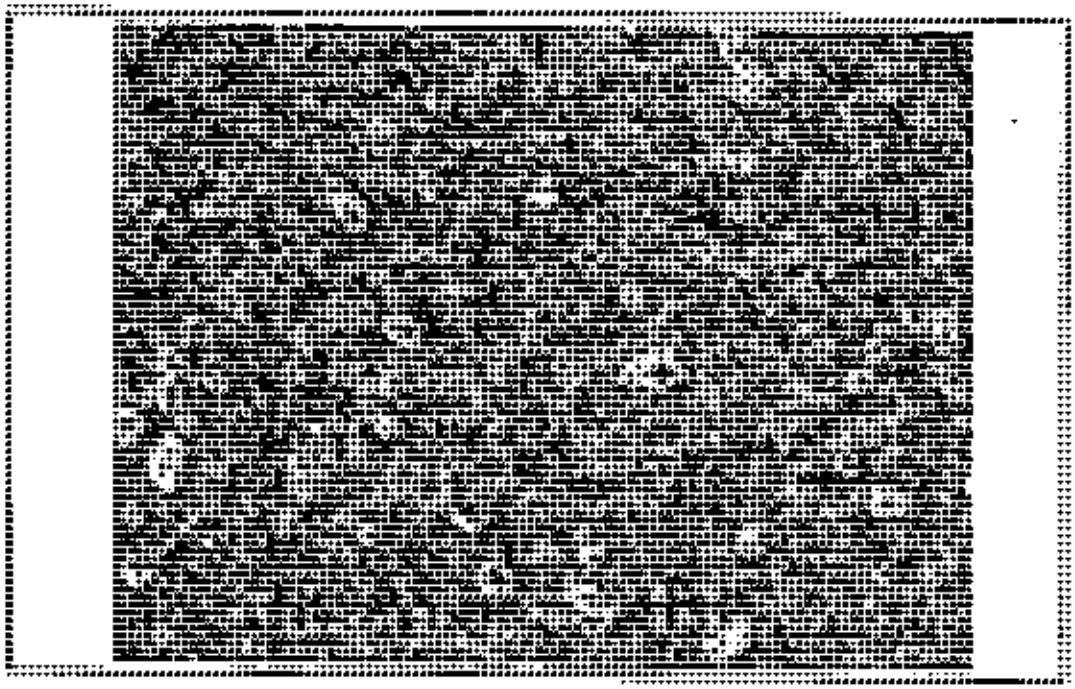

Figure 4-2 SEM Micrograph of un etched $BaTiO_3$

and the microstructure shown in Figure 4-4. Fully sintered grains are surrounded by loose particles that make up the pores. Un-reacted powder might be BaO and Ba_2TiO_4 that are soluble in concentrated HCl but not $BaTiO_3$. This can be explained as during etching the un-reacted powder were leached away leaving a spongy structure while $BaTiO_3$ remained intact. There was no doping in this sample.

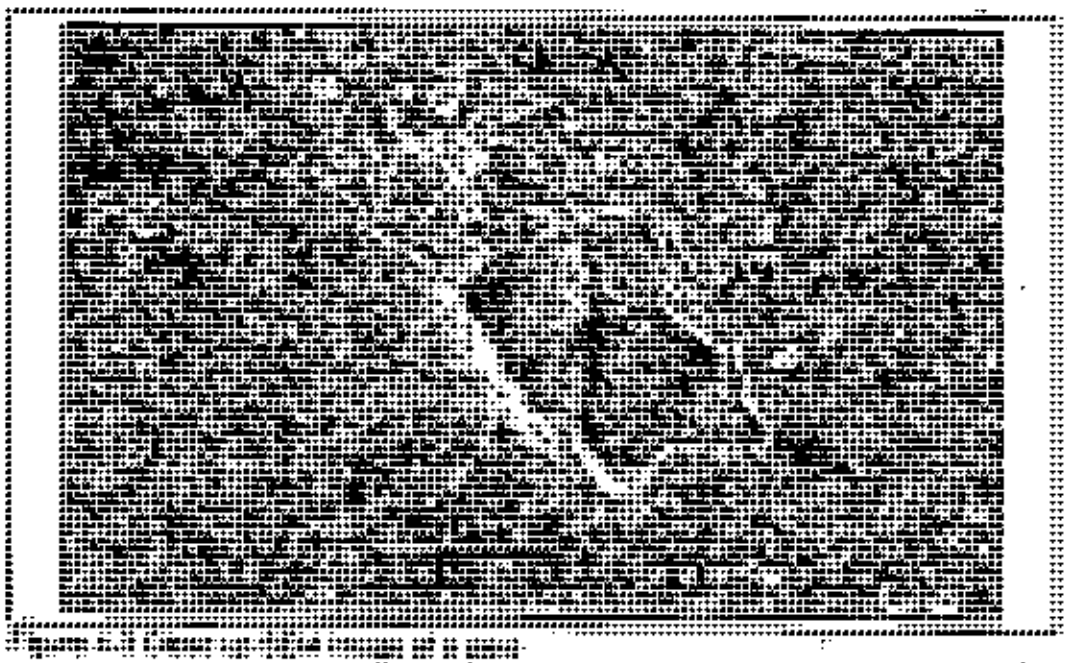

Apart from BaO and Ba_2TiO_4 other contamination might have accelerated this leaching process. There are sufficient evidence of contamination present in set A sample; this would be discussed in following section. From Table 4-3, comparison of densities of P samples of set A sintered at different temperature indicate the effect of sintering temperature on density as these samples were calcined under identical conditions. However, this is not the case for the samples of batch E-M, EI-M and EII-M of set B. Sample E-M was calcined at 900°C for 3hrs and sintered at 1300°C for 3hrs whereas EI-M was calcined at 1000°C for 2hrs and sintered 1250°C for 1hrs but the density was almost the same, about 85% of TD. On the other hand, the calcination thermal profile of EI-M and EII-M was identical but EII-M was sintered at 1350°C for half an hour yet its density was almost 92% of TD. Calcination temperature and time governed the final density of the material in this case. Dense material can be prepared sintering at lower temperature for long time or high temperature for short time provided the calcination temperature was high and soak time was longer. This condition fulfills the heat requirement criteria for solid-state reaction, forming $BaTiO_3$. Hence, eliminate gas formation, volume change etc. leading to pores and cracks.

XRD examination also supports this conclusion. XRD pattern of milled mixture of powder shown in Figure 4-5 confirm the presence $BaCO_3$ and TiO_2 in mixed state. XRD pattern of the same powder was calcined at 900°C for 3h was super-

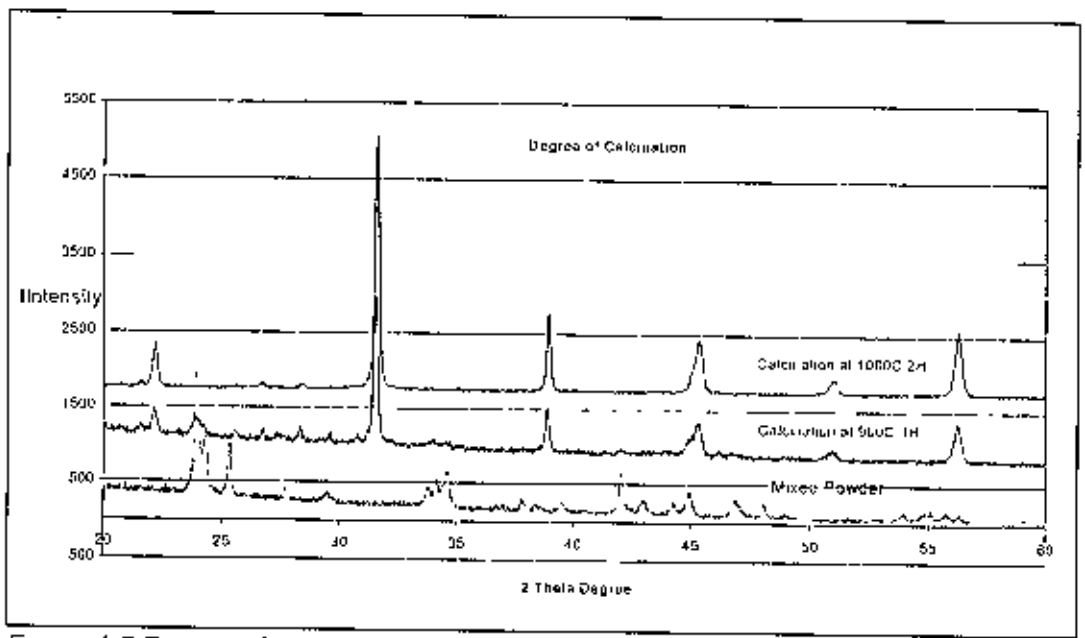

Figure 4-5 Degree of calcination in terms of $BaTiO_3$ formation

imposed above the mixed powder pattern showing the formation of $BaTiO_3$ but still enough un-reacted $BaCO_3$ and TiO_2 is present. These peaks owing to un-reacted powder are absent in the XRD pattern (the top one in the figure) of powder of identical composition calcined at 1000°C for 2 hours. This sample (EII-M) was sintered at 1350°C for half an hour; formed sintered body density of 92% of TD. The dielectric properties are better for this sample as discussed in later section.

4.2.2 Thermal Profile

The physical appearance of the sintered body summarized in Table 4-4 below.

Table 4-4 Physical appearance of sintered body

		Sintering		Physical Quality of sintered body			
Set	Batch	°C	Hrs	P	Q	R	S
A	B – I	1225	3	Ash brown stain on substrate	Olive / ash some cracked, staining	Olive some cracked, staining	Ash no stain
	B – II	1200	3	lighter stain than B-I	lighter stain than B-I	lighter stain than B-I	no stain
	B – III	1300	1	green brown stain	brown stain, broken, stuck with substrate	stain, broken, stuck with substrate	stain on substrate
B	E – M	1300	3	light brown	Ca Doped sample was not prepared		
	E – B	1300	3	light cream			
	EI – M	1250	1	light brown			
	EI – B	1250	1	light cream			
	EII – M	1350	0.5	light brown			
C	B – IV	1325	2.5	biscuit colour no stick substrate	Partial stick to substrate	Partial stick to substrate	Partial stick to substrate
D	B – V	1350	4	biscuit colour no stick substrate	not prepared	biscuit colour partial melt stick with substrate	light biscuit colour fused and stick with substrate

Brown coloured staining on the substrate during sintering of set A samples were unusual for $BaTiO_3$ ceramics, some sample even stick with the alumina substrate and cracked, as shown in Figure 4-6. Sample E-B and EI-B were prepared using identical powder source yet there was no staining or crack on these samples. However, these samples did not sinter to even 75% of TD. So, the staining and discolouration must had resulted from either powder or the processing. Set A samples were milled

with steel balls in distilled water media (Table 3-3) whereas others sets were with zirconia and acetone. $BaCO_3$ forms $Ba(OH)_2$ through tribochemical reaction with water during milling. Furthermore, reactive compound CaO was added as a source of Ca. During milling iron balls certainly reacted in this strong alkaline environment forming iron hydroxide. Set A was calcined three times and milled subsequently which increased iron contamination successively. This iron and possibly with other contaminates reacted with $BaCO_3$, TiO_2 and $BaTiO_3$ during calcination forming different phase or doping modification of the $BaTiO_3$. Discoloration of green samples (pallets) does suggest inclusion of impurities during milling process.

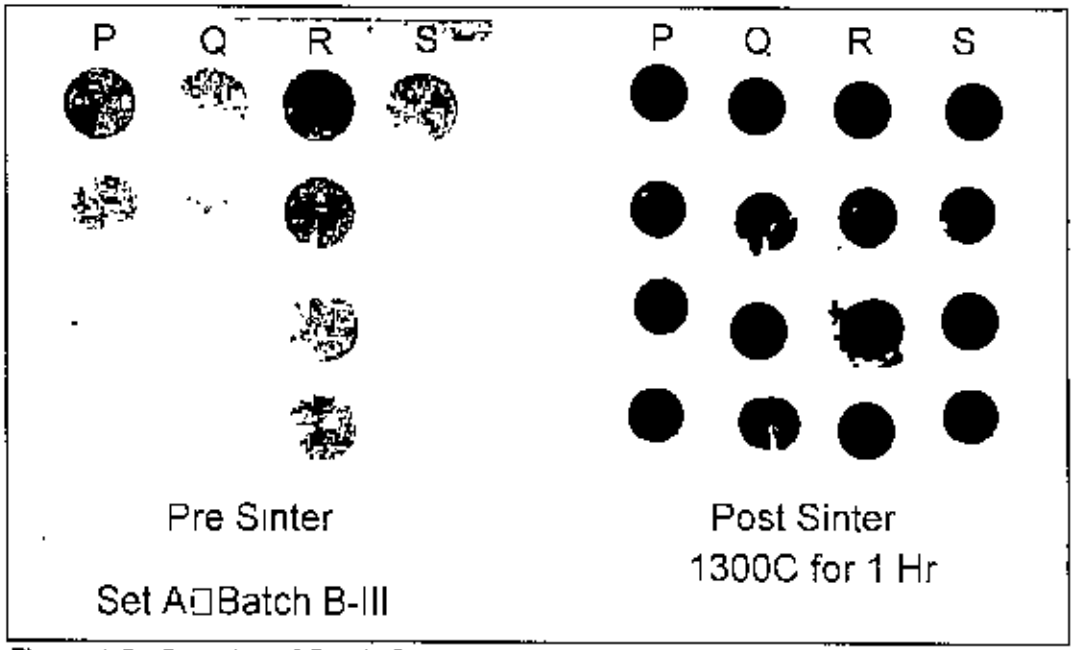

Figure 4-6 : Samples of Set A, Batch B-III, pre and post sinter state

In Figure 4-6, the physical appearance of pallets before and after the sintering is shown. Ca doping should not have changed the colour of green pallets but as seen in the left side of the Figure 4-6, the colour of batch R and P were gray compared to R and S. Physical state of sintered pallets are shown on the right hand side of the Figure 4-6. Sample were cracked, shattered and stained the substrate.

Sintered density difference between Set A and E-B & EI-B indicate that these impurities acted as sintering aid. Level of inclusion was uncertain and uncontrolled Effect of this can be seen in the variation of densities in Set A that did not follow a clear pattern in accordance with sintering temperature and time.

4.2.3 Ca Doping

Pattern of physical appearance and density from Table 4-3 and 4-4 suggest that the Ca doping also affect the density to a certain degree. For instance, relative density is higher for doping level 5% and 12% mole but lower for 8% mole. The same pattern observed for Set A and C. Ca doping effect on density is illustrated graphically in Figure 4-7. However, it was reported [45] that the dielectric property change with the concentration of Ca doping following this pattern. This effect is much pronounced for the sample sintered at relatively higher temperature and longer time. Confident result was reflected from sample with density above 90%. The density curve of B-IV sintered at 1325°C for 2.5hrs might be considered as an ideal.

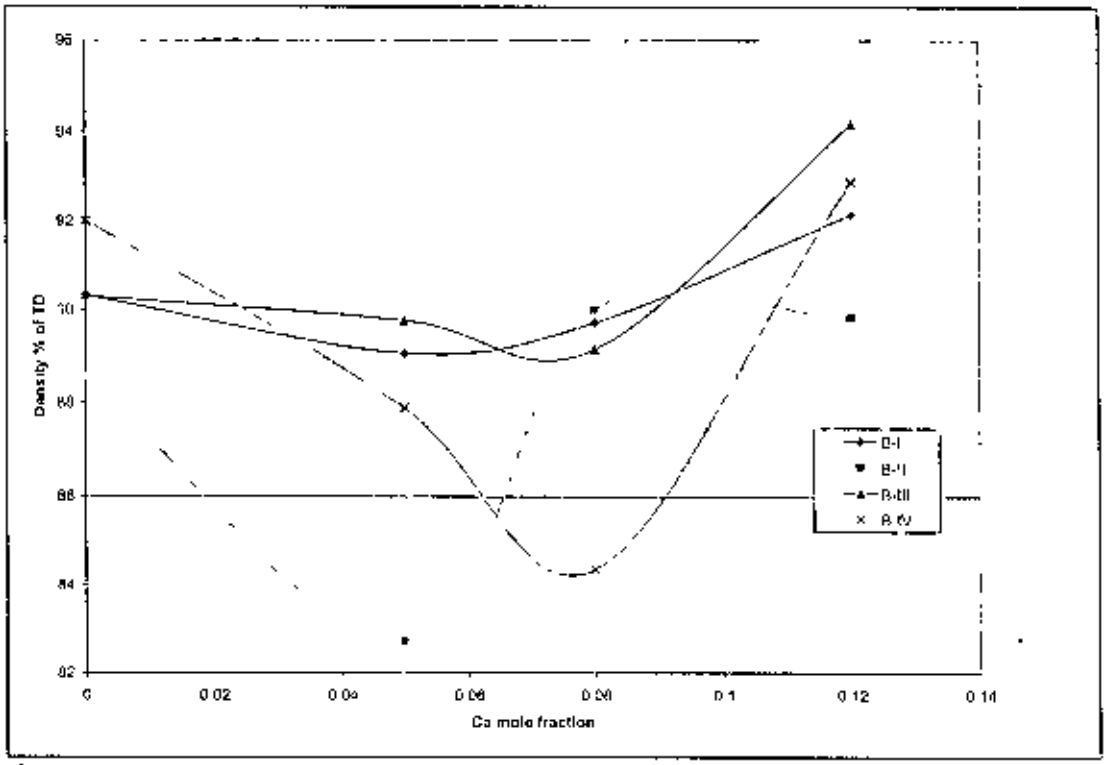

Figure 4-7 : Ca doping effect on density

4.2.4 Raw powder

Following identical processing, the sample of batch E-B and EI-B did not even attain 75% of TD whereas E-M and EI-M did. The only difference between these batches was the raw powder source. Powders of both sources were investigated using XRD and compared, shown in Figure 4-8 and 4-9 for $BaCO_3$ and TiO_2 respectively. Both TiO_2 used were anatase and almost identical but the twin peaks at around 55° are much resolved for MTEC powder than MME powder. The $BaCO_3$ powder seems to differ crystallographically. MTEC $BaCO_3$ matched with PDF# 45-1471 while MME $BaCO_3$

with PDF# 05-0378. The colour of MME TiO_2 was pale and MTEC was white. The same colour difference was observed in $BaCO_3$ also. Impurity level below 2% is difficult to identify in XRD very accurately. X Ray Florescence (XRF) is needed to confirm quantitative elemental analysis. Another significant impurity (as declared by the manufacturer) in $BaCO_3$ of MTEC source was ~1.5% Sr. This might have aided sintering of E-M, EI-M and EII-M samples. The Ba/Ti molar fractions of un-doped sample are given in Table 4-5. The Ba/Ti ratio of E-B was higher compared to the sample E-M and EII-M. The effect of Ba/Ti ratio variation studied by Lee *et al* [12] showed that excess Ti causing better densification and excess Ba inhibiting grain growth.

Table 4-5 Ba/Ti molar fraction of the un-doped series P samples

E-M	E-B	EII-M	B-IV	B-V
0.9896	1.0046	0.9998	1.0005	1.0091

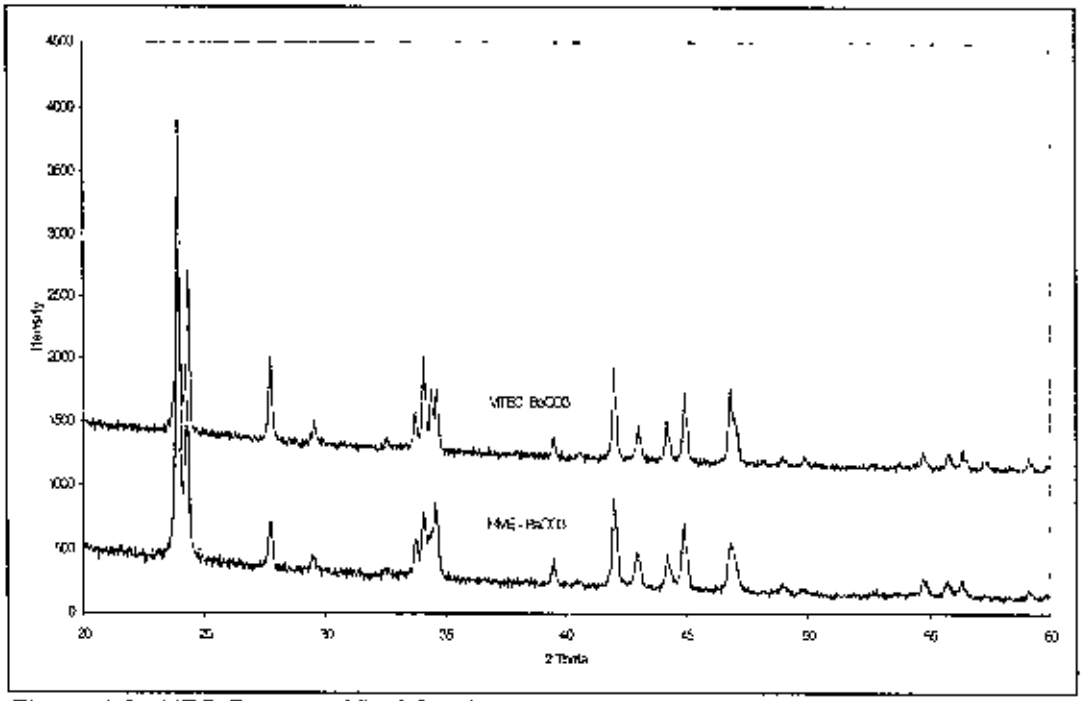

Figure 4-8 : XRD Pattern of $BaCO_3$ of MME and MTEC source

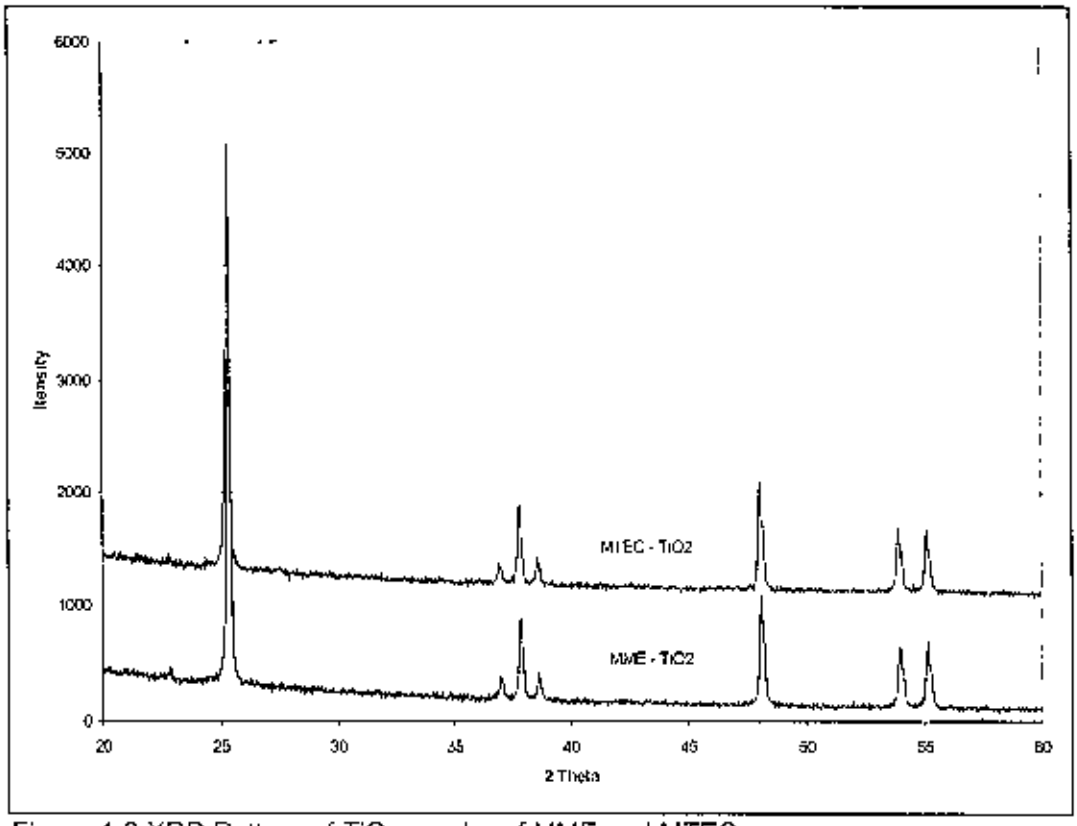

Figure 4-9 XRD Pattern of TiO_2 powder of MME and MTEC

4.2.5 TGA Analysis

Some samples developed crack during sintering and excessive pores leading decreased density. The evaporation or burn out characteristics of PVA (binder) was examined and result shown in Figure 4-10. The sample was of batch EII-M.

It was observed from the graph that large mass loss occurred at about 90°C. This is due to moisture evaporation as PVA used was as solution in water. The second loss is rather gradual from 220°C to 400°C, attributed to the burn out of PVA. Still the sample was losing weight up the test temperature of 850°C. This suggests as mentioned earlier, the incomplete reaction during calcination. This weight loss beyond 400°C is due to calcination reaction of un-reacted particles from the previous calcination step. The holding temperature was increased to 550°C and slower heat rate was used for sintering. However, no significant effect was observed. Crack developed only in doped sample of Set A which might have resulted from impurities

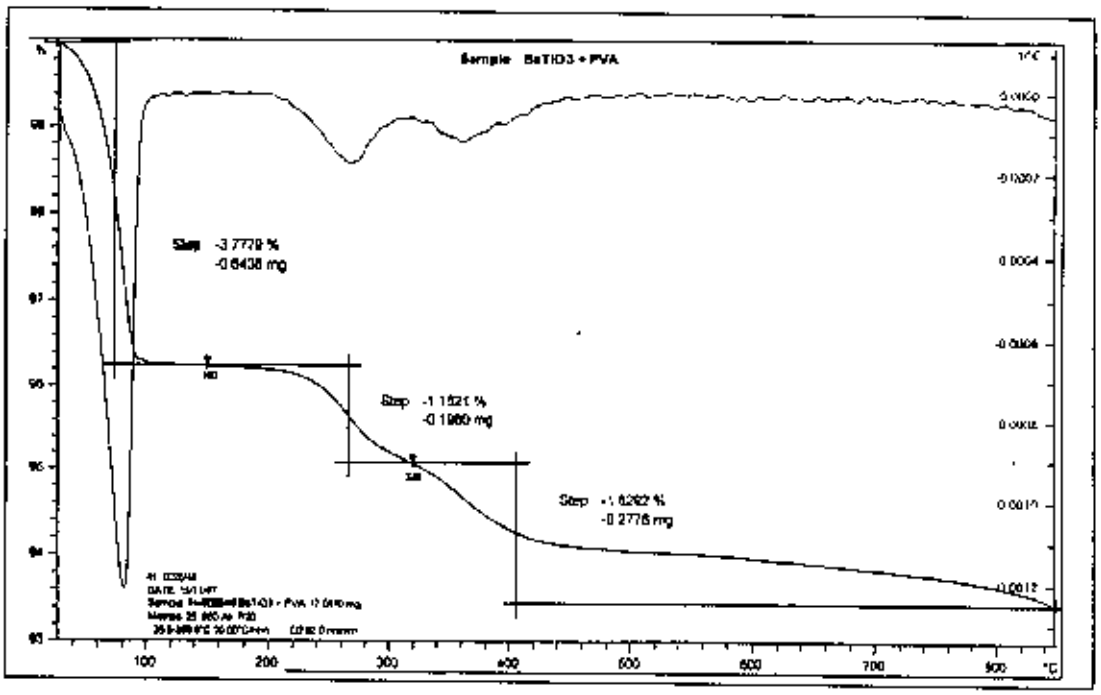

Figure 4-10 TGA analysis of pre sintered powder mixed with PAV

4.3 Dielectric Properties

4.3.1 Set A

Five samples of each batch were progressively heated to the test temperatures simultaneously in the heating chamber and electrical property were measured. The average of these five samples' dielectric constant and tangent loss are plotted in the following Figures (4-11 to 4-18) Temperature dependence of electrical properties presented in these graphs is at a fixed frequency of 100kHz. Densities, in terms of percentage of TD, of the samples are indicated on the corresponding curves in the graphs. Frequency dependence of electrical properties at 60°C is also shown in Figure 4-19 to 4-22. All the curves were plotted using smoothing technique based on moving point average in *EXCEL* spreadsheet.

Universally accepted Tc of $BaTiO_3$ is 120°C but in this study samples of P, Q and R series showed Tc at around 55°C. This was unexpected and surprising. Ca doping was not reported to decrease Tc that much At least un-doped sample should have shown Tc at around 120°C. Apart from doping concentration difference, all samples of set A under gone identical processing except sintering temperature profile

Hence, the degree of calcination reaction does not arise. The only significant factor was the impurity inclusion during processing, as mentioned earlier. This impurity made the transition affect smooth or hump shape over a broad temperature range, rather than sharp change at Tc. There is however, a small peak observed at ~125°C for the samples sintered at 1225°C for 3hours. This peak is absent for other sample of the same series and also in the samples of other batches. Samples of batch B-1 were tested to 175°C while others were to 120°C. Peak of this kind might had been beyond temperature of 120°C. These two peaks at 55°C and 125°C indicate the presence of two distinctive phases. It seem that the impurities formed different phase along with $BaTiO_3$, not substituting any constituents of $BaTiO_3$ or forming solid solution, as expected the doping would have.

In general, k' were higher for denser sample of the same batch. Highest k' value recorded was for the un-doped sample of batch B-I sintered at 1300°C for 1hr. The k' value was 4510 and the density was 90.3% of the TD. The transitional peak (hump) are relatively shaper for denser sample also. Highest transition temperature of around 100°C recorded was for series S (Ca x= 0.12) samples, (Figure 4-18) while for others were about 55°C.

From Figure 4-19 to 4-22, it can be seen that within the frequency range of 1kHz to 100kHz the k' are almost constant and a slight increasing trend towards 1MHz range for all samples of the set. The same frequency dependence has been observed for the loss tangent also. The loss was almost constant with in the frequency range of 1kHz to 100kHz than a slight increasing trend to wards 1MHz range. This increasing trend however, increased as the Ca concentration increased

Dielectric loss is related to the homogeneity of the material. This pattern was observed in the sample of set A as shown in Figure 4-12, 4-14, 4-16 and 4-18. Loss tangent was low with in the test temperature for sample with density >= 90% of TD. No loss peak was observed except for the un-doped sample sintered at 1200°C with density of 88.5% of TD. This peak was at ~100°C. At the transition temperature loss tangent seem to increase following the pattern of k' especially for doped S series samples. The curve of loss tangent of series S was uniform i.e. bell shaped about the transition temperature. The density was also about ~90% for this series. Loss peak at phase transition is normal due to disorder in the lattice. For other doped samples the loss characteristics was not consistent.

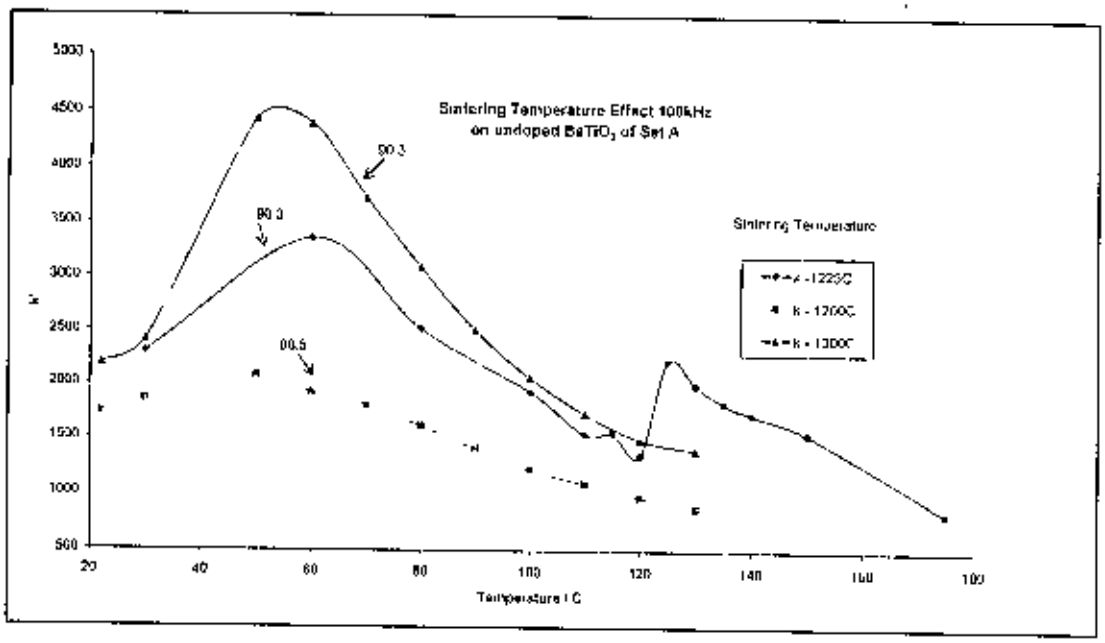

Figure 4-11 : Dielectric constant as function of temperature for $BaTiO_3$ (un-doped - P)

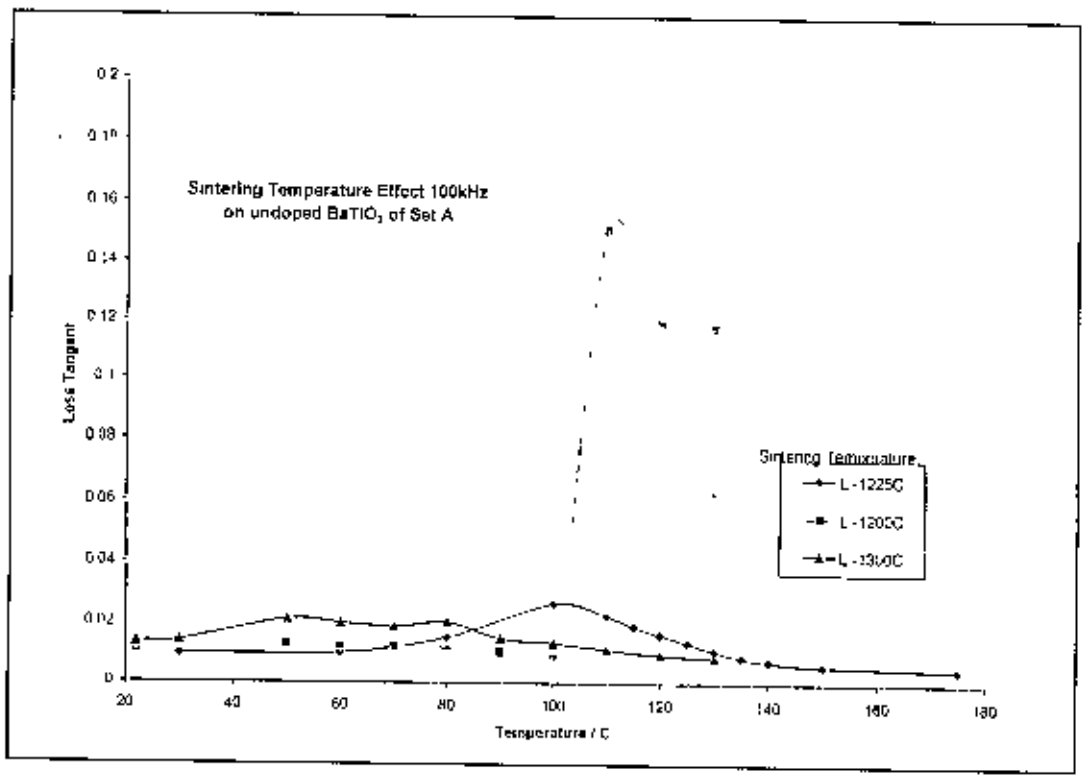

Figure 4-12 :Tangent Loss as function of temperature for $BaTiO_3$ (un-doped - P)

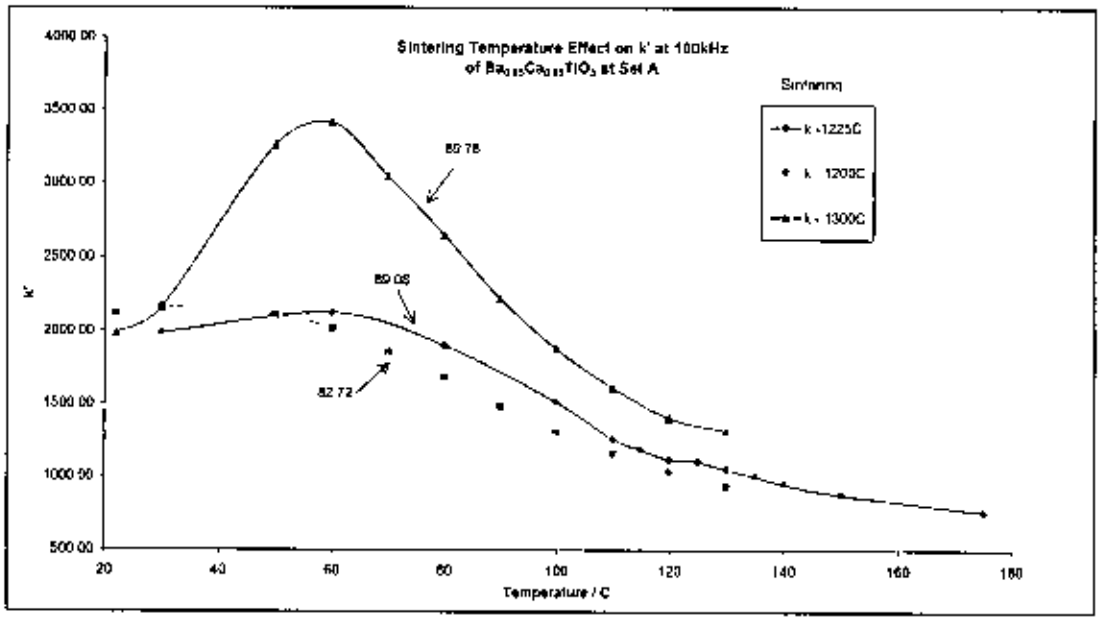

Figure 4-13 : k' as function of temperature for BaTiO3 (Ca doped x=0.05 - Q)

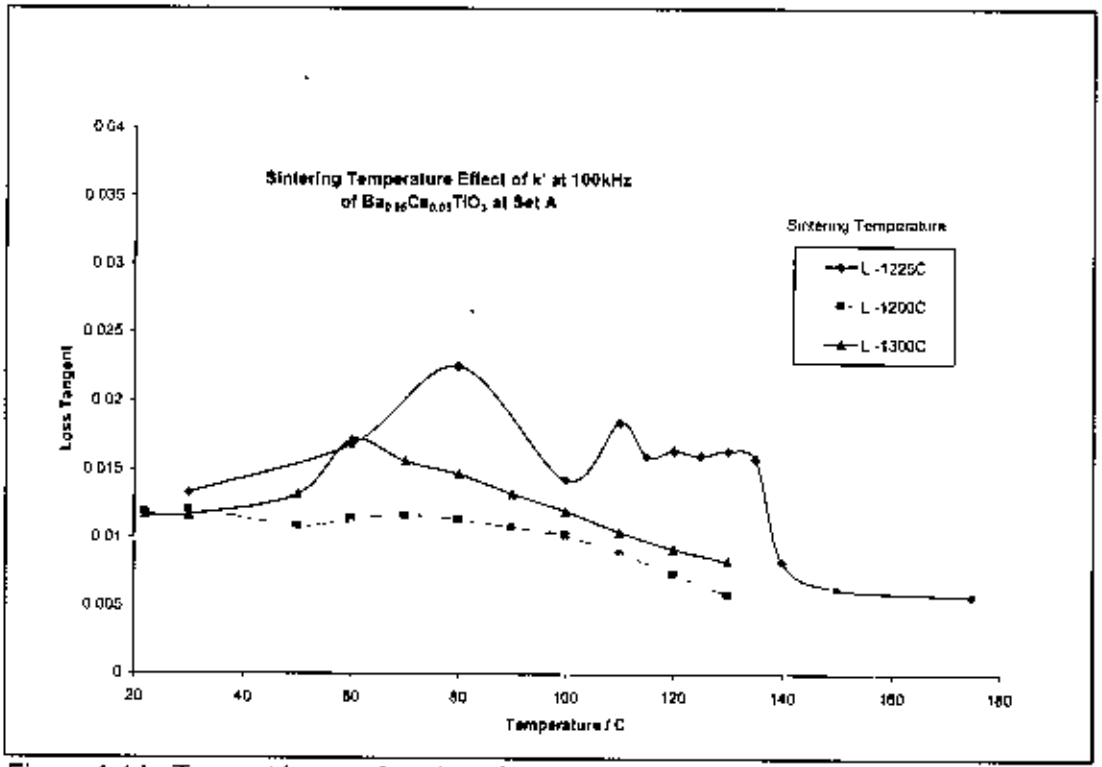

Figure 4-14 : Tangent loss as function of temperature for BaTiO3 (Ca x=0.08 - Q)

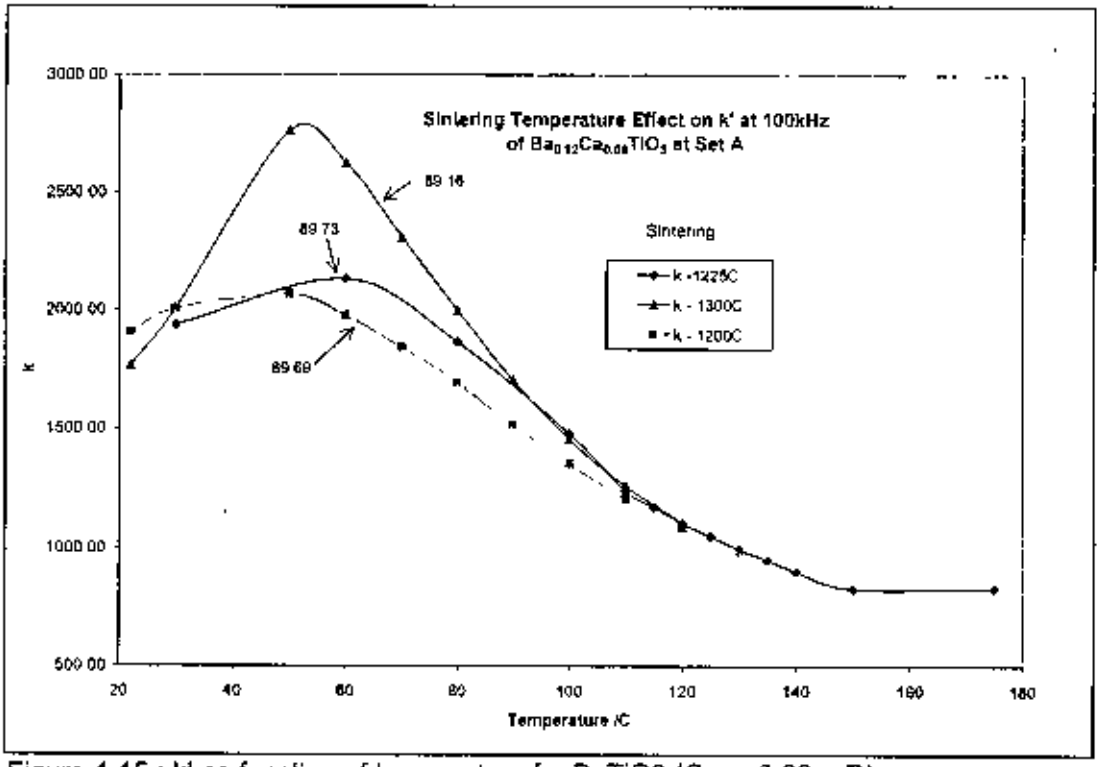

Figure 4-15 : k' as function of temperature for BaTiO3 (Ca x=0.08 - R)

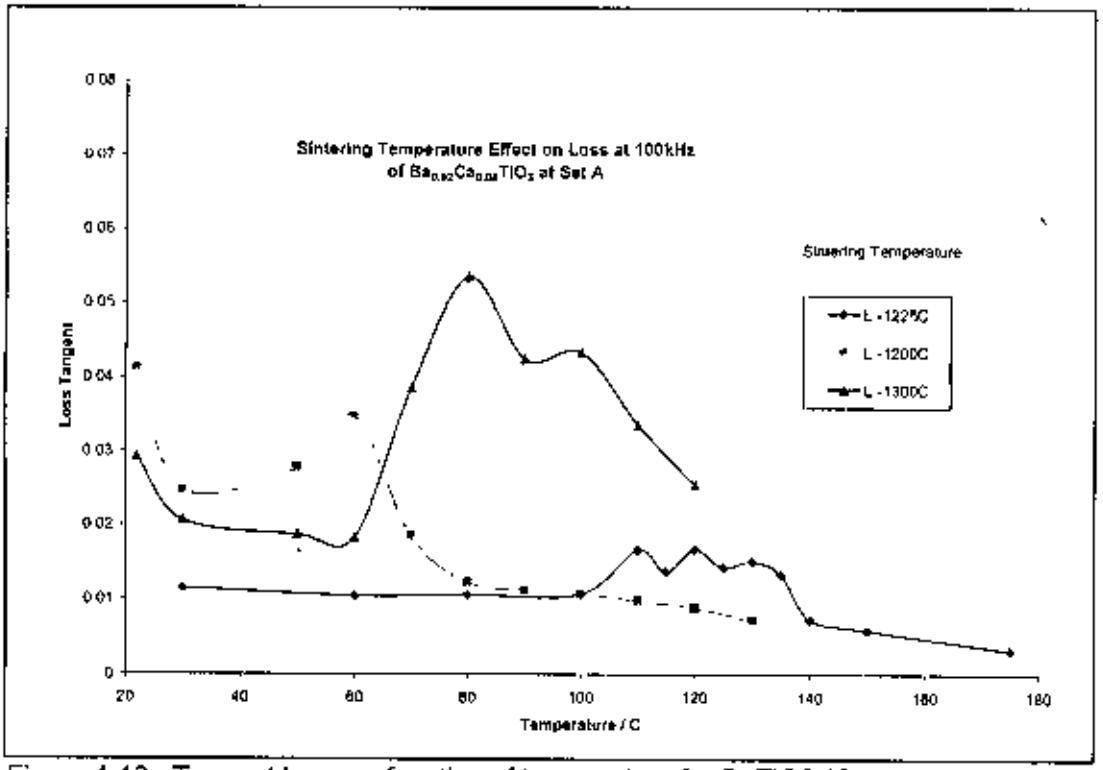

Figure 4-16 : Tangent Loss as function of temperature for BaTiO3 (Ca x=0.08 - R)

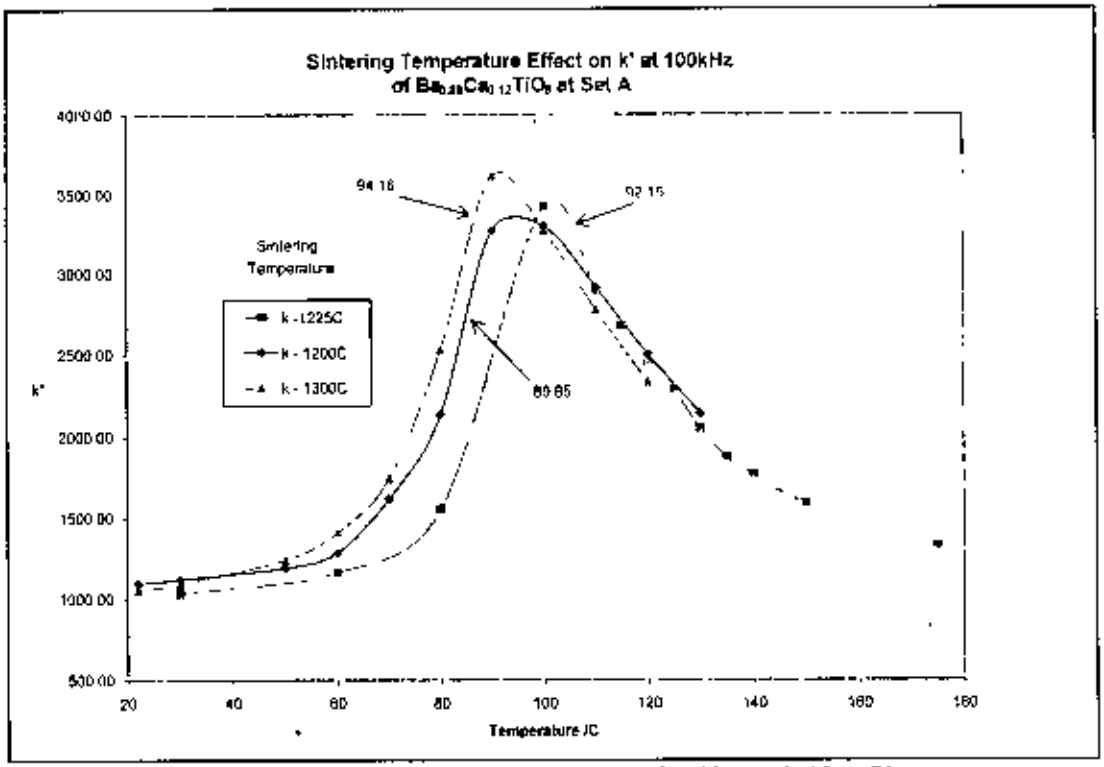

Figure 4-17 : k' as function of temperature for BaTiO3 (Ca x=0.12 - S)

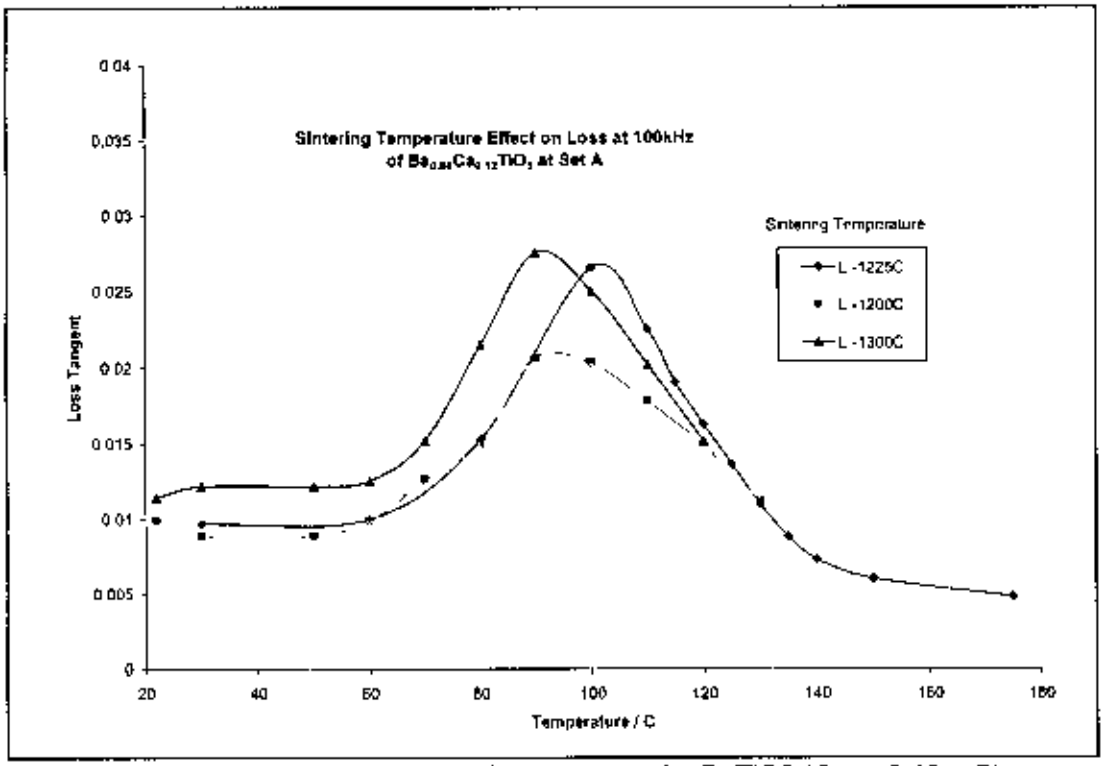

Figure 4-18 Tangent loss as function of temperature for BaTiO3 (Ca x=0.12 - S)

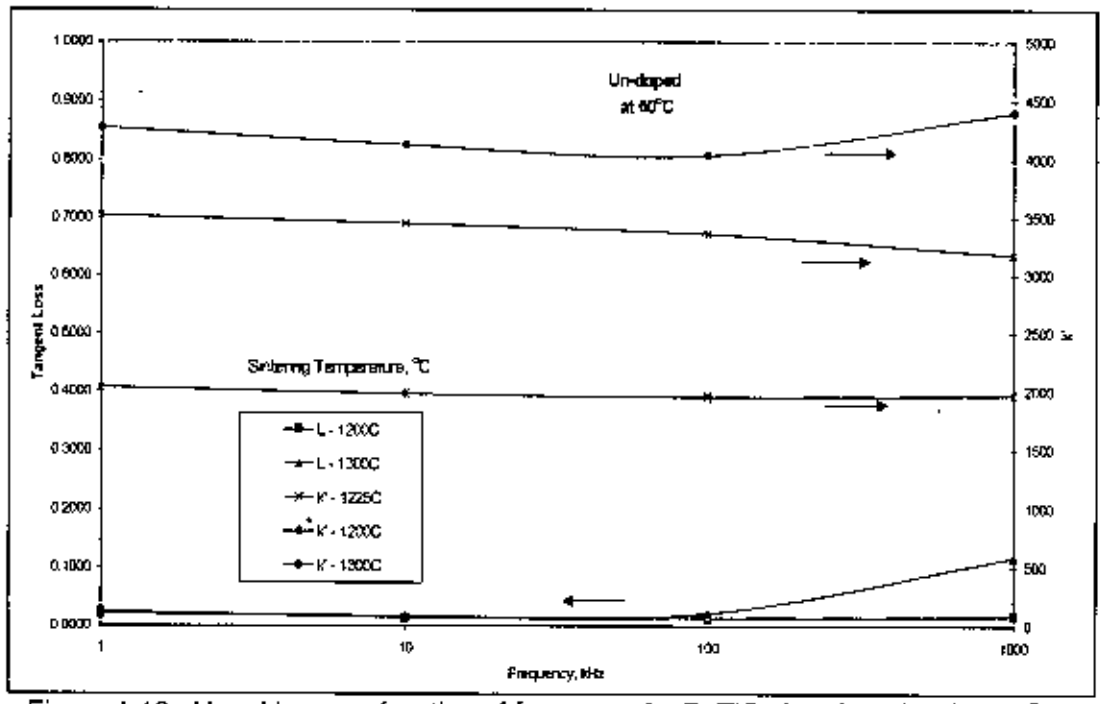

Figure 4-19 : k' and Loss as function of frequency for $BaTiO_3$ (un-doped - P) at 60°C

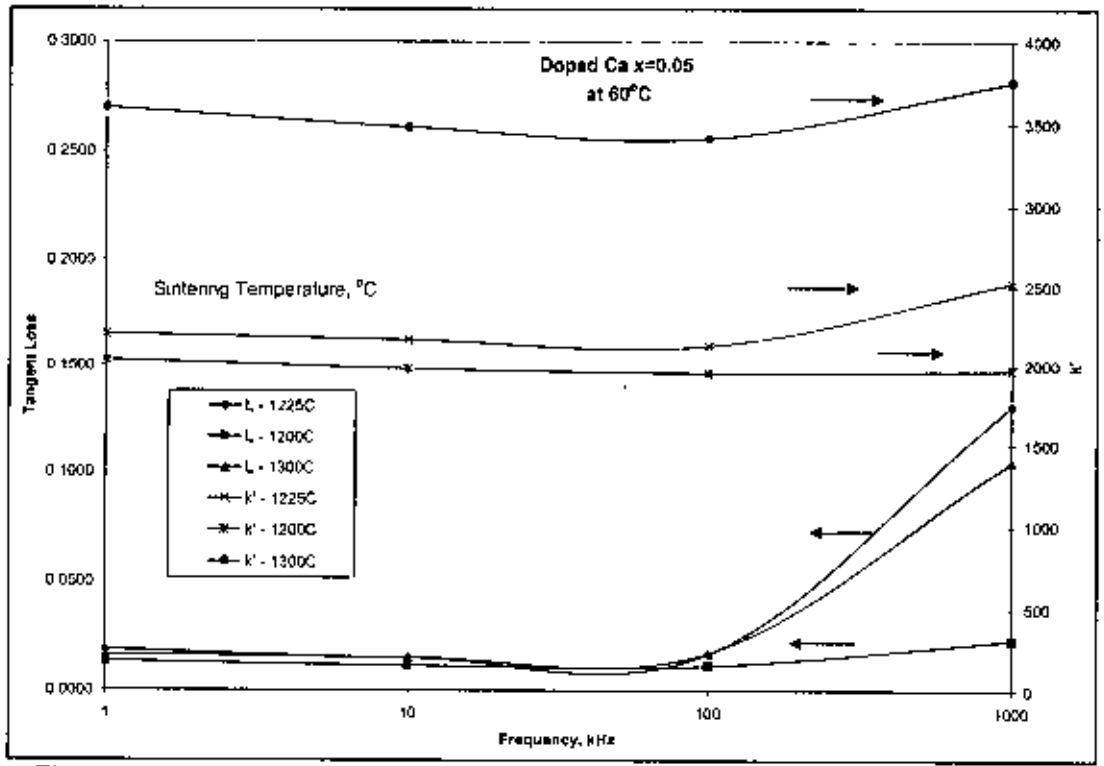

Figure 4-20 : k' and Loss as function of frequency for $BaTiO_3$ (Doped - Q) at 60°C

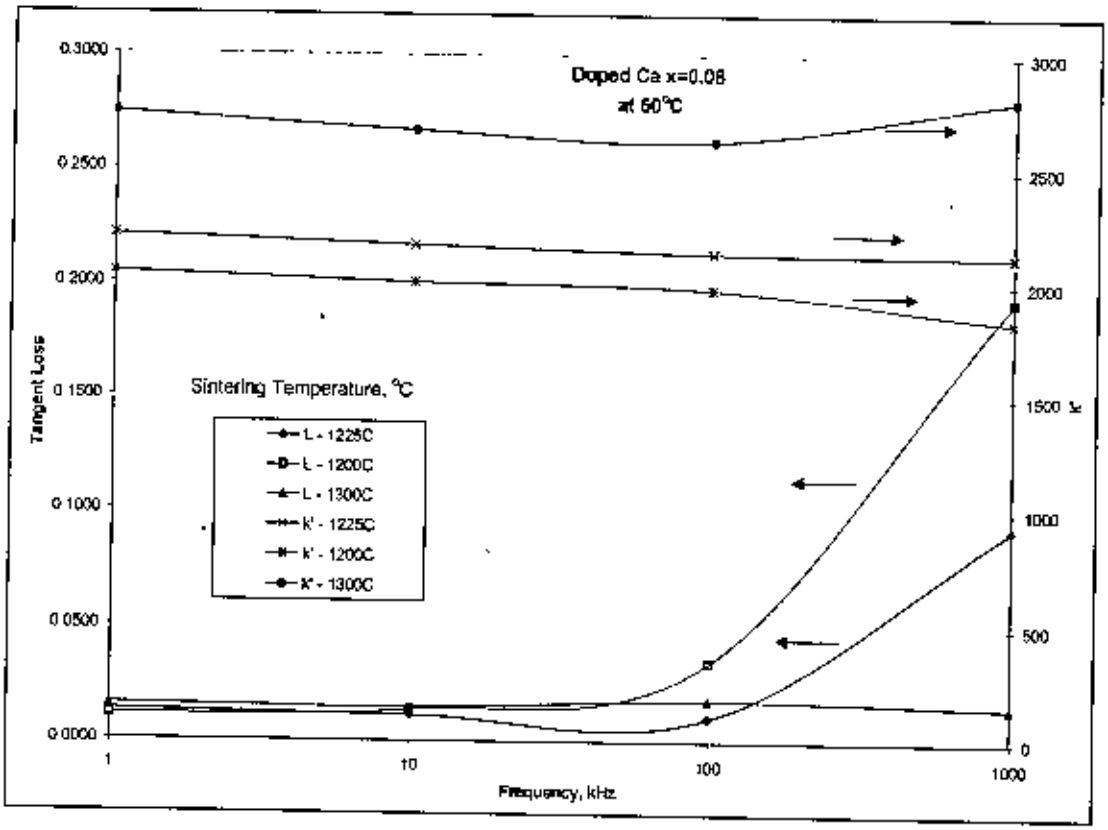

Figure 4-21 : k' and Loss as function of frequency for $BaTiO_3$ (Doped - R) at 60°C

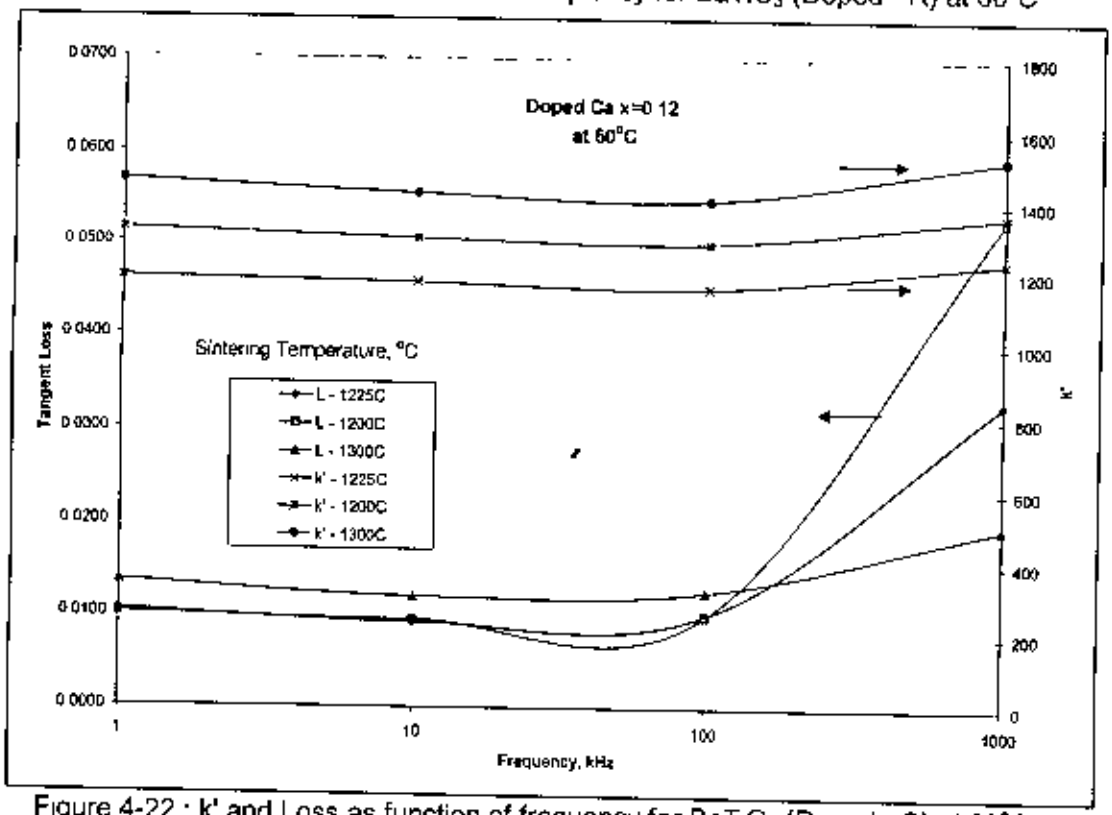

Figure 4-22 : k' and Loss as function of frequency for $BaTiO_3$ (Doped - S) at 60°C

4.3.1.1 Ca Doping

The variation of k' on Ca doping concentration illustrated in Figure 4-23 for samples sintered at 1300°C shows a distinctive trend. It is apparent from the graph, increased Ca doping concentration up to a certain level, lowered the k' value over the whole test temperature range. This trend seem to change for Ca doping concentration above 0.08mole fraction where k' value started to increase and Tc shifted from 55°C to 90°C. The variation of k' with the Ca doping concentration were plotted in Figure 4-24 for three batches of samples of this set. The same trend was also observed. It is apparent from the curves in Figure 4-24 that minima of Ca doping concentration exist.

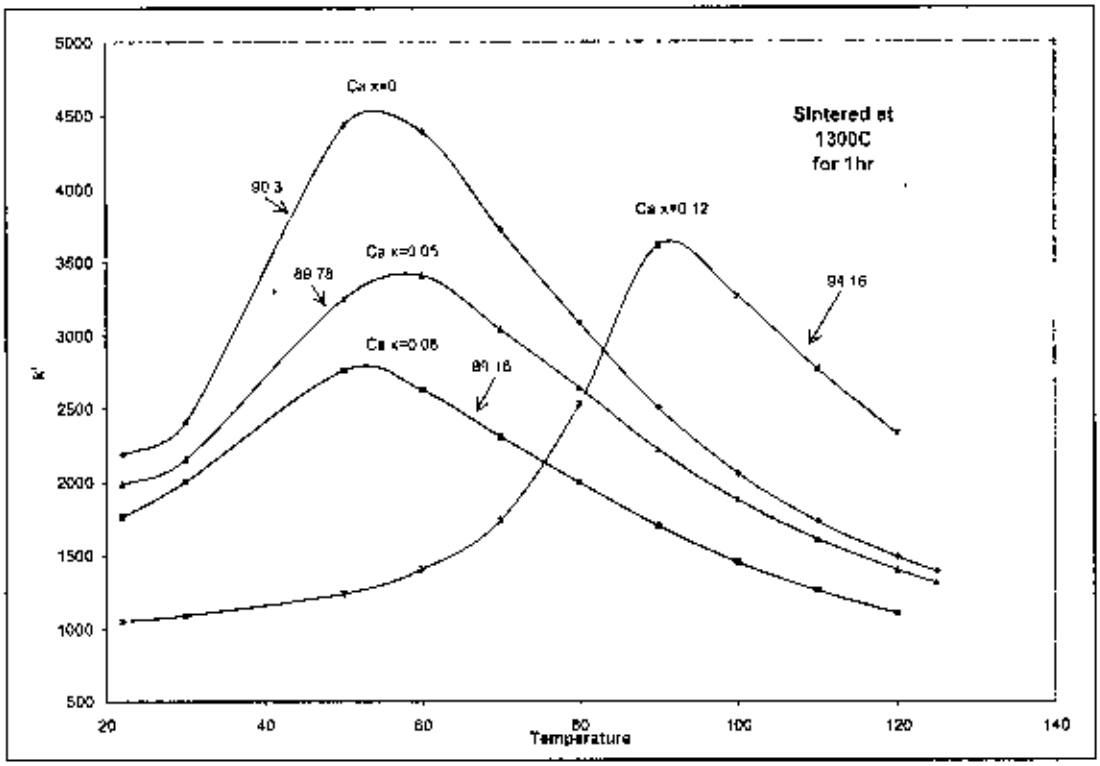

Figure 4-23 : Effect fo Ca doping for samples sintered at 1300C

Dielectric constant tends to decrease to that point, and beyond that start to increase This point is observed to be at 0.07mole fraction of Ca. Regard less of sintering temperature and density the doped samples follow this trend. This effect cannot be attributed to the density apparent from the graph. Doped samples of Q (0.05) and R (0.08) had densities almost identical, yet this effect was there. The difference of density reflected in offsetting the curve only This non-linear relation seems to be an intrinsic property of Ca doping in $BaTiO_3$ ceramics. Even with the impurity in the sample, the effect is pronounced. The effect was also reported [45] earlier and this point was suggested to be around 0.08mole fraction.

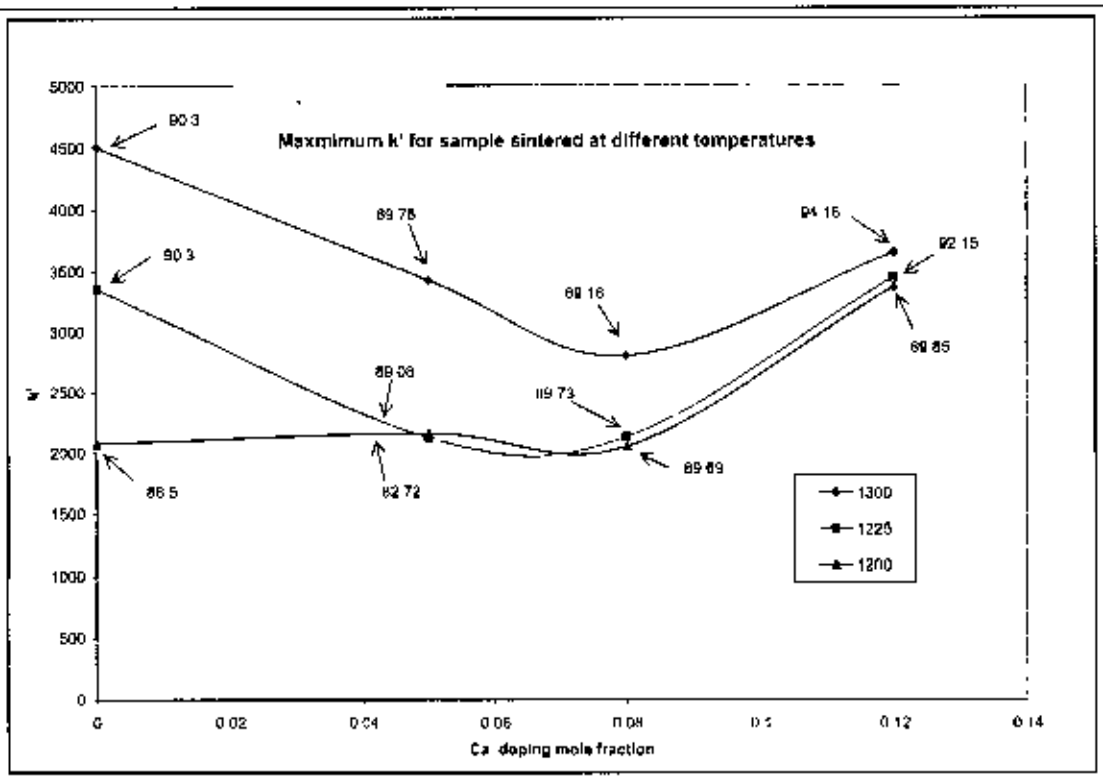

Figure 4-24 : Ca doping effect on k' at different sintering temperatures

The origin of this effect might be in the crystal structure of the sample. Un-doped and doped (x=0.12) samples of B-I and B-II were examined using XRD to identify phases present and lattice parameters. XRD patterns was taken from the polished sintered sample and shown in Figure 4-25 to Figure 4-28 at room temperature. At this temperature, expected crystal structure is tetragonal. The identification of tetragonal lattice is the twin peak resulting from the close values of lattice parameter *a* and *c*. As per JCPDS standard, attached in appendix 7-7, for tetragonal $BaTiO_3$ {PDF# 05-0626} five sets of twin peaks exist with in the scan range (20° to 60°) in this experiment. Underneath each pattern of the sample, the standard pattern of $BaTiO_3$ and $BaFeO_{3-x}$ {PDF# 23-1023} are also attached indicating the line position and relative intensities of respective line. The first twin for (001) and (100) has angular difference only 0.224° that would be difficult to resolve at lower angle about 22°. The second twin is also not resolved according to standard. Third and fifth twin peaks must be resolved due to angular difference of 0.522° and 0.298° respectively at such higher angle and intensity. Twin peak separation was reported [37] as degree of tetragonal $BaTiO_3$ formation during calcination and discussed in section 2.4.1.1.

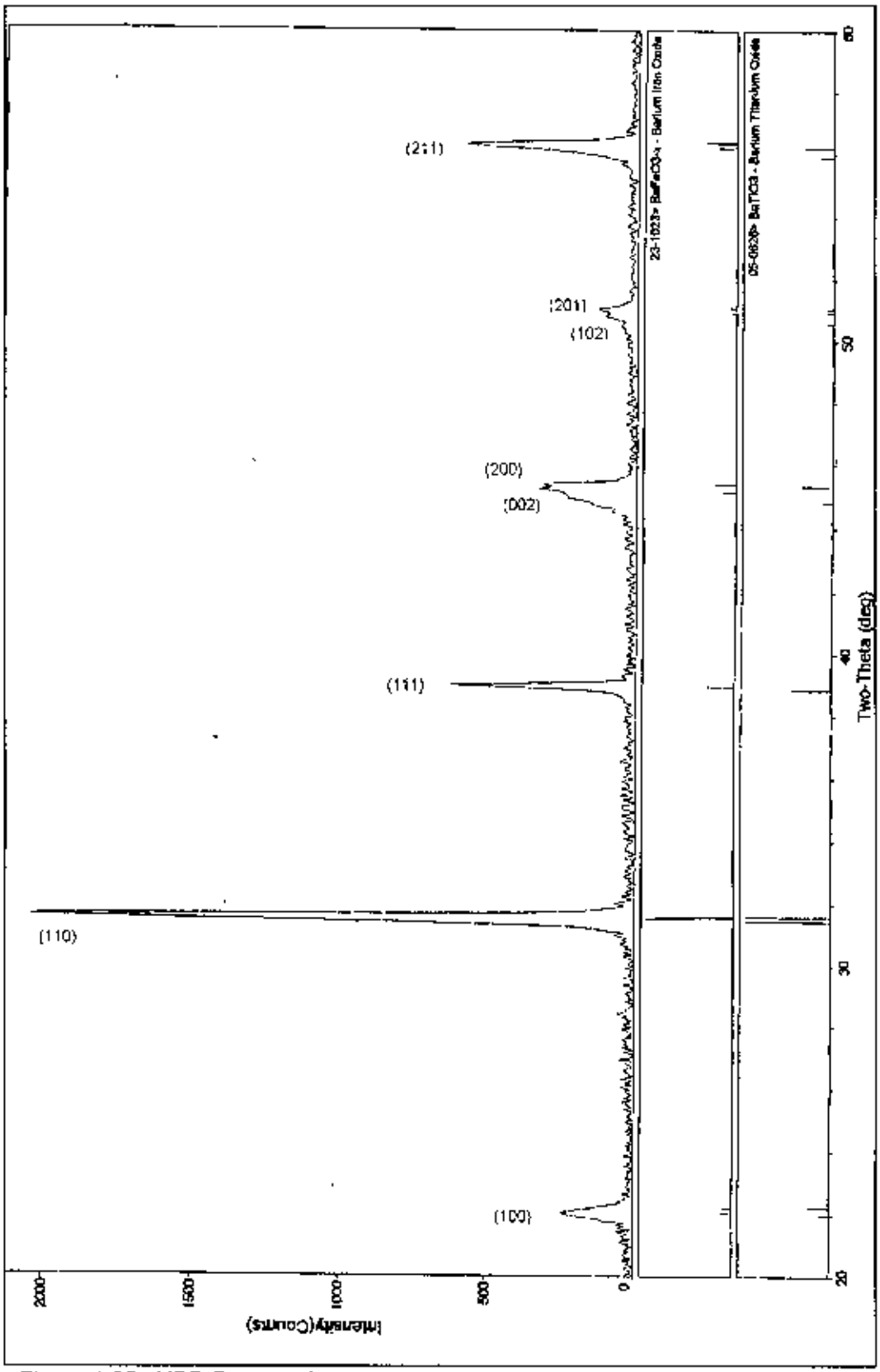

Figure 4-25 : XRD Pattern of un-doped sample of B-I

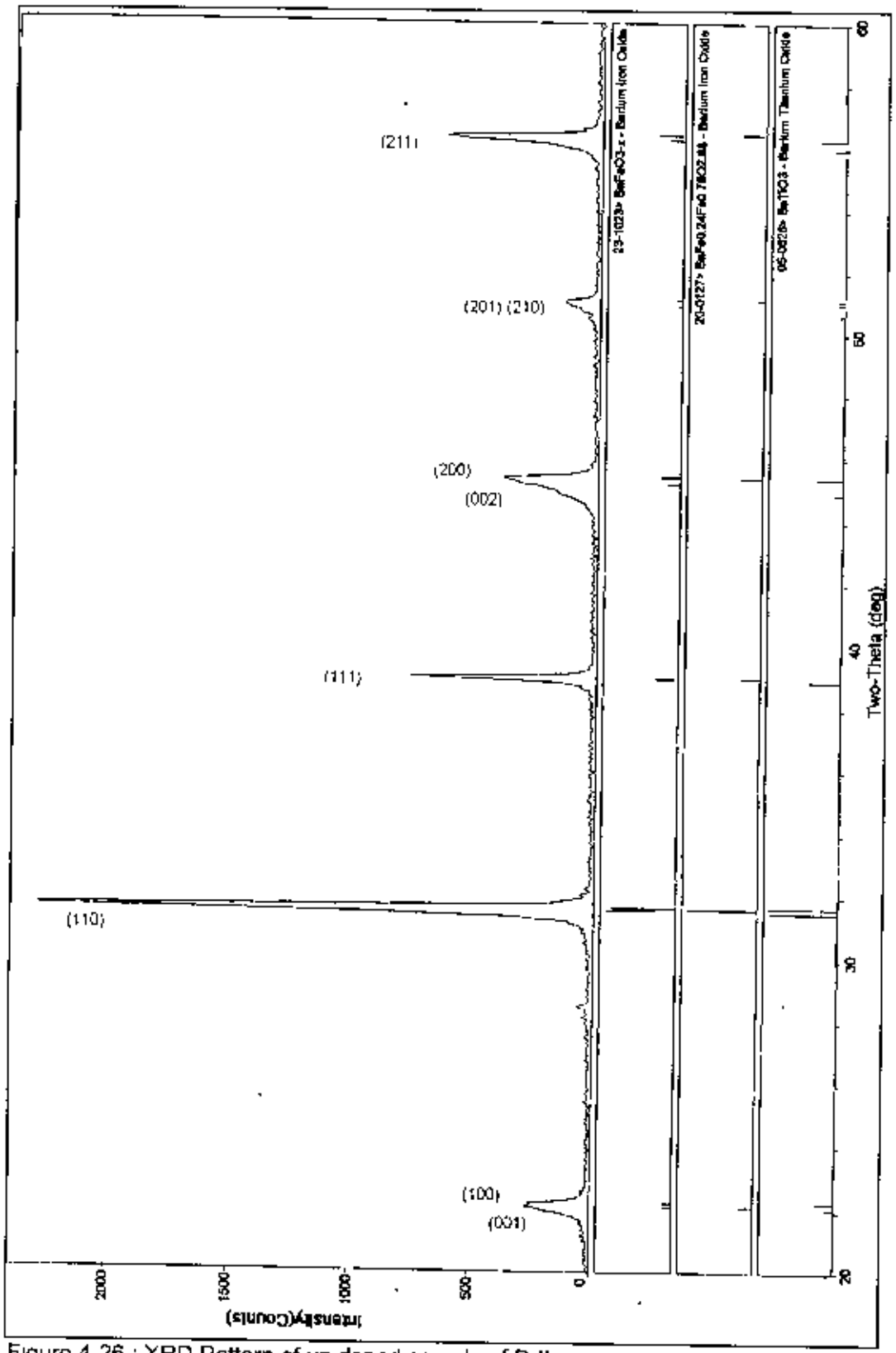

Figure 4-26 : XRD Pattern of un doped sample of B-II

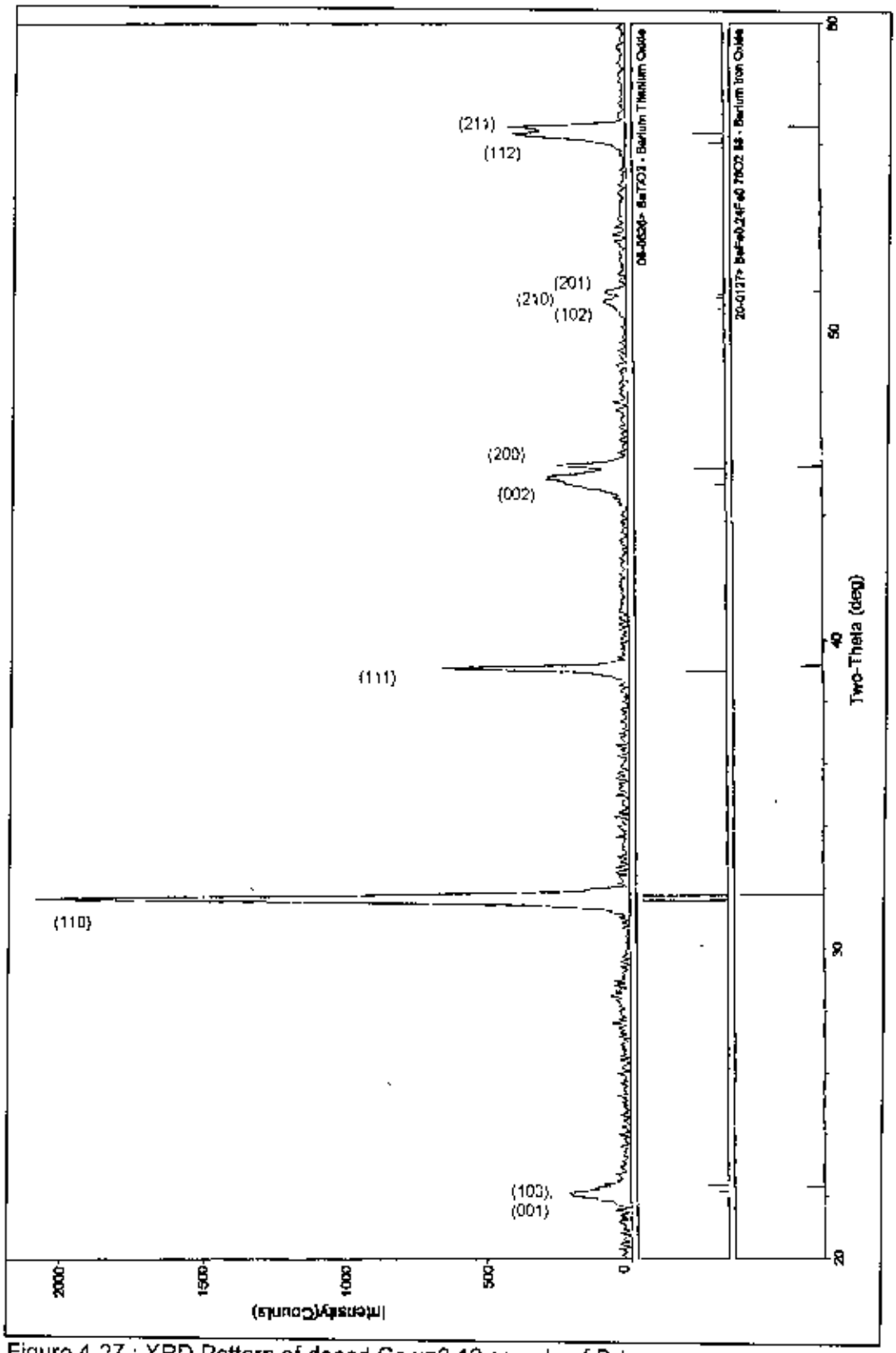

Figure 4-27 : XRD Pattern of doped Ca x=0.12 sample of B-I

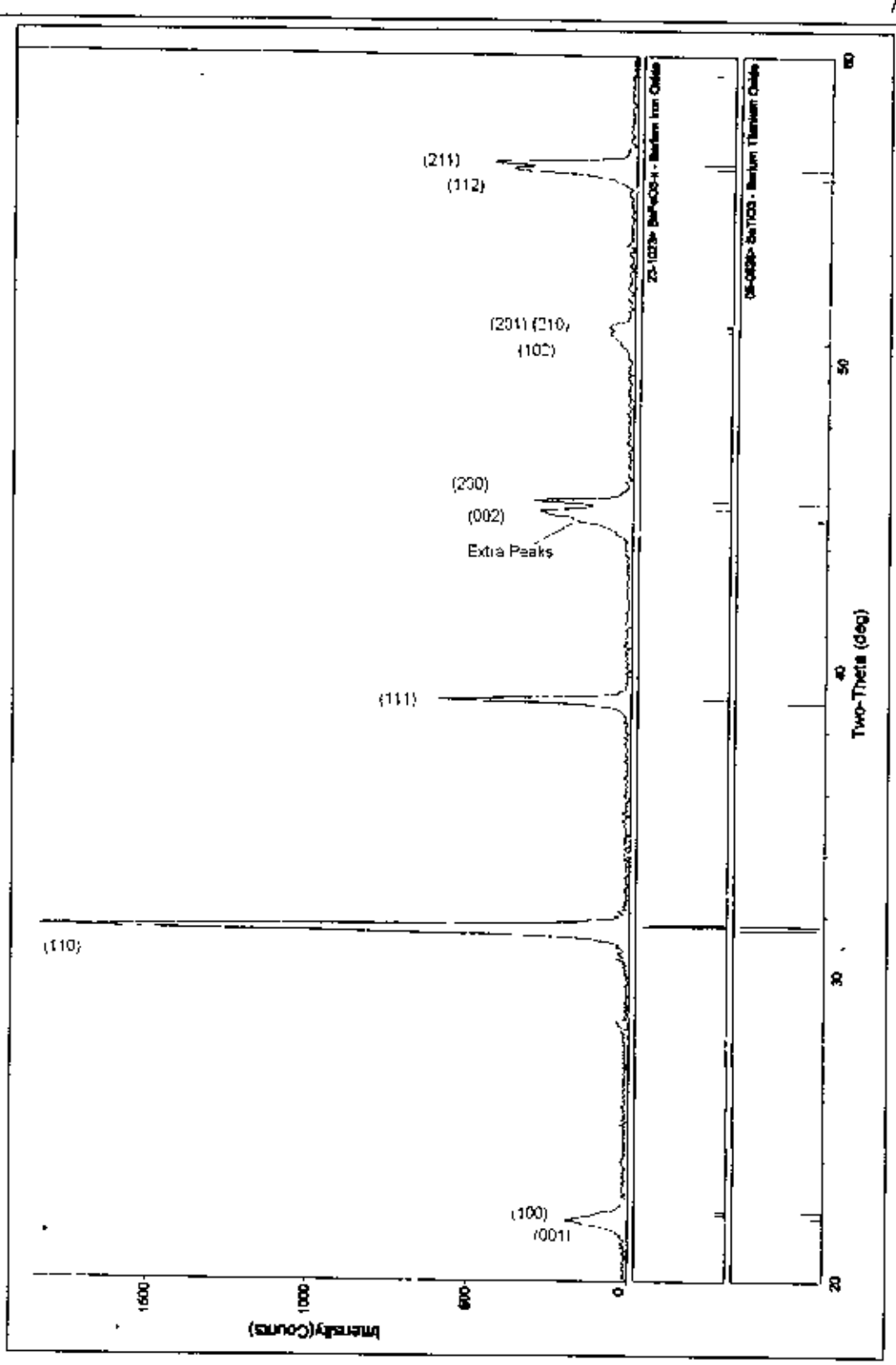

Figure 4-28 : XRD Pattern of doped Ca x=0.12 sample of B-II

It can be readily seen from the XRD pattern shown in Figure 4-25 and 4-28 that, tetragonal distortions in the form of twin peak were almost absent for un-doped samples. Whereas, for doped sample of S series i.e. Ca doping x=0.12 tetragonal distortion was present and twin peaks resolved. However, these twins were superimposed with another set of twin peaks from the impurity phase. The lattice parameter and tetragonal distortion data are given in Table 4-6

Table 4-6 Lattice parameters and tetragonal distortion

Sample identity			Lattice Parameter Å		Distortion
Set	Batch	Series	a	c	c/a
A	B-II	Un-doped	3.9952	4.0189	1.0059
A	B-II	(S)Ca x=0.12	3.9828	4.0514	1.0172
B	E-M	Un-doped	3.9956	4.0232	1.0069
B	EI-M	Un-doped	3.9914	4.0263	1.0088
B	EII-M	Un-doped	3.9916	4.0224	1.0077

Degree of this tetragonal distortion translates into abnormal dielectric constant peak at the transition temperature, where tetragonal phase transforms to cubic. From the Table 4-6, it can be seen that the tetragonal distortion was much higher for doped S sample than the un-doped sample. Hence, sharper k' peak was observed for Ca doped of x=0.12 and hump for un-doped samples.

4.3.1.2 Contaminations

The unusual Tc at about 50°C, for series P, Q and R cannot be attributed solely to the distortion of tetragonal lattice as such. Closer examination and comparison with the standard (attached at the bottom of each pattern) suggest the co-existence of different phase such as $BaFeO_{3-x}$ (PDF 23-1023) in the samples of set A. Part of the diffraction pattern of doped (Ca x=0.12) shown in Figure 4-29 (enlarge of Figure 4-28). By comparison with the standard, the diffraction pattern of $BaFeO_{3-x}$ and $BaTiO_3$ is almost identical and peaks (also twin peaks) do overlap. Lines might broaden or shift owing to factors other than inclusion of impurities. Even though, at around 45° degree region there are more than two sets of twin peaks present, indication of presence of two phases. Moreover, line positions and relative intensities do match better to $BaFeO_{3-x}$ than $BaTiO_3$.

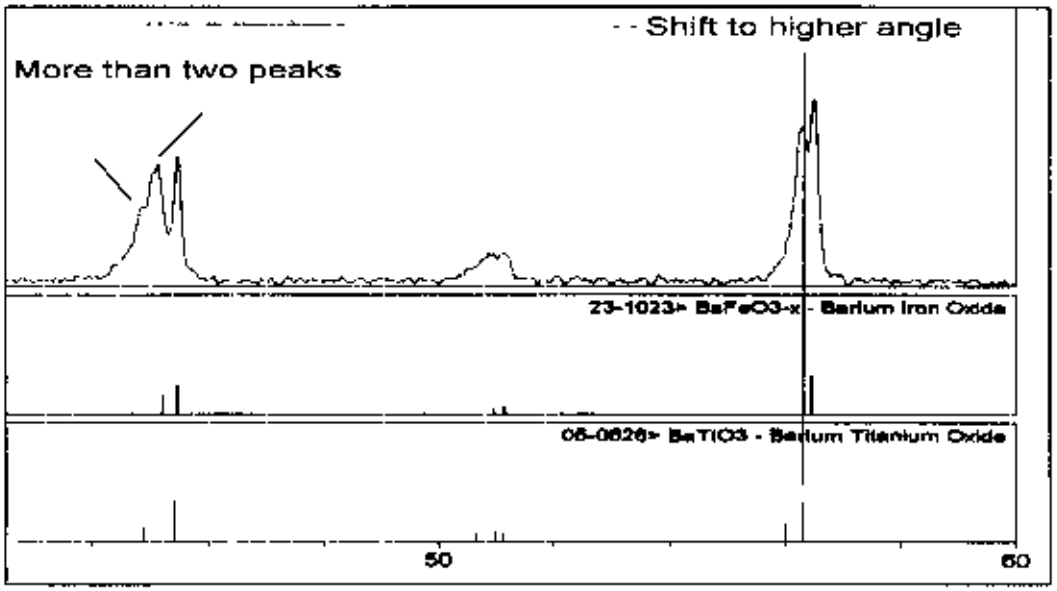

Figure 4-29 : Part of Diffraction pattern of Doped $BaTiO_3$ of set A

The diffraction pattern of EII-M sample of set B shown in Figure 4-30 closely match to the standard $BaTiO_3$ and there are no more than two peaks in the twin peak region. This set of sample was milled with zirconia balls in acetone media. Combined effect of mixed phases might have shifted the Tc to 55°C of series P, Q and R samples

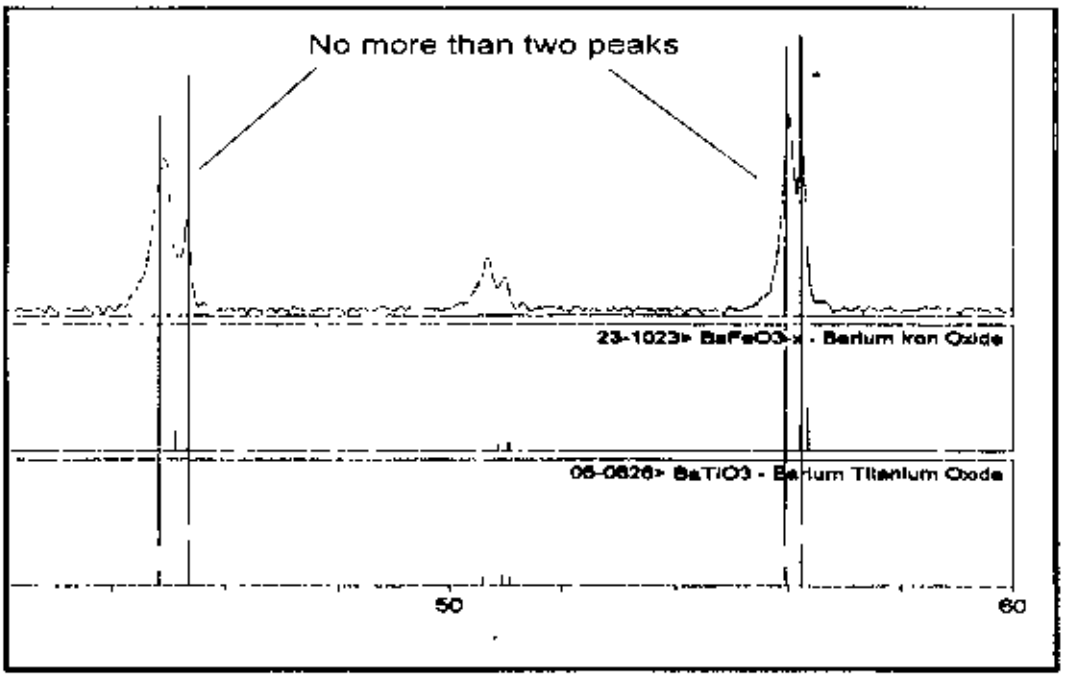

Figure 4-30 : Part of Diffraction pattern of BaTiO3 of MTEC

This explanation however, cannot be extended to Ca doped sample of series S (Ca x=0.12) that showed Tc at around 90°C. Iron contamination was present in all samples of set A as they were all milled with iron ball under identical conditions. In

the XRD pattern of sample S, the impurity effect was present but the increase Ca doping had caused the contraction of lattice *a* and extension of lattice *c*. The decrease of *a* enhanced the polarizability of Ca^{2+} ion due to relatively closer proximity of O^{2-} ion On the other hand, increased *c* make the tetragonal crystal harder transform to cubic. The non-linear relationship between Ca doping level with density and k' was discussed in the preceding sections. Density is related to the unit cell dimensions or lattice parameters and did change with the doping concentration as shown in Table 4-6. Although the unit cell volume was identical and so, was the density but the distortion was much higher for doped (Ca x=0.12) than that of un-doped sample of the same batch. This higher distortion along with iron impurities might have cause shift of Tc at 90°C.

4.3.1.3 Effect of contaminations

The effect of frequency on the dielectric constant with in the temperature range is shown in Figure 4-31 The characteristic was of an ideal relaxor dielectric material; dielectric constant gradually decreasing with the increase of frequency. This is purely the effect of impurity in the sample Apart form shifting the Tc to lower temperature the impurity transformed the expected normal ferroelectric ceramic in to relaxor type ferroelectric ceramic.

Differences between these two types of ferroelectric material are summarized in Appendix 7.6. Closer scrutiny of the electrical properties of set A sample match with the relaxor type ferroelectric ceramic The Tc was broad and diffused, strong frequency dependence and no twin peak in the XRD pattern

The level of impurity was not determined hence the exact origin of this relaxor not characterized

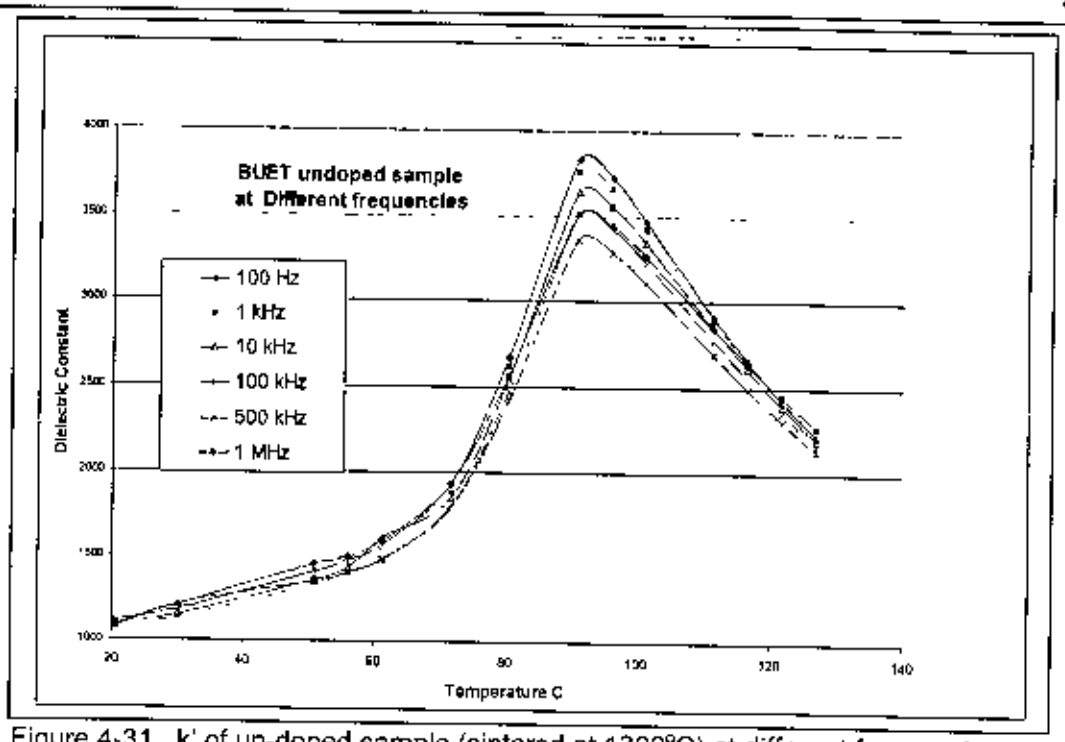

Figure 4-31 . k' of un-doped sample (sintered at 1300°C) at different frequencies

4.3.2 Set B

Only un-doped samples were prepared to verify the abnormal results obtained for samples of Set A. XRD examination of MME source powder revealed the presence of impurities. Hence, two batches of sample were prepared, E-M, EI-M and EII-M

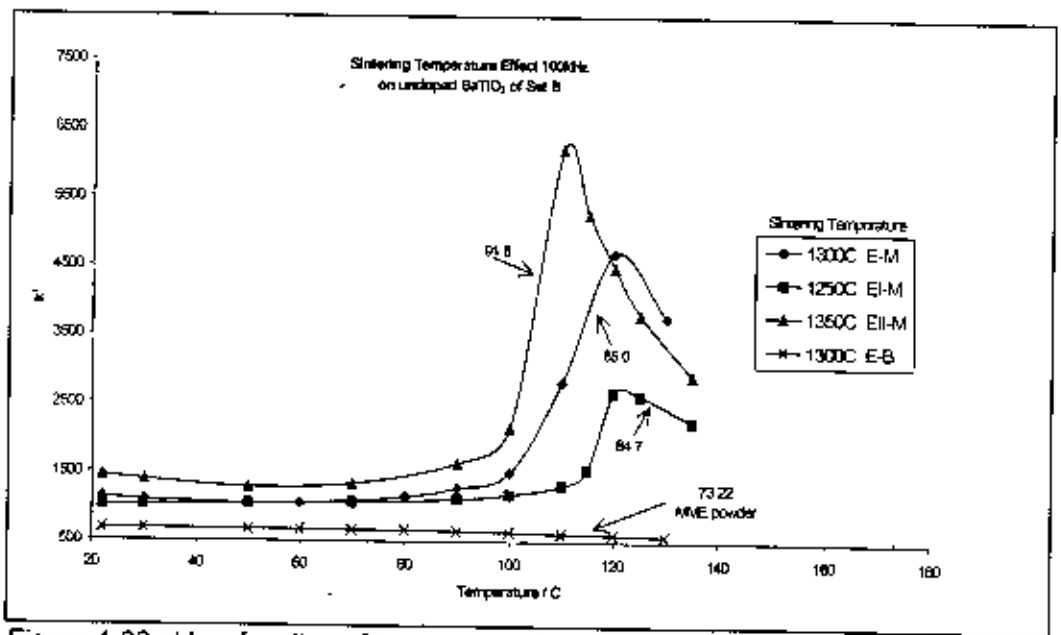

Figure 4-32 : k' as function of temperature for $BaTiO_3$ (un-doped; MTEC powder)

using powder source of MTEC and E-B and EI-B using MME source powder. Details of process parameters were given in Table 3-1. Ceramic balls (zirconia) were used to

avoid metal contamination during milling of this set of samples. Entire processing of these two batches was identical yet samples made from MME powder source did not even sinter to 75% of TD whereas MTEC powder sample did (Table 4-3). Appearance of MME powder samples was chalky. As a result, the dielectric constants of MME samples are below 700 and do not exhibit any transitional peak with in the test temperature range. In Figure 4-32 the dielectric constant of samples Set B were shown as function of temperature. The corresponding densities of samples are labeled on the respective curves.

The Tc was about 110°C for un-doped sample EII-M prepared using MTEC powder sintered at 1350°C for half an hour. This sample was denser than the other two of the same batch. Density of E-M and EI-M were almost identical. Difference of

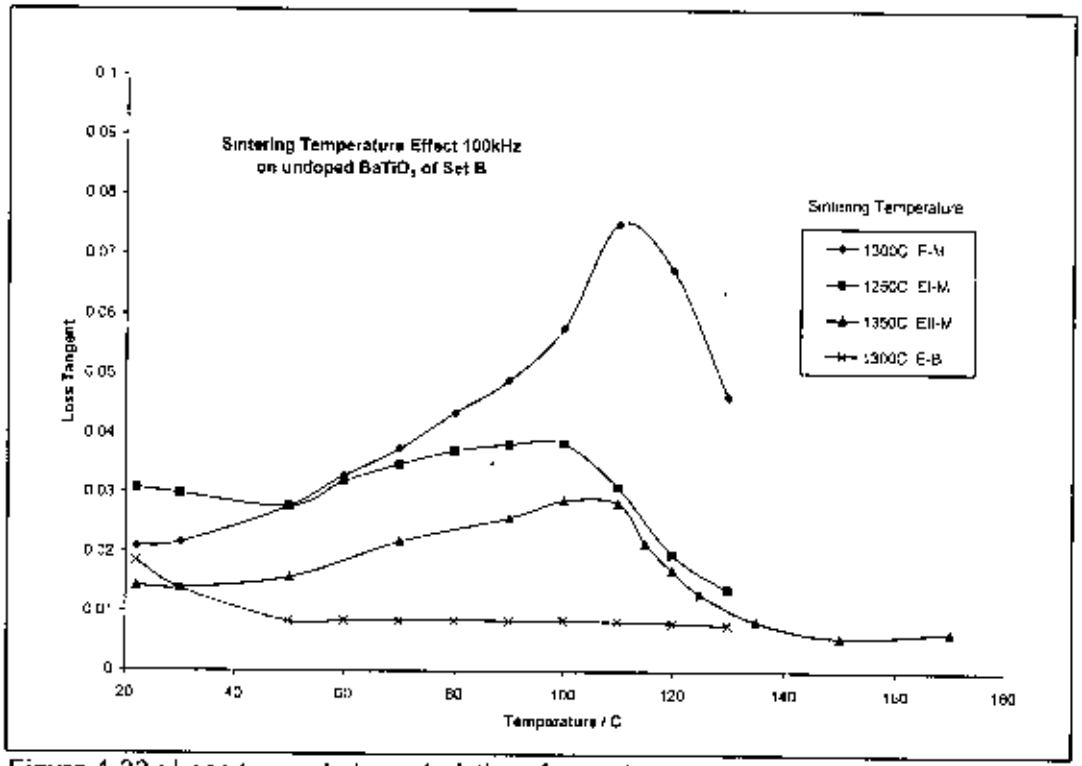

Figure 4-33 : Loss tangent characteristics of samples prepared using MTEC powder

density resulted in dielectric constant difference below the Tc, as can be readily seen from Figure 4-32. Identical density however, did not fix the Tc of the sample at the same temperature. It is observed that the sharpness of peak and k' depends on the density of the material. The peak k' values of these samples differ by more than 2000 from each other. Both E-M and EI-M sample were sintered at 900°C for 3hour whereas; EII-M was for 1000°C for 7hours. It is clear from the graph and thermal history, that complete calcination is required for densification and for better dielectric

property. The Ba/Ti mole ratio of E-M and EI-M was 0.9896 and of EII-M was 0.9998. Relatively higher Ba content might have suppressed the grain growth and attributed to the increased k' of EII-M samples [13].

The Tc is more dependent on the tetragonal distortion than the density. It can be seen from the Figure 4-32 that the Tc of sample E-M and EII-M would have been almost same had their density been identical. The on-set of Tc in this case is identical at 100°C. However, for the sample EI-M the on-set is at 115°C. By comparison, of tetragonal distortion of samples from Table 4-6, the highest (1.0088) distortion was for EI-M that was relatively higher from the other two.

The tangent loss characteristics of this set of sample followed the same pattern observed earlier as shown in Figure 4-33. Denser material showed less loss over the test temperature. There is however, a trend of increasing loss at the transition of phase at Tc. This effect is much pronounced in the sample E-M that showed sharp transitional peak. However, loss characteristics of E-B samples are featureless; no increase of loss at transition and remained constant over the test temperature.

The frequency dependence on k' and tangent loss are shown in Figure 4-34 to 4-36. Both k' and loss are constant with in the frequency range of 100Hz to 100kHz. At the frequency of 1MHz k' peak to a maximum then started to decrease for samples sintered at 1300°C and 1250°C. On the other hand k' peaked at 1.2MHz for the samples sintered at 1350°C but whether it decreased further on was not detected due to frequency limitation of the instrument. Same pattern observed of tangent loss of the samples. It is worth mention here that the silver paint applied to the samples and the test fixtures used during measurement are not recommended to use over 1MHz range due to unacceptable level of noise generated. This might have attributed to the abnormal properties above 1MHz range.

XRD pattern of E-M, EI-M and EII-M are given at Figure 4-37, 4-38 and 4-39 respectively. Tetragonal twin peaks are present in all of these samples. Whereas, these twin peaks are completely absent in the XRD pattern of E-B (Figure 4-40), the sample made from MME powder source. Tetragonal $BaTiO_3$ phase was not formed in E-B samples, hence, its k' was low and no transitional peak observed.

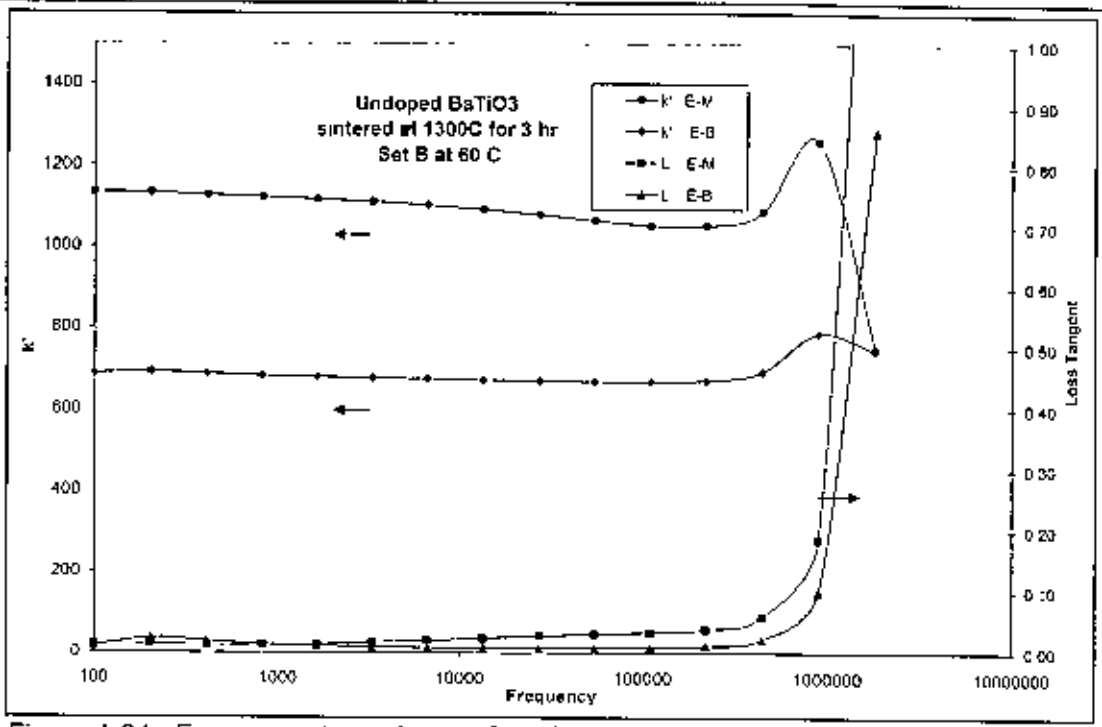

Figure 4-34 : Frequency dependence of un-doped $BaTiO_3$ of Set B at 60°C

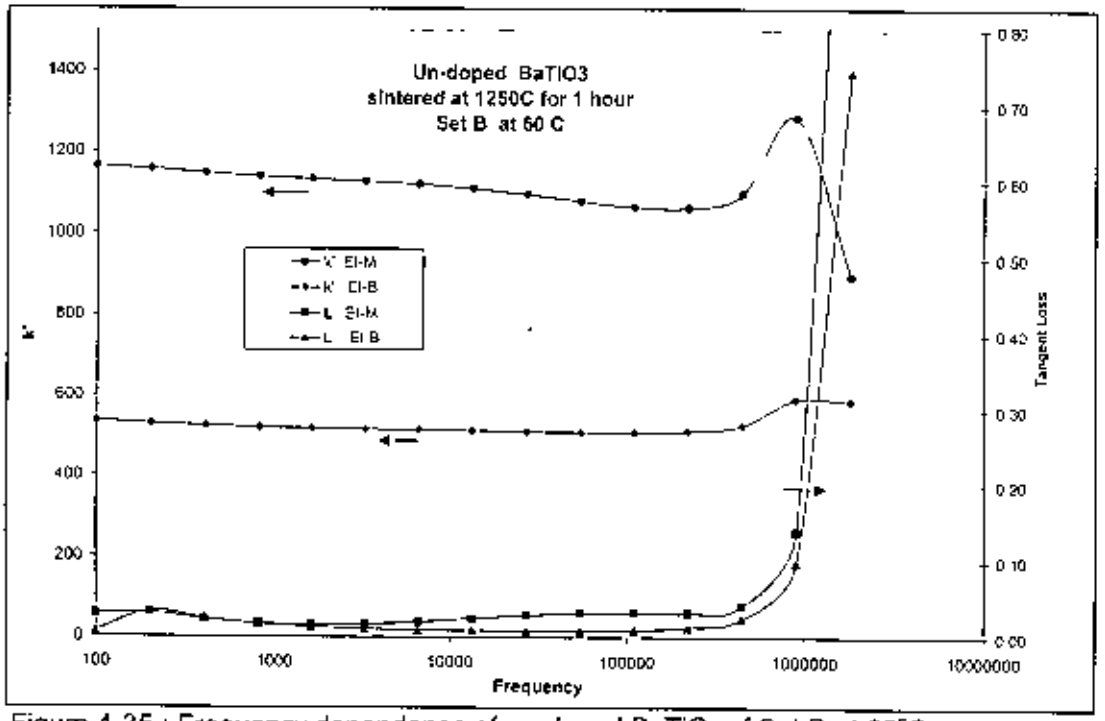

Figure 4-35 : Frequency dependence of un-doped $BaTiO_3$ of Set B at 60°C

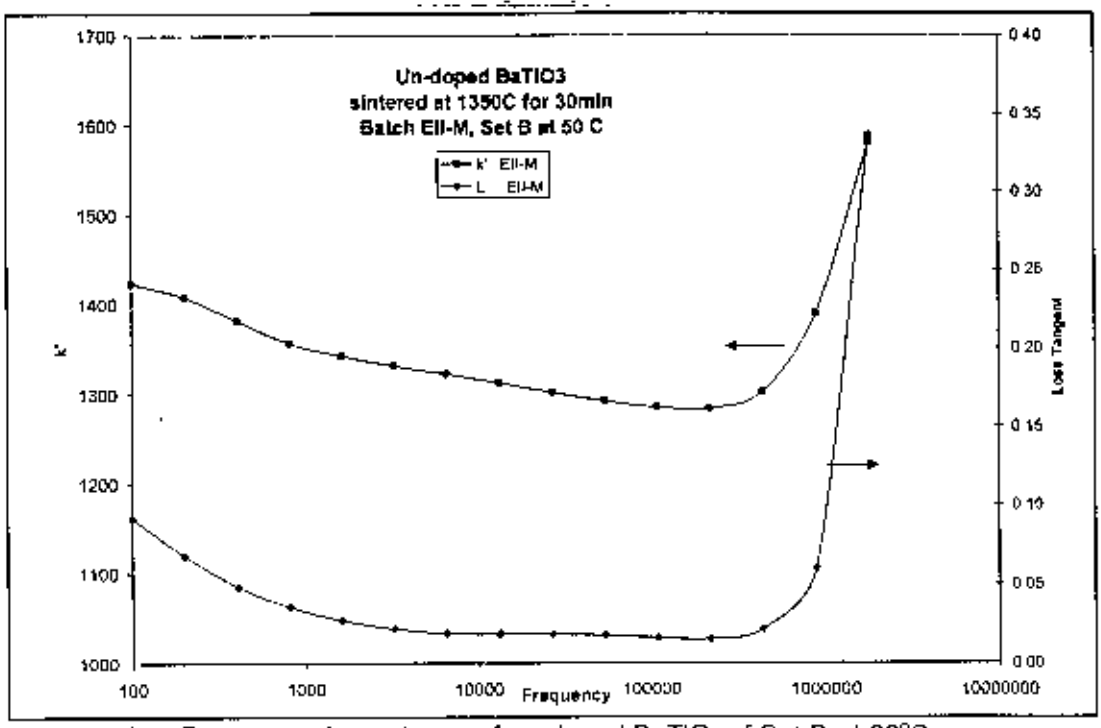

Figure 4-36 : Frequency dependence of un-doped $BaTiO_3$ of Set B at 60°C

4.3.2.1 Preferred orientation

All sintered samples were ground then polished before XRD examination. The XRD pattern of EI-M shown in Figure 4-38 is of as sintered surface of the sample whereas others are of ground surface. The twin peaks are much resolved with higher intensities than those of the other samples. However, this increased tetragonal peaks or increase of intensity did not reflect in increased dielectric properties. Another 'as sintered' sample of EII-M was tested to confirm this affect. It can be seen that the effect is much more intense for this sample as shown in Figure 4-41 Intensity of {200} plane was almost double of the standard XRD pattern for that peak. Also other twin peaks' intensity was increased at the expenses of the standard highest peak {101}. This seems to be a preferred orientation {200} planes oriented parallel to the surface.

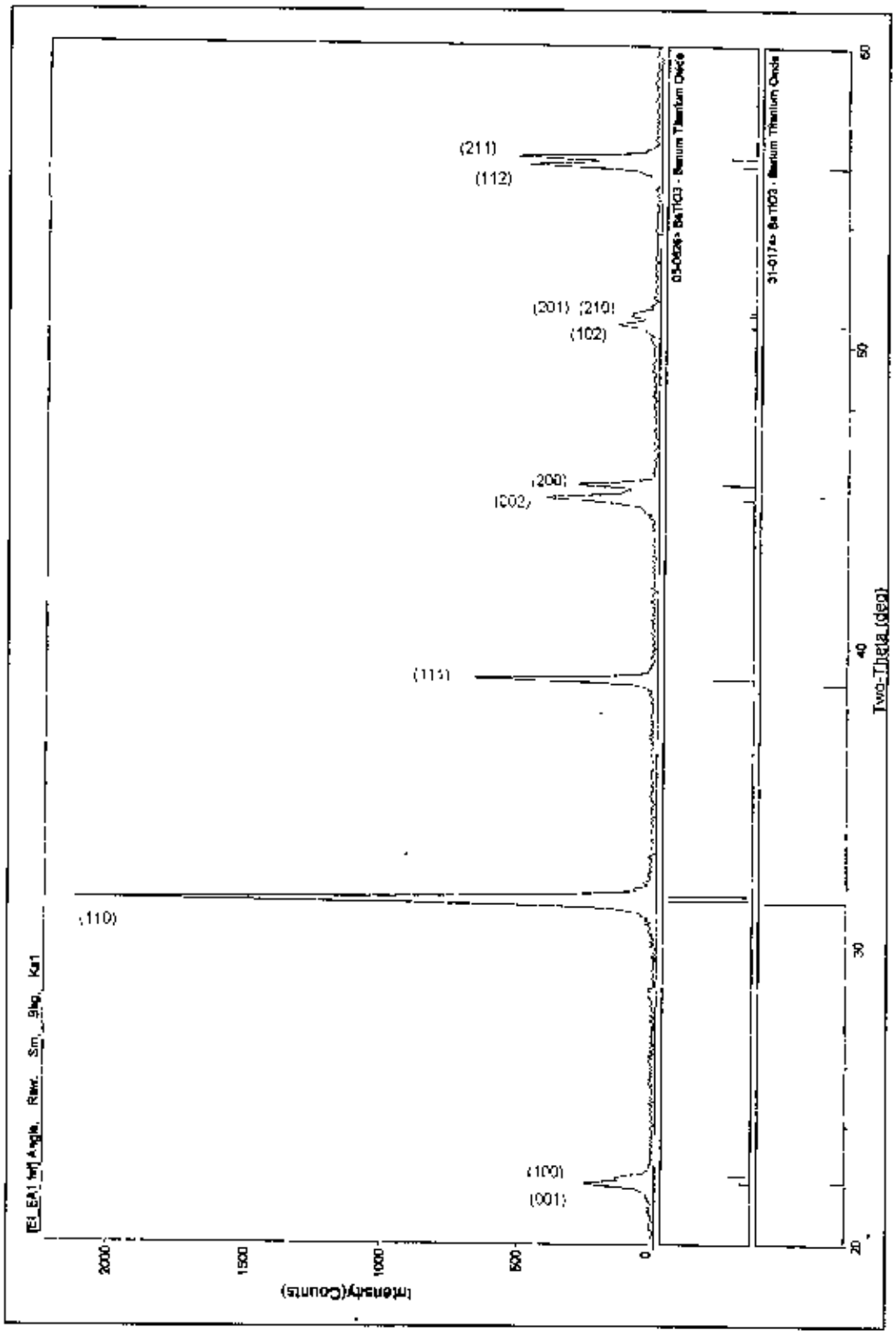

Figure 4-37 : XRD Pattern of E-M pallet (surface ground)

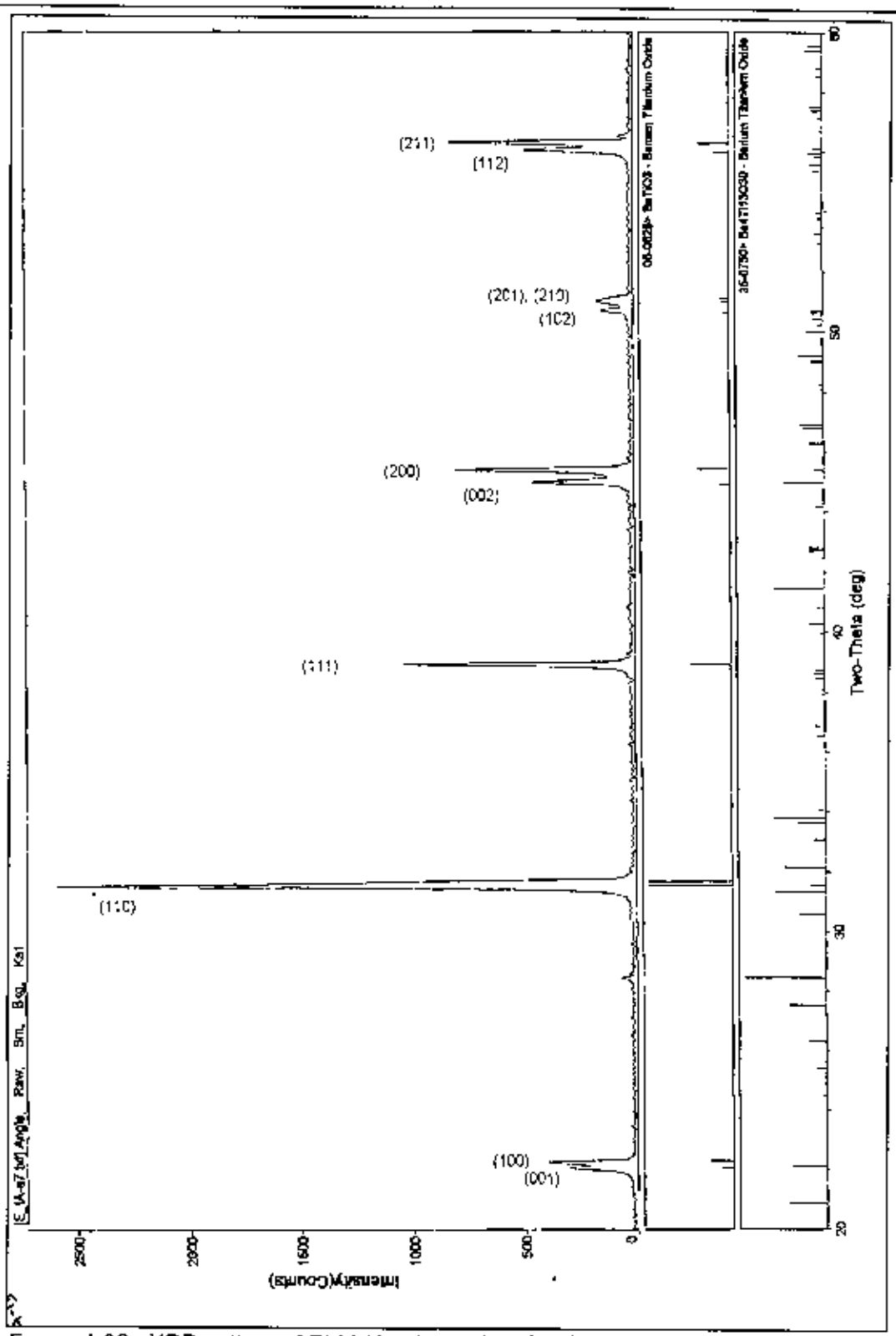

Figure 4-38 : XRD pattern of EI-M (As sintered surface)

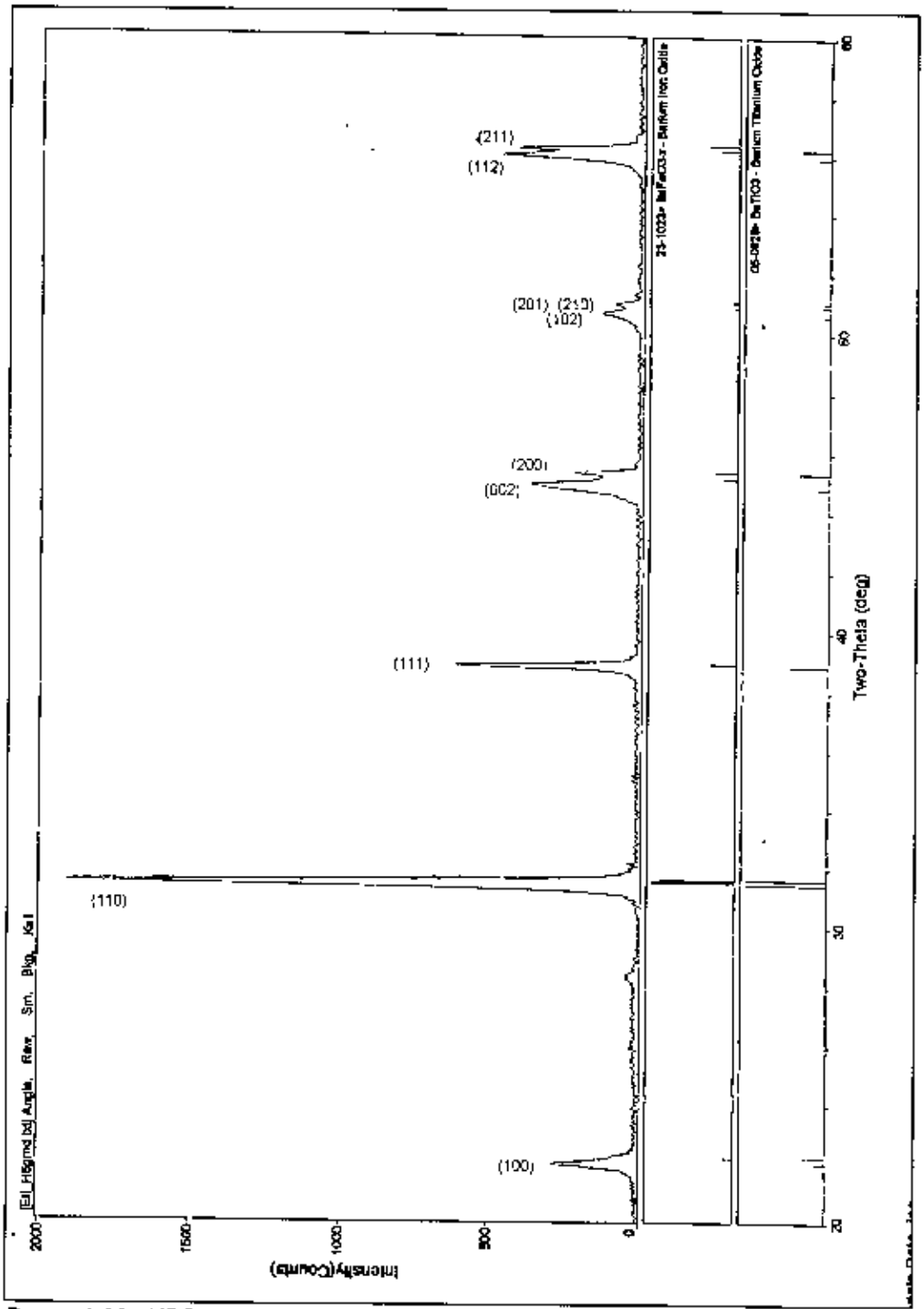

Figure 4-39 : XRD pattern of EII-M

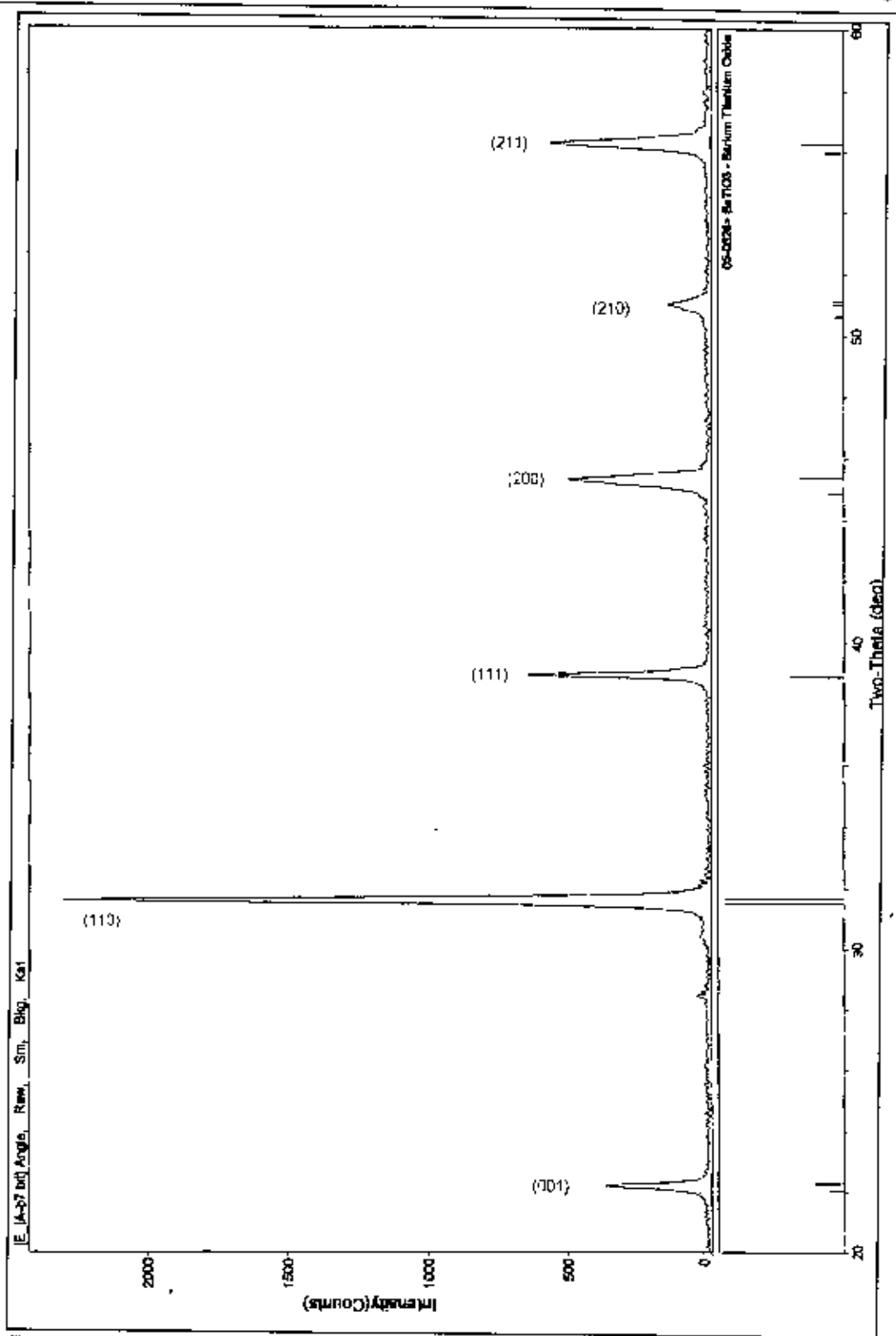

Figure 4-40 : XRD Pattern of E-B sintered at 1300C

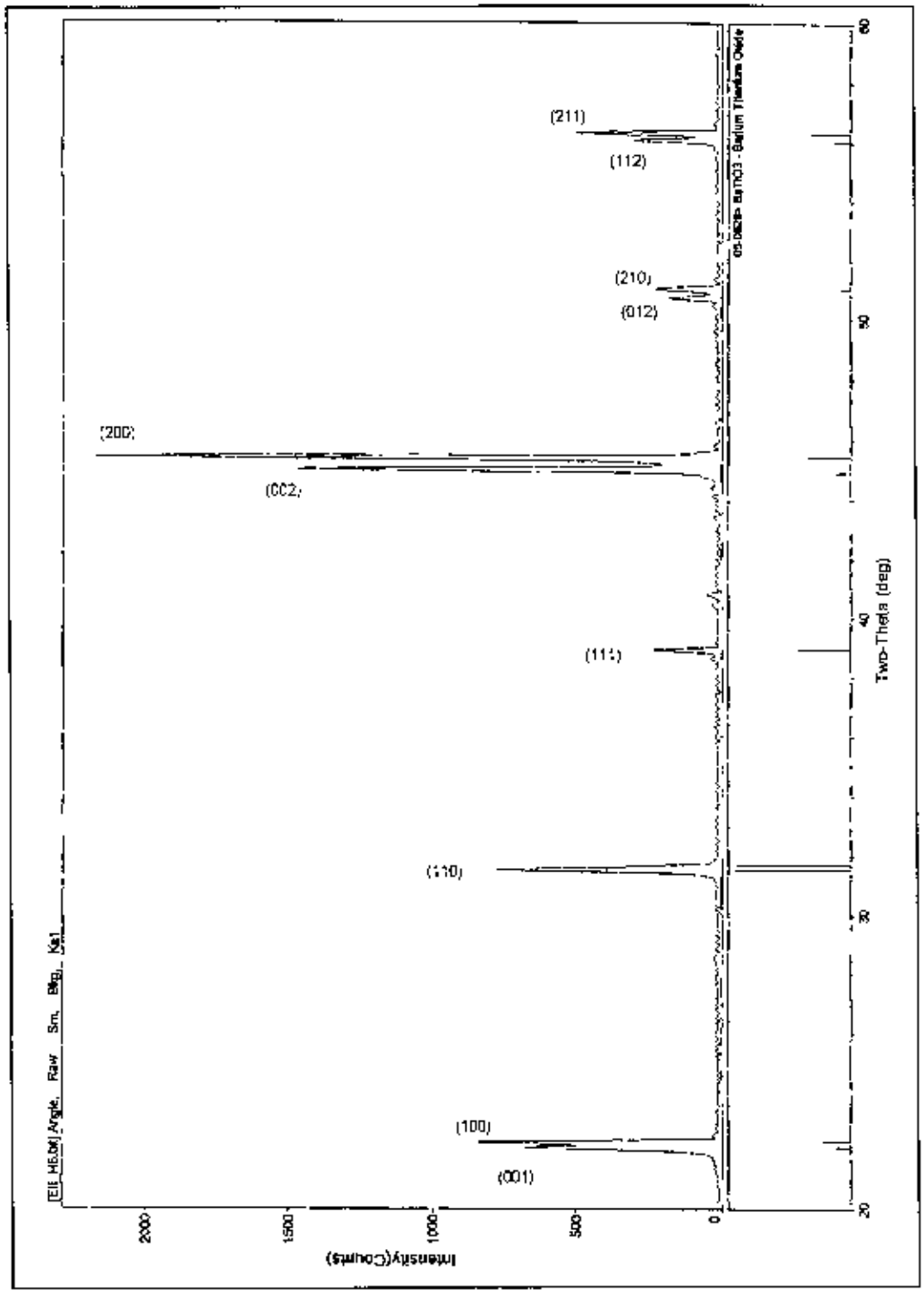

Figure 4-41 : XRD pattern of EII-M showing the preferred orientation of {002} planes at the surface.

The oriented planes are oxygen rich. The oxygen in the furnace atmosphere might have encouraged formation and growth of this plane at the surface. Anion vacancies were annihilated at the surface due to oxygen diffusion from the atmosphere that might have also encouraged preferential formation of these oxygen rich planes

Effect of this preferred orientation at the surface on dielectric property was examined for sample of series EII-M. Firstly, the samples were tested with the surface "as-sintered" (un-polished) state than the samples were ground and polished. The polished samples were tested again. The dielectric constant (k') of these two conditions are illustrated in Figure 4-42 as function of temperature. The k' values were identical up to the T_c then started to differ by 700 at the Tc and beyond.

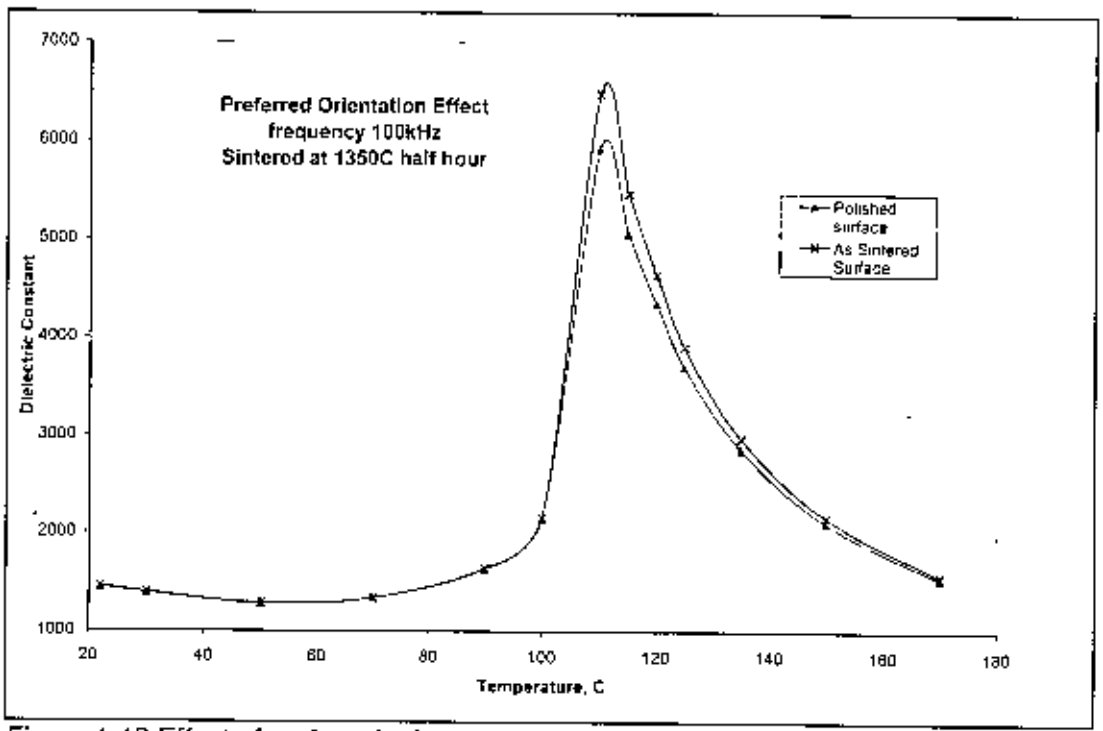

Figure 4-42 Effect of preferred orientation on k'

4.3.3 Set C

This set of sample was prepared entirely at MME, using different powder (Appendix 7-3) and as Ca doping agent; $CaCO_3$ was used instead of CaO. Details of processing parameters were given in Table 3-1 Density of sintered samples were given in Table 4-3 and discussed in section 4.2. The Ba/Ti molar ratio was 1.0005. Due to iron contamination in samples of Set A, the Ca doping effect on electrical property was not realized This set of sample was prepared with the aim to optimize density and observe Ca doping effect on electrical properties.

The electrical properties of this set of samples were measured at Physics Department of BUET Samples were heated to the test temperature using the tube furnace made at MME Department. In Figure 4-43 dielectric constant (k') at 100kHz

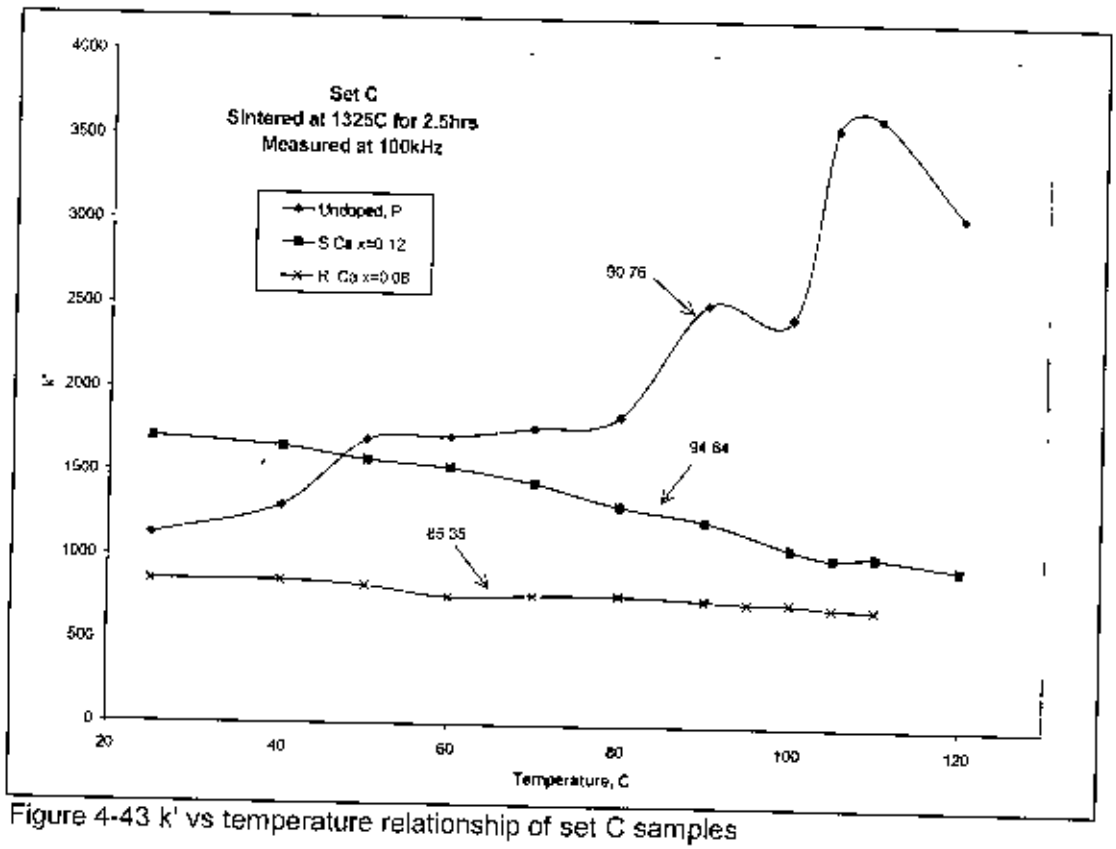

Figure 4-43 k' vs temperature relationship of set C samples

is plotted as function of temperature for the sample sintered at 1325°C. Densities of respective series are indicated in the figure Curie Temperature of un-doped (P) samples seems to be at 107°C, but there possibly other than $BaTiO_3$ phase is present This other phase might have contributed to another peak at 95°C and increase of k' at 50°C from room temperature. XRD examination was carried out on this un-doped sintered sample and diffractogram is shown in Figure 4-44. The primary peaks are of

$BaTiO_3$ but the extra peaks, as indicated in the figure might have contributed to the extra k' peaks observed in the Figure 4-43. Extensive analysis of these peaks (Figure 4-44) confirmed the presence of different phases closely resembling to BaCuOCl (PDF# 71-1029) Probability of Cu inclusion is very much remote as the powder used were of high purity and metal bearing implements were not used. The amount of Cu impurity was not even mentioned (Appendix 7-3) and other impurities would not have caused reflection of such intensity. Even the $BaTiO_3$ formed are of different crystallographic structure (PDF# 79-0461) than $BaTiO_3$ of set B (PDF# 05-0626). A slight tetragonal distortion of 1 004 was calculated from the reflection from (002) and (200) planes. Together with the density of 90.79% and this crystal structure might have shifted the Tc to 107°C. It seems that the dielectric property of the un-doped sample is the combined effect of different phases present.

Although, computer analysis of XRD diffractogram does suggest the presence of BaCuOCl (PDF# 71-1029), Quartz (PDF# 79-1913) and FeS_2 (PDF# 79-0617) responsible for the extra peaks can be ruled out. The inter-planner spacing and the relative intensities of these phases closely matched with the phase formed in the sample. The phase so formed has significant effect on the electrical property yet its structure not fully understood.

Doped R (Ca x=0.08) sample however, exhibited no transitional peak at all. The k' value remained constant over the test temperature range. Density was about 85.64% and k' was ~750. The same kind of characteristics was observed in the sample E-B of Set B (density 73.22%), which was prepared form MME powder at MTEC Chemically, the difference between these two sets of sample was $BaCO_3$ and Ca doping source. For identical doping concentration. k' hump was observed for R series samples of set A whereas for this set completely constant.

It seems that the observation made earlier regarding iron contamination was vindicated. The XRD diffractogram of this sample shown in Figure 4-38 reveal the amplification of extra peak than the un-doped sample. The computer analysis of the peaks match with a different modification of $BaTiO_3$ and no tetragonal distortion detected. None of the peak matched with any Ca bearing compound or Ca. Hence, Ca incorporated in the crystal structure but formed a different phase.

The extra peaks of doped sample S (Ca x=0.12) were different from those of sample R as can be seen in Figure 4-46. Effect of this was reflected in the dielectric property. There is no tetragonal distortion hence, no sharp peak or hump observed. However, k' decreased with the increased temperature in a linear manner. Density of this sample is about 95% which a good achievement and the k' value is on average 1400. Considering the commercial formulation shown in Figure 2-26 for NPO type capacitor which has k' values up to 75, this is a good result in a way.

The SEM micrograph of etched sample illustrated in Figure 4-47 and Figure 4-48 indicate the presence of different phases and the flaky morphology of the sample Considerable amount of porosity were also present.

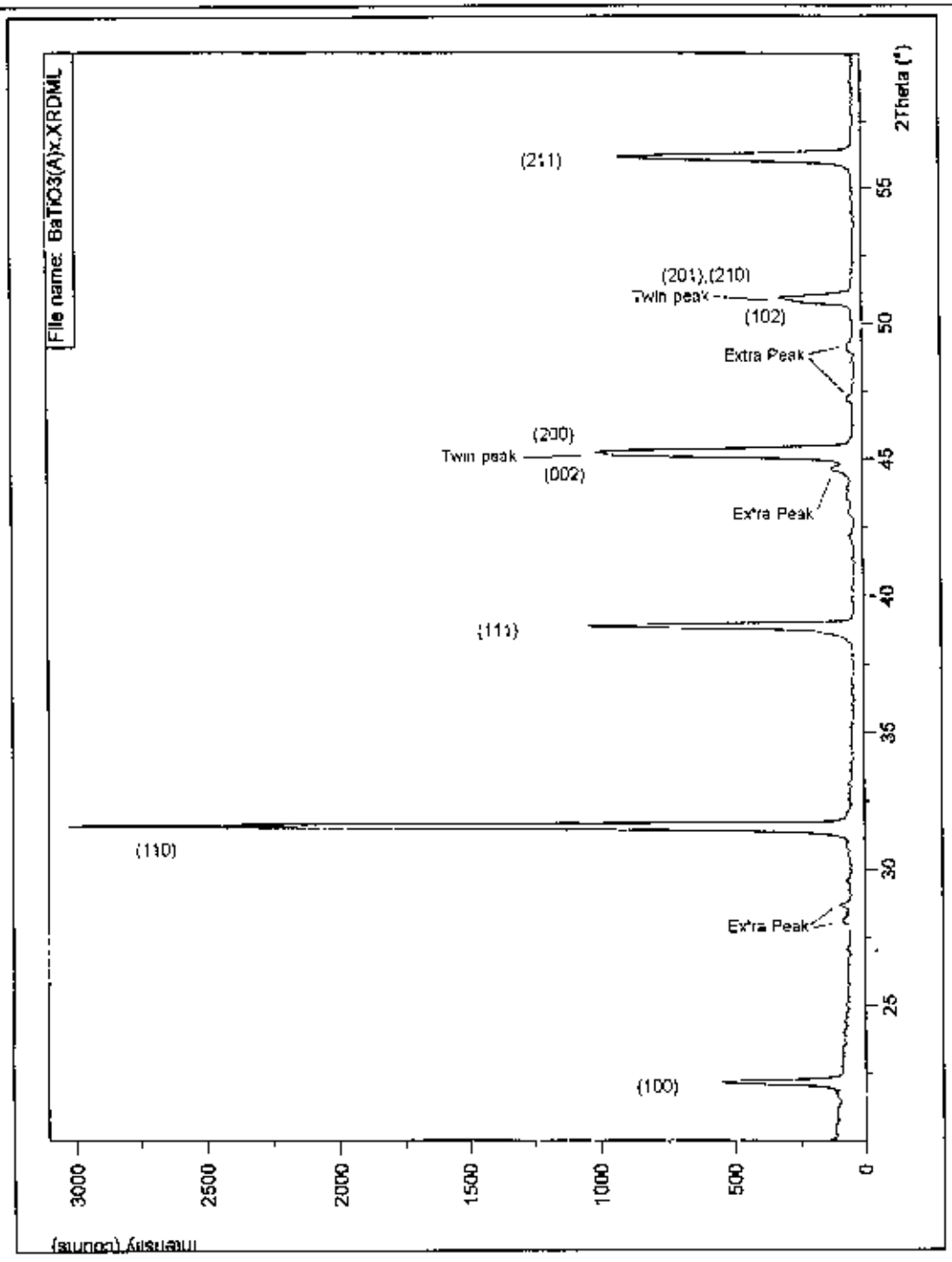

Figure 4-44 : XRD pattern of un-doped (P) sample of set C; sinter 1325C

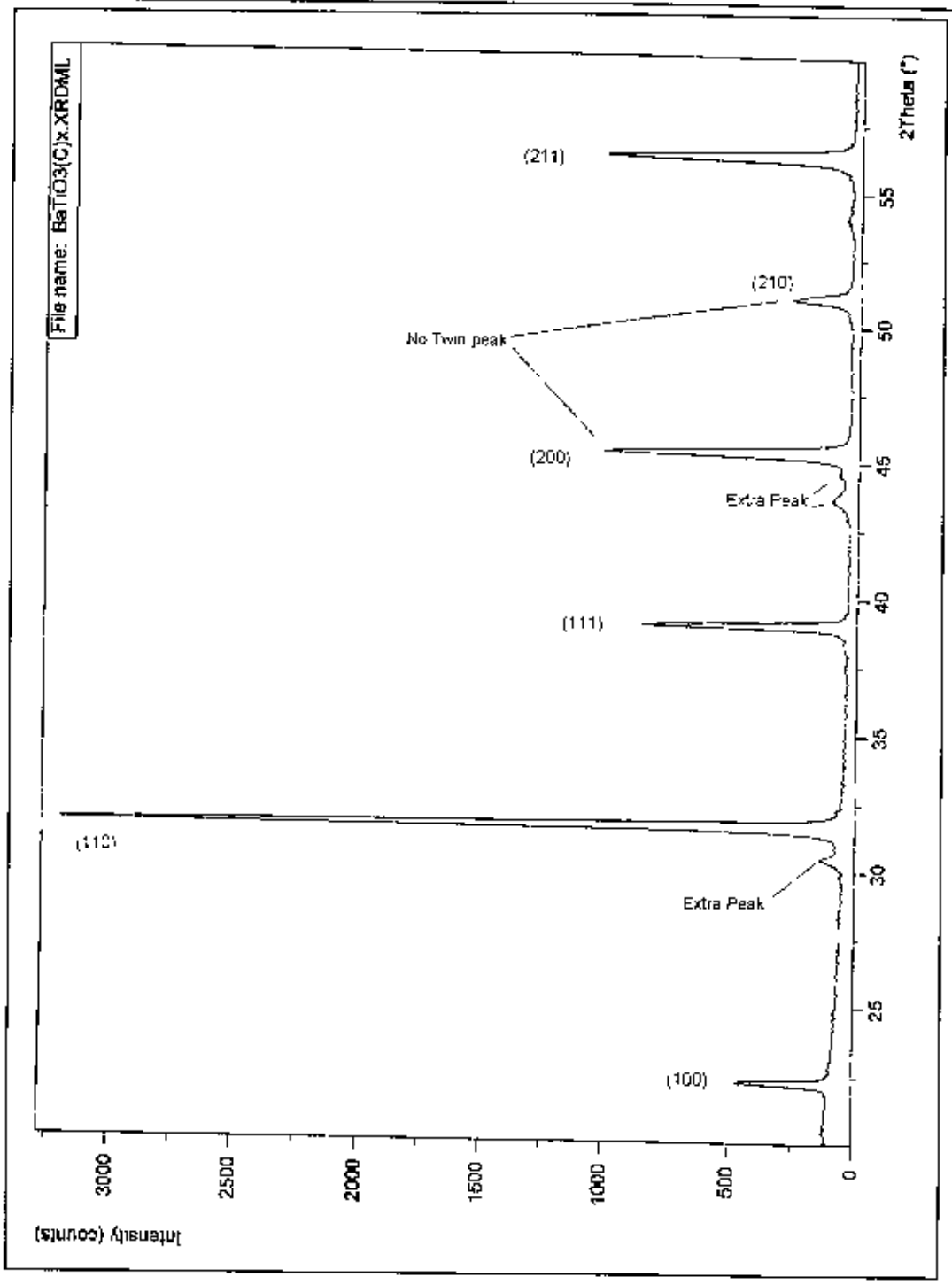

Figure 4-45 : XRD pattern of doped R (Ca x=0.08) of set C

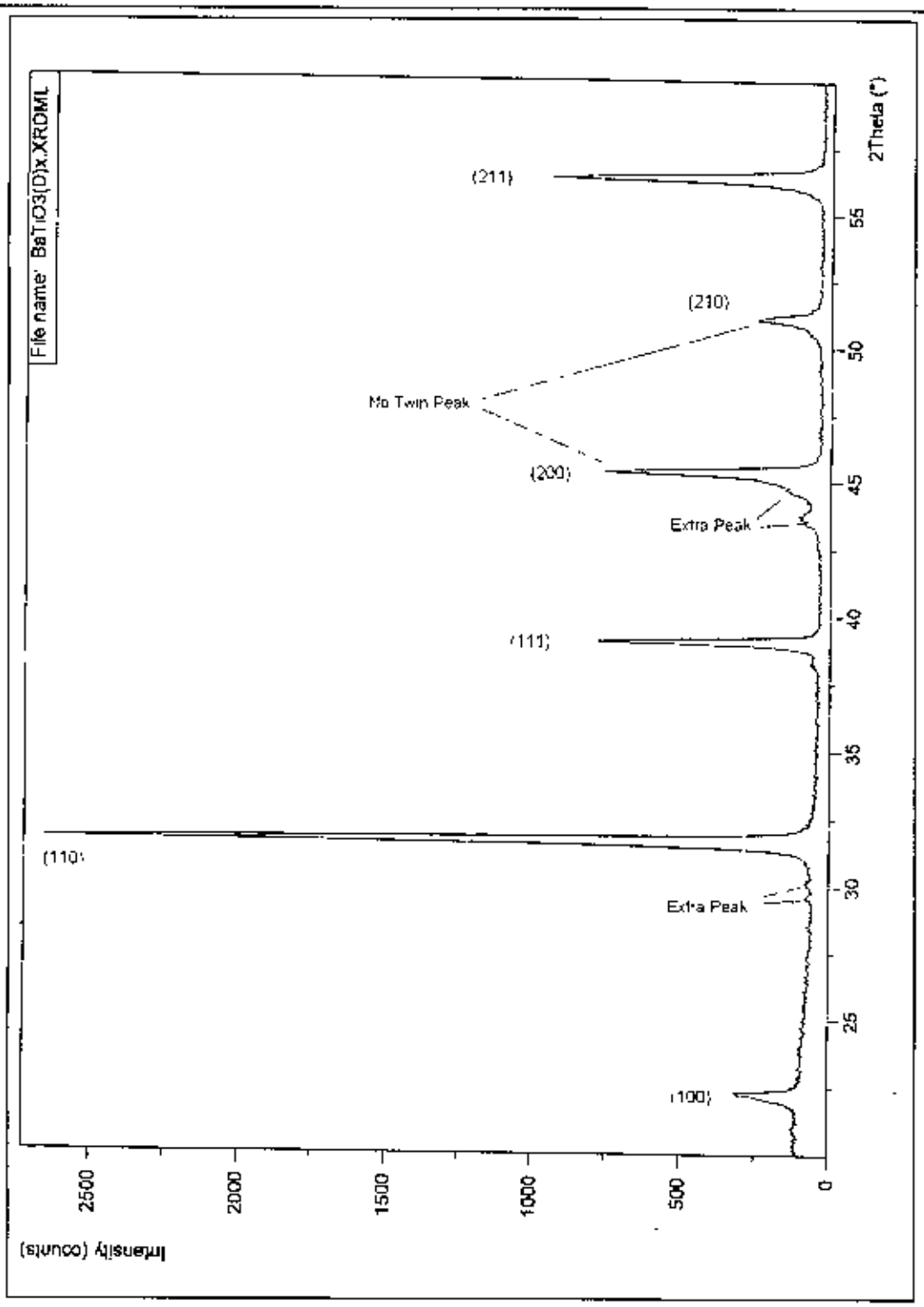

Figure 4-46 : XRD pattern of doped S (Ca x=0.12) of set C

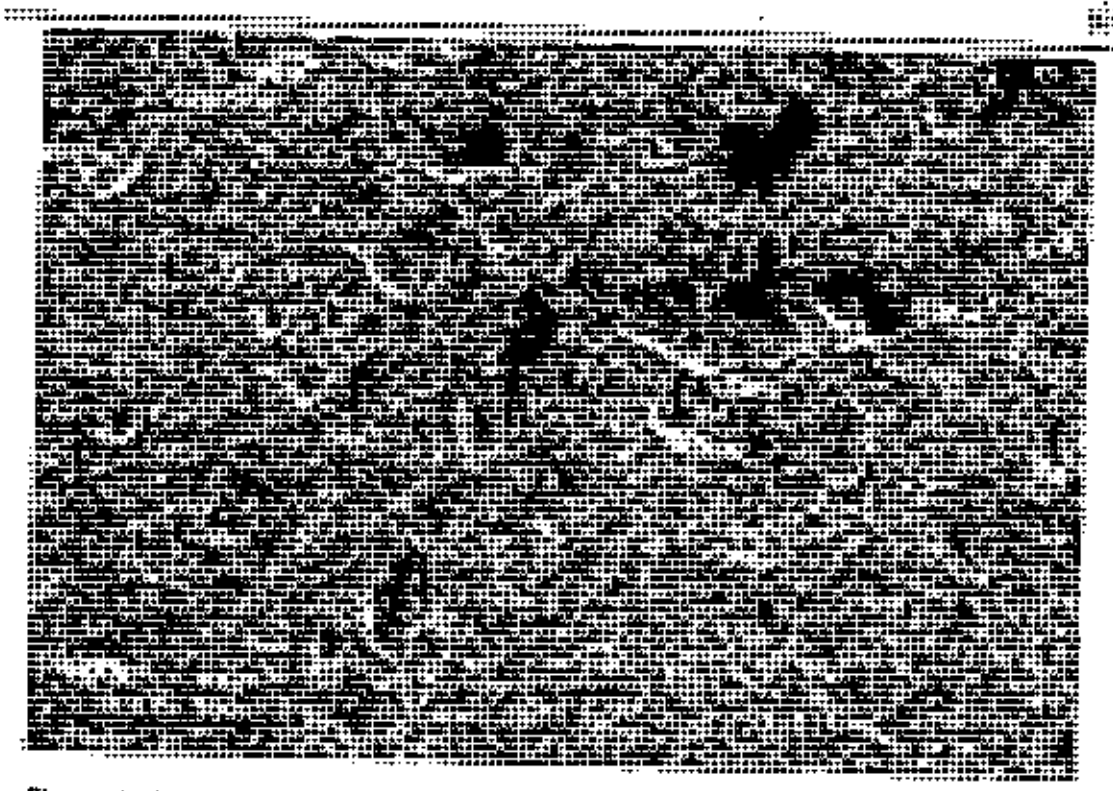

Figure 4-47 : SEM micrograph of doped S (Ce x= 0.12) etched sample

Figure 4-48 : SEM micrograph of doped S (Ca x= 0.12) etched sample (enlargement of figure 4-47)

4.3.4 Set D

The final set of sample was prepared to obtain usual $BaTiO_3$ that would match with the powder pattern of the standard tetragonal phase of $BaTiO_3$. Since the very same TiO_2 was used in the preparation of samples so far and none of the sample exhibited usual property of $BaTiO_3$, hence new source of TiO_2 was used for this set. As doping agent $CaTiO_3$ was used instead of CaO or $CaCO_3$. Milled powder was calcined at 1100°C for 5 hours then again calcined at 1200°C for 5 hours (Table 4-3) and sintered at 1350°C for 4 hours. All of the sample were fused or cracked, hence dielectric property was not measured. The un-doped sample was ground to powder and XRD pattern was taken and shown in Figure 4-49. Diffractogram of un-doped sample (Figure 4-49) almost matched, peak to peak, intensity to intensity with the tetragonal $BaTiO_3$ (PDF#05-0626). Exception is the extra peak observed at 2theta angle of 44.58°. The tetragonal distortion is about 1.007. Origin of the extra peak might have came from the $BaCO_3$ powder being used for sample preparation of set C and D.

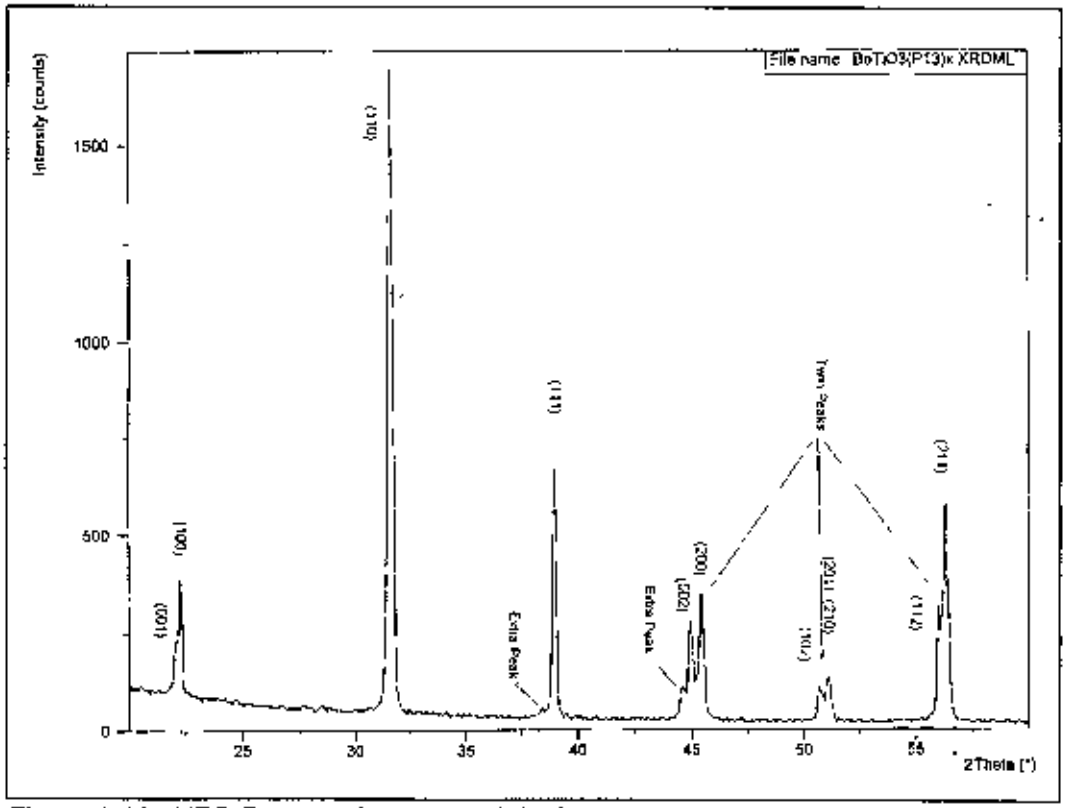

Figure 4-49 : XRD Pattern of un-doped (P) of set D

5 Conclusions

5.1 Process Variables

Selection of raw powder as starting material is an important factor. Impurities may hinder or devastate the desired properties of the ceramic. Much care is needed in selection of raw material, if necessary; purity should be confirmed before proceeding.

The optimum density of the sintered body has to be with in the range of 92% to 95% of theoretical density in order to deduce reliable, reproducible and confident property measurement. Every step in ceramic processing, the conditions have to be tuned to obtain such dense product

Complete reaction during calcination is the most important factor governing the final density and dielectric properties of $BaTiO_3$ based ferroelectric material. Incomplete calcination, or incomplete reaction, leads to the evolve of gas forming blowhole during sintering and most importantly desired properties are not realized owing to non-formation (or partial formation) of required phase(s). It has been observed in samples the formation of Ba_2TiO_4 that was leached away during etching and leaving a spongy structure as seen in the micrograph. This phase is detrimental and must be avoided through proper calcination. Due to sluggish nature of solid-state reaction, calcination at 1100°C for 7 hours seems to be satisfactory.

Iron impurity in samples hindered the effect of Ca doping on dielectric property of $BaTiO_3$. Steel ball used in aqueous media caused iron inclusion in the samples. Steel ball should have been avoided. It is however observed that the transition temperature has lowered and the peak has been flattened in the sample of set A, especially the doped ones. Furthermore, CaO used in set A samples has reacted with the steel ball during milling caused formation of $BaFeO_{3-x}$ hindering the effect of Ca doping. Instead of CaO, $CaCO_3$ could have been used. These findings were confirmed by comparison with the samples prepared at MTEC. The mechanism of shifting of T_c in this case is not certain.

None of samples achieved density more or equal to 95% of the theoretical density. The sintering temperature should be around 1350°C, varying only the holding time to optimize the maximum density. Other factor attributes to the density is the Ba/Ti ratio, which also controls the microstructure and electrical properties.

It is observed that Ca acted as a sintering aid for doping level of 0.08 mole fraction and above. Densities of doped sample do follow a non-linear relationship with doping concentration and the change over takes place at 0.07 mole fraction. This effect is observed irrespective of sintering thermal profile.

5.2 Dielectric Properties

The density of sintered ceramic has to be around 95% of TD to deduce tangible dielectric properties Under the identical processing conditions, denser sample have relatively higher dielectric constant (k') and sharper transitional peaks. The Curie Temperature (Tc) depends on the tertragonaly of the material. Samples with identical tetragonal distortion exhibited k' peak at different temperature due to lack of adequate density. However, the on-set of Tc are almost identical. It has been observed in this study that tetragonality fixes the on-set of Tc and the density causes the sharpness of the peak. Absence of tetragonal distortion (c/a) usually translate into absence of transitional peak of k'.

Iron inclusion in samples of set A turned the expected normal ferroelectric ceramic into relaxor type, with peak k' nearly 4000. The k' dependence on frequency of this sample is remarkable. In conjunction with Ca doping the Tc was shifted to 55°C which with the increase of Ca doping level above 0.08 mole fraction shifted the Tc to 90°C. The k' also changed non-linearly with the Ca concentration level. What aspect of microstructure has exactly attributed to this could not been ascertained in this study Overall loss tangent characteristics do follow the same pattern of k', denser material with lower loss and in some samples hint of loss peak at the Tc.

The doping effect of Ca seems to be not that straightforward. Doping source material seems to affect the crystal structure and different phase formation. Due to problem with the purity of the powder neither pure $BaTiO_3$ was prepared nor the doping effect of Ca was realized However, Ca seems to effect the density, sintering and flattening of k' peak at Tc; possibly shifting of Tc as well.

The preferred orientation of {002} parallel to the surface might have been due to oxygen in the oven. This increases k' at T_c, that may a valuable hint as to find the way to manipulate k' of ABO_3 type ceramics.

6 Bibliography

Listed according to the first citation in the text.

INTRODUCTION

01 Thurnauer, H. and Deaderick, J , U.S. Patent 2429588, Oct 1947 (file Oct 1941) .. 1

02 NIC Components – official web site www nic-component.com 2

03 J C. Burfoot. *Ferroelectrics*, Von Nostrand, New York, (1969) 2

04 W. D. Kingery, *Introduction to Ceramics*, Jhon Wily & Sons (1975) 2

05 D W. Richerson, *Modern Ceramic Engineering*, Marcel Dekker, Inc., (1992) 2

06 R. C. Buchanan, *Ceramic Material for Electronics*, Marcel Dekker, Inc., (1991) .. 2

07 M. A. Omar, *Elementary Solid State Physics*, Pearson Education, Inc., (1999) 2

08 B. Jaffe, W. R. Cook and J. Jaffe, "*Piezoelectric Ceramics*". Academic Press Limited (1971) 2

09 J. P. Remeika, *J Am Chem Soc.*, 76. 940-1, (1954) 2

10 D Hennings,B. S. Schreinemacher and H. Schreinemacher, *J. Am Ceram Soc.*, 84(12), 2777-82 (2001) 3

11 G. Arlt, D. Hennings and G. de With, *J. Appl. Phys* **58** (4), 1619-25, 1985 3

12 J. K. Lee, K. S. Hong, and J W Jang, *J. Am. Ceram Soc.*, **84**(9), 2001-2006, (2001) 3

LITERATURE REVIEW

13 W. J. Merz, *Phys. Rev.* **91**,513 (1953) 5

14 M. Saifi, B Dubois, E. M. Vogel, *J Mater. Res.*, **1**, 452, (1986) 7

15 J. C. Chen, Y. C. Lee, S. P. Lin, *Jpn. J Appl Phys.*, **39**, 1812-1814, (2000) 7

16 T. J. Yang, V. Gopalan, P J. Swart, U. Mohideen, *Phys. Rev. Lett.*, **82**, 4106, (1999) 7

17 M. Muller, E. Soergel, M. C. Wengler, K. Buse, *Appl. Phys. B* , **78**, 367-370, (2004) 7

18 Z. Wang, J. E. Blendell, G. S. White, Q. Jiang, *Smart Mater. Struct.*, **12**, 217-222, (2003) 8

19 A Panupath, PhD Thesis, 1999 8

20 A. von. Hippel, *Rev Modern Phys.*, **22** 221 (1950). 8

21 J. A. Hooton and W. J. Merz, *Phys. Rev.* **98**, 409 (1955) 8

22 D. P. Cameron, *IBM Journal*, **January** 1957 8

23 U. Bottger, '*Polar Oxides: Properites, Characteriazation and Imaging*'. Wiley-VCH, Weinheim, **2005** 8

24 R. E. Newnham, ' Structure - Property Relations', Springer-Verlag, New York, 1975 10
25 R E. Nettleton, Ferroelectrics, 1, 3, 87 207, 221 (1970)..... 10
26 R. E. Nettleton, Ferroelectrics, 2, 5, 77 93, (1971)..... .10
27 R. E. Newnham, L. J. Bowen, et al., *Matl. Engg.*, **2**, 107 (1980).. 12
28 F. S. Galasso, *Structure, Properties and Preparation of Perovskite Type Compounds*, Pargamon Press, London, (1969). 13
29 H. D Megaw, *Acta Cryst.*, 7, 187-94, (1954) 13
30 R. E. Newnham, Structure - Property Relations, Springer-Verlag, New York, 1975 .... .18
31 C. Kittel, *Introduction to Solid State Physics*, Wiley, New York, 1996..... 19
31 T. Izuhar, *et. al., Appl. Phys. Lett.*, **82**, 4, 616-618, (2003).... 20
32 H.L. Hasegawa, M. R. Morelli, P. I. Paulin Filho, *Acta Microscopia*. **12**, C. 2003 20
33 Z C Chen, T. Ring, J. Lematre, *J. Am. Ceram. Soc.*, **75**, 3201-208, (1992) ..... .21
34 A. Bauger, J. Mutin, J. C. Niepce, J. Mater. Sci , 18, 3548, 1983. 22
35 I. K. Templeton, J. A. Pask, *J Am. Cerm. Soc* . **42**, 212, 1959..... 22
36 W. Kwestroo, H. A M. Paing, *J Am. Ceram. Soc.*, **42**, 292-9, (1959).....23
37 W. Maison, et al., *Science Asia*, **27**, 239-243, (2001). 23
38 S. L. Swartz, *IEEE Trans Electrical Insulation*, **25**, 935 (1990).....32
39 W. R. Buessem, L.E. Cross. A K Goswami. *J. Am. Ceram. Soc* . **75**, 2927 (1966) 32
40 R. Gerson, J. M. Peterson, D. R. Rote, *J. Appl. Phys.*, **34**, 3242-5, (1963) 33
41 D. A. Berlincourt, F. Kulesar, *J. Acoust Soc Am.*, **24**, 709, (1952) 36
42 R. C DeVries, R. Roy, *J. Am. Ceram. Soc* , **38**, 142, (1955) 36
43 M. C. McQuarrie, F. W. Behnke, J. Am. Ceram. Soc., 37, 539, (1954).....36
44 W. J. Merz, *Phys. Rev.*, **78**, 52, (1950) 36
45 T. Mitsui, W. B. Westphal, *Phys. Rev.*, **124**, 1354-59, (1961) 36
46 Y Baba, et at., *J. Phys. : Condens. Matter*, **8**, 7847-56, (1996) 37
47 K. Askan, et al., *J. Phys : Condens. Matter*, **13**, 11087-95, (2001).....38
48 M. Kahn, *Technical Information - Multilayer Ceramic Capacitors - Materials and Manufacture*, AVX Corporation, USA..... 38
49 D. Hennings, G. Rosenstein, *J. Am. Seram Soc.*, **67**, 249, (1984)..... 39
50 T. R. Shrout, J P. Doughery, *J Am. Ceram Soc.*, **57**, 1990..... 41

EXPERIMENTAL

51 Material Data Sheet, *http:/www.goodfellow.com* 48

7 Appendix

7.1 Raw Powder Chemical Specification – MME

Data provided here are taken form the label on the container.

7.1.1 Titanium Oxide

Manufacturer	Lobe	India
MW = 79.90	Min Assay = 99%	**TiO_2**
Impurities:		
H_2O – 0.5%	As - 0.005%	
Substance soluble in HCl –0.5%	Fe - 0.005%	Note:
Sulphate - 0.05%		Anatase
Heavy Metal (Pb) – 0.003%		

7.1.2 Barium Carbonate

Manufacturer	E. Merck	India
MW = 197.35	Min Assay = 99%	**$BaCO_3$**
Impurities:		
Choloride - 0.01%	Pb - 0.002%	
Na - 0.01%		
Fe - 0 005%		

7.1.3 Calcium Oxide

Manufacturer	Lobe	India
MW = 197.35	Min Assay = 95%	**CaO**
Impurities:		
Choloride - 0.1%	Pb - 0.02%	
Sulphate - 0.5%	Loss on ignition	
Fe - 0.1%	10%	

7.2 Raw Powder Chemical Specification – MTEC

Data provided here are taken form the label on the container.

7.2.1 Titanium Oxide

Manufacturer	Fluka	UK
MW = 79.90	Min Assay = 99%	**TiO_2**
Impurities:		
	As - 0.005%	
Substance soluble in HCl –0.1%	Fe - 0.005%	Note:
Sulphate - 0.05%	Loss on ignition	Anatase
Heavy Metal (Pb) – 0.003%	<= 0.5%	

7.2.2 Barium Carbonate

Manufacturer	Fluka	UK
MW = 197.37	Min Assay = 98.5%	**$BaCO_3$**
Impurities:		
Choloride - 0.03%	Ca - 0.05%	**Sr ~ 1.5%**
Cd, Co, Cu, Fe, Ni, Pb, Zn each <= 0.005%		
K - 0.01%	Na - 0.2 %	
Note the addition of Sr		

7.3 Raw Powder Chemical Specification – MME (2)

Data provided here are taken form the label on the container.

7.3.1 Barinm Carbonate

Manufacturer	BDH	UK
MW = 197.35	Min Assay = 99%	**$BaCO_3$**
Impurities:		
Choloride - 0.01%	Na <= 0.2%	
Fe <= 0.005 %		
Pb <= 0.002 %	S <= 0.05 %	

7.3.2 Calcinm Carbonate

Manufacturer	Merck	India
MW = 100.086	Min Assay = 99.5%	**$CaCO_3$**
Impurities:		
Choloride - 0.05 %	Ca - 0.05%	
Substance soluble in HCl –0.05 %		
SO_4 - 0.5 %	Pb - 0.005 %	
Fe - 0.05 %		

7.4 Basic Data of Elements involved

Element	Atomic Weight	Atomic Number	Crystal Structure	Atomic Radius nm	Ionic Radius nm	Common Valance	Melting Point °C
Ba	137.33	56	BCC	0.217	0.136	2+	725
Ti	47.88	22	HCP	0 145	0.068	4+	1668
Ca	40.078	20	FCC	0 197	0.100	2+	837
O	15.99	8	-		0 140	2-	-218 4
C	12.011	6	HCP*	0.071	0.016	4+	-

7.5 Symmetry of crystal system

Crystal Structure	Point Groups	Centro-Symmetric	Non-centrosymmetric	
			Piezoelectric	Pyroelectric
Triclinic	1, $\bar{1}$	1	1	1
Monoclinic	2, m, 2/m	2/m	2, m	2, m
Orthorhombic	222, mm2, mmm	mmm	222, mm2	mm2,
Tetragonal	4, $\bar{4}$, 4/m, 422, 4mm, 42m, (4/m)mm	4/m, (4/m)mm	4, $\bar{4}$, 422, 4mm, 42m	4, 4mm
Rhombohedral	3, $\bar{3}$, 32, 3m, $\bar{3}$m	3, 3m	3, 32, 3m	3, 3m
Hexagonal	6, $\bar{6}$, 6/m, 622, 6mm, 6m2, (6/m)mm	6/m, (6/m)mm	6, $\bar{6}$, 622, 6mm, 6m2	6, 6mm
Cubic	23, m3, 432, 43m, m3m	m3, m3m	23, 43m	----

7.6 Differences between normal and relaxor ferroelectrics

Property	Normal Ferroelectric	Relaxor Ferroelectric
Dielectric temperature dependence	Sharp 1st or 2nd order transition at Curie point T_c	Broad diffused phase transition at Curie maxima
Dielectric frequency dependence	Weak Frequency dependence	Strong frequency dependence
Dielectric Behavior in paraelectric range ($T > T_c$)	Follows Curie - Weiss law	Follows Curie - Weiss square law
Remnant polarization (P_R)	Strong P_R	Weak P_R
Scattering of light	Strong anisotropy	Very weak anisotropy to light
Diffraction of X-Rays	Line splitting due to deformation from paraelectric to ferroelectric phase	No X-Ray line splitting

7.7 JCPDS PDF file of BaTiO3

2θ	Int	h	k	l	2θ	Int	h	k	l
22.037	12	0	0	1	92.320	12	3	2	1
22.261	25	1	0	0	99.486	1	0	0	4
31.496	100	1	0	1	100.975	2	4	0	0
31.643	9	1	1	0	103.859	1	1	0	4
38.826	10	1	1	1	104.492	1	2	2	3
44.852	12	0	0	2	104.981	1	3	2	2
45.375	37	2	0	0	105.352	1	4	1	0
50.611	8	1	0	2	108.246	3	1	1	4
50.974	6	2	0	1	108.935	1	3	0	3
51.087	7	2	1	0	109.783	5	4	1	1
55.951	15	1	1	2	113.545	2	3	3	3
56.249	33	2	1	1	114.951	2	3	3	1
65.756	17	2	0	2	117.494	3	2	0	4
66.418	10	2	2	0					
70.354	5	2	1	2					
70.577	2	3	0	0					
74.331	5	1	0	3					
75.080	7	3	0	1					
75.158	9	3	1	0					
78.782	3	1	1	3					
79.466	5	3	1	2					
83.458	7	2	2	2					
86.968	1	2	0	3					
87.260	1	3	0	2					
88.082	1	3	2	0					
88.578	2	2	1	3					
92.053	12	3	1	2					

Ref Swanson Fuyat, Natl Bur Stand (U S) Circ 539 3, 45 (1954)

Ref Ibid

Color Colorless
X-ray pattern at 26 C Sample from National Lead Company CAS # 12047-27-7 Annealed at 1480 C in MgO Spectroscopic analysis <0 1% Ba Sr <0 01% Al Ca Fe Mg Pb Si <0 001% Mn Sn Inverts to cubic form at 120 C Merck Index 10th Ed , p 122 PSC 1/3 Plus 10 additional reflections Mwt 233 23 Volume[CD] 64 41

2θ	Int	h	k	l
22.30	14	1	0	0
31.387	100	1	1	0
38.876	30	1	1	1
44.966	35	2	0	0
50.628	10	2	1	0
65.910	25	2	1	1
65.501	15	2	2	0
70.001	5	3	0	0
74.472	1h	3	1	0
78.580	6	3	1	1
83.00	4	2	2	2

Ref Naka, S , Private Communication, (1978)

Sample was prepared by hydrolysis of titanium tetraisopropoxide in aqueous solution of barium hydroxide and has submicron size of particles Absorbs about 6% of OH and alcoholic radicals Metastable form It changes to stable tetragonal form above 800 C Mwt 233 23 Volume[CD] 66 50